Development of Novel Technologies for Direct Cellular Patterning for the Establishment of Well Controlled Microenvironments to Facilitate Studies on Cellular Signaling, Sensing, and Other Diffusion-Based Phenomena

---

A Dissertation
Presented to

Colleges of Nanoscale Science & Engineering

In partial fulfillment
of the requirements for the

Doctor of Philosophy Degree

State University of New York

Polytechnic Institute

By

William F. Hynes

May 2016

ABSTRACT

This work focuses on the utilization of novel bioprinting technologies for the investigation of cellular signaling, sensing, and other diffusion-based phenomena with spatiotemporal dependencies. Two different printing techniques were developed for the purpose of fabricating controlled microenvironments comprised of cells, nutrients, hydrogels, and soluble signaling molecules in a repeatable fashion.

The first application explored was the development of a novel, bioprinted, cell-based biosensor as a nondestructive method for the monitoring of the cellular redox environment. Mammalian cells were engineered to express a redox sensitive protein and were patterned and immobilized within a photopolymerizing hydrogel matrix, resulting in biocompatible, three-dimensional microenvironments which supported cell growth and facilitated small molecule sensing. Exposure of the printed, redox sensitive cells to oxidative and reductive compounds and monitoring via confocal microscopy demonstrated proper and reversible functioning of the living biosensor.

Bioprinting was also used to generate complex, micro-scale, multi-species populations of bacteria in order to evaluate the effects of distance and various forms of competition on syntrophic relationships. An artificial, syntrophic bacterial consortium was printed within controlled microenvironments confined by geometry and nutrient availability. The growth of the printed strains was monitored, analyzed, and compared to the predictions of an experimental, computational bacterial growth model known as COMETS. Results indicated that the general trends exhibited *in vitro* by most of the examined micro-scale interactions can be predicted *in silico*, and that the effects of microbial interactions on the micro-scale can differ considerably than those observed at the macro-scale.

TABLE OF CONTENTS

Chapter 1: Bioprinting Technologies

Section 1.1. Bioprinting: A Definition

Bioprinting is an expanding field that is addressing the growing requirement for the precise spatial arrangement of live cells and biomaterials onto solid and semi-solid surfaces [1]. Bioprinting is defined as the use of computer-aided transfer processes for patterning and assembling living and non-living materials with a prescribed two (2D) or three dimensional (3D) organization [2]. It encompasses many different contact and non-contact patterning technologies. The importance of this biofabrication approach is becoming fully understood in many fields, including tissue engineering [3], regenerative medicine [4], development of high-throughput biosensors [5], as well the more fundamental fields of microbiology [6] and stem cell research [7]. Currently, there are several well established methods for the rapid deposition of live cells onto solid, semi-solid, and liquid substrates. These printing technologies can be separated into two broad classifications depending on their method of introducing cells to the substrates, direct contact, or non-contact (indirect) printing [Fig 1]. In the case of contact methods, the printing device directly touches the substrate to transfer cells, while in the case of non-contact methods, cells and materials are transported to the surface via an ejection or settling process. It should be noted that all of the discussed bioprinting technologies are generally considered to be complementary, rather than competing technologies. Each method has its own strengths and weakness, and the decision as to which approach, or combination of approaches, will be used is chosen based on the specific requirements of the research group and the task at hand [8].

Section 1.2. Contact Cell Patterning Techniques

Direct contact cell printing encompasses several different approaches which posses the shared characteristic of delivering cells and other materials directly to the receiving substrate while under the control of the printing apparatus. Some of the most commonly utilized contact patterning technologies are based on extrusion pump methods, where cells are suspended in solution and loaded into syringe pumps or pneumatically driven nozzles [Fig 1]. Pressure is then applied to force the solution through the printing tip and onto the print surface in a well controlled fashion [9]. By utilizing this technology, Forgacs *et al.* have successfully fabricated vascular grafts *in vitro* by depositing aggregates of smooth muscle cells onto 3D agarose templates. The aggregates were permitted to coalesce over time, as a result of tissue liquidity, forming the necessary tubular structure [10]. Typically extrusion-based printing systems are utilized in order to pattern large numbers of cells with relatively low resolution ($\geq$ 100 μm in diameter [11]). This relatively low resolution is necessary as higher shear forces are generated when using narrower nozzle diameters, which can potentially cause cell damage. Some additional control over print volume can be gained upon the incorporation of a micro-solenoid or pneumatically driven flow-controller within the print nozzle. This additional flow-control also enables the extrusion system to switch between continuous flow and single droplet deposition modes [12]. Extrusion systems are well suited for tissue engineering applications where these characteristics are necessary to ensure rapid and accurate positioning of cell aggregates at the required densities within the printed organ and tissue constructs [13].

Microcontact printing and microfluidic patterning together are among the earliest and most widely adapted methods for directly patterning surfaces with proteins and other bioactive molecules on the micro-scale, and together they share many of the same strengths and

weaknesses in terms of their patterning ability. These methods involve the fabrication of either polymeric "stamps" possessing raised and recessed features, or micro channels molded into a polymeric matrix, using a process known as soft lithography. In brief, the soft lithography approach involves fabricating a "master mold" out of photoresist or silicon, using micro-fabrication techniques such as photolithography and silicon etching to produce a negative of the intended surface features desired for the final stamp or microfluidic device. After fabrication of the master, an elastomeric material such as polydimethylsiloxane (PDMS) is cast over the features, cured and removed resulting in a solid, flexible polymeric matrix with features opposite those of the master. In the case of microcontact printing, this results in a stamp which can be coated in protein solution and used to pattern a surface, with the raised features of the stamp depositing the solution onto the patterning substrate when the two are brought into contact [14] [Fig 1].

For microfluidic patterning, the trenches in the PDMS "stamp" (as described above) function as micro-channels when the PDMS is bonded to a glass substrate. Solutions can be pumped or pulled through via capillary force in order to deposit them onto the glass surface [15]. Both of these patterning approaches have been converted into direct contact, whole-cell patterning techniques [Fig 1]. The conversion of microcontact printing of proteins to cells has been termed "hydrogel-based cell patterning and transferring" or HPT [16]. This method involves coating the stamp with cells suspended in a hydrogel solution, allowing the solution to fill the recessed areas, followed subsequently by cross-linking to encapsulate the cells and transferring them to a receiving substrate via stamping. Currently, the only recorded application of HPT was to qualitatively analyze artificially engineered genetic circuits in live bacterial cells, and was performed by the group responsible for its conception. The HPT technique possesses a

great deal of promise, as it can tightly control the number of cells deposited, the deposition volume, and the spacing between depositions, resulting in an ideal platform for cell signaling studies and high-throughput screening applications. The conversion of microfluidic devices into direct cell patterning devices is quite straight-forward by comparison. Substituting the protein solution for cells suspended in solution, multiple cell types can be patterned simultaneously and in close proximity via transport through the micro-channels [17]. An example of the application of direct microfluidic cell patterning is the development of 2D and 3D cell cultures consisting of one or more cell types which have been patterned via laminar flow of cell-containing solutions through micro-channels. For 2D microfluidic cultures, cells in solution are pumped through the device and allowed to settle and attach to the basal surfaces, while in 3D microfluidic cultures the cells are pumped through the device while suspended in a hydrogel precursor and encapsulated within the hydrogel via cross-linking. These approaches have been used to generate cell cultures within environments that more closely resemble the cell's *in vivo* conditions for the purpose of studying the cells in a more physiologically relevant setting [18]. Both microcontact printing and microfluidic patterning rely on the fabrication of a master mold, which can be challenging to fabricate without access to cleanrooms and photolithography tools, and can also delay the development of novel prototypes as new photolithographic masks must be developed anytime a new design is desired. In the case of microcontact printing specifically, only one solution or cell type can be patterned at a time, whereas with microfluidic patterning multiple solutions and cell types can be patterned simultaneously or sequentially within the same channels [19].

Molecular printing systems designed for the fabrication of microarrays, such the MicroSys 5100-4SQ microarray spotter (Cartesian Technologies), typically possess many of the

characteristics necessary to be considered viable whole-cell bioprinter, such as computer-aided, controlled transfer of biomaterials with precise 2D, and potentially 3D, organization. These printing systems are capable of achieving patterning resolution in-line with the non-contact technologies described in section 1.3. Microarryer systems can accomplish this without exposing printing solutions to the high shear forces, acceleration, or thermal stresses normally experienced with most other patterning methods. This is because these systems utilize either pin- or cantilever–based patterning tools that both load and dispense solutions via comparatively gentle capillary forces, which are generated upon the printing solutions interaction with the micro-scale channels and tips of the patterning tools. When the tip of the printing pin or cantilever is brought into contact with a substrate, the fluid meniscus is able to interact with the surface and, if the surface is sufficiently hydrophilic, a small volume of solution is pulled out of the tip and deposited [Fig 1]. In addition to being capable of patterning whole-cells, microarray printers can also be used as non-contact bioprinters by patterning solutions containing proteins or other attachment molecules, such as hydrogels and extracellular matrix components. Surfaces patterned with these molecules can be subsequently seeded with cells to promote their attachment to the patterned locations, which is very similar in function to the indirect patterning of cells using the microcontact and microfluidic patterning methods.

Microarray printers are well suited for the development of high-throughput, miniature cell-based screening assays for the identification and characterization of therapeutic or toxic compounds. This is due to the fact that they utilize very small amounts of material, large amounts of which can be very costly when examining possible drug candidates, while enabling the screening of up to thousands of compounds simultaneously [20]. Examples of microarrayer-based cell printing include the development of the Data Analysis Toxicology Assay Chip or

DataChip for high-throughput toxicity screening of drug candidates using printed cells [21], and the development of an immunoflorescence-based assay which uses printed cells to enable the high-throughput screening of cellular protein levels upon exposure to chemical stimuli [22].

The final direct-contact technology that will be covered is the optical tweezers method, which utilizes focused light to trap cells from solution and guide them directly to the receiving substrate. The optical tweezers method uses an infrared laser focused through a high-power objective to trap cells and other microscopic materials in the focal region of the beam via the forces of radiation pressure, electromagnetic induction of dipoles within the manipulated object, and the dipole's interaction with the electromagnetic field of the beam itself [Fig 1] [23]. This technique could also be considered non-contact, due to the electromagnetic forces acting on the cells over a distance. However, due to the fact that cells must be directly guided into contact with the substrate in order to be patterned, we will consider it as a direct contact technique for the purposes of this review. Optical tweezers enable the manipulation and positioning of single cells and other biological materials without requiring removal from their normal liquid media environment. This enables the printing process to proceed without a reduction in cell viability due to drying or possible contamination events. This technique currently possesses the highest possible printing resolution due to its ability to deposit single cells with sub-micron precision [24]. The laser beam can also be split via diffraction to increase the number of traps available at the same time, increasing patterning throughput, resulting in a technique known as holographic optical tweezers (HOT). HOT's ability to generate complex histoarchitectures was demonstrated by Kirkham *et al.* through the patterning of biological 3D microenvironments consisting of deposited cells, ECM and polymer materials in order to facilitate the observation of cellular regulatory mechanisms within a tunable environment [25].

Section 1.3. Non-contact Cell Printing Techniques

Non-contact patterning methods encompass several printing approaches, the most well known of which are based on ablative laser and ink-jet printing technologies. Laser-based technologies, such as matrix-assisted pulsed-laser evaporation direct writing (MAPLE DW), utilize the forward momentum produced when photons from a laser strike the backside of a transparent target ribbon. Interaction of the laser beam with the cell-laden matrix spread on the front of the target induces rapid heating and vaporization in order to eject cells/materials from the target and onto the receiving substrate [26]. Recently, more refined laser-based processes known as absorbing film assisted laser induced forward transfer (AFA-LIFT) and biological laser printing (BioLP) have been developed to improve upon the existing technology by using a metal, light-absorbing thin film between the irradiated target surface and the cell containing matrix material [Fig 1]. The thin film is designed to absorb the wavelength emitted by the laser, preventing the beam from penetrating into the matrix material, which assists in the transition from beam to kinetic energy and protects the cells from potential damage arising from direct interaction with the laser beam [27]. In the case of BioLP, this layer also acts as a sacrificial layer which undergoes rapid thermal expansion when struck by the laser, ejecting the printing solution from the target ribbon without significant heating of the cells in the matrix material [28]. BioLP has recently been used by Wu and Ringeisen to pattern branch and stem structures of human umbilical vein endothelial and smooth muscle cells onto thin hydrogel substrates [29]. This patterning was performed in order to guide cell growth and subsequent angiogenesis, demonstrating BioLP's feasibility for patterning complex microstructures for *in vitro* tissue fabrication.

Ink-jet bioprinters represent another non-contact patterning method, which are classified based on their method of droplet ejection from the printing nozzle. Thermal ink-jet printers utilize a small resistive heating element to vaporize the printing solution, forming a bubble which expands and collapses within microseconds, ejecting a droplet from the nozzle due to the pressure pulse [Fig 1] [30]. Piezoelectric ink-jet printers function similarly by employing the pulsing pressure of a piezoelectric membrane within the printing nozzle, which mechanically flexes rapidly in order to eject droplets of printing solution [31]. While both ink-jet technologies are viable for laboratory bioprinting, piezoelectric printing systems are considered more challenging to employ, as they are only able to optimally print a comparatively narrow range of printing solutions, limited by the ink's viscosity, surface tension and composition. Printing solutions are often aqueous, but contain polymers for immobilization and salts to maintain the physiological osmotic pressure of the cells within; this can be an issue for the piezoelectric mechanism which can gradually degrade and short under these printing conditions [32]. Despite these drawbacks, piezoelectric ink-jetting is still considered a viable cell patterning method and has been recently used by Aria *et al.* to demonstrate live printing of HeLa cells into complex, 3D alginate gel structures [33]. Meanwhile, thermal ink-jet cell printing has been widely used by many groups, including Xu *et al.* who have used it to demonstrate the fabrication of complex 3D tissue constructs incorporating multiple cell types for the purpose of developing functional tissues for *in vitro* assays and *in vitro* implantation [34].

Bioprinters that utilize either laser-based or ink-jet deposition methods share several characteristics, including their non-contact nature and their capability to rapidly print small spots (diameters < 50 μm) with high spatial precision [35], [36]. However, there are some differences to note between the laser and ink-jet methods in that laser-assisted technologies are generally

capable of greater control over printed cell density and can only pattern multiple samples in a serial manner, while ink-jet-based printers can typically pattern samples at higher throughputs and multiple samples in parallel [11]. The non-contact nature of these systems usually requires cells to be subjected to high accelerations as they pass through the gap toward the printing surface. This means special considerations must be taken when selecting printing substrates in that they must deform sufficiently upon cell impact in order to prevent damaging the cells, which often restricts these printers to patterning substrates consisting of gels or liquids [37]. In comparison to extrusion-based methods, the higher resolution, non-contact patterning methods are more readily suited toward recreating the 2D and 3D microstructures found in native tissues and organs on the appropriate scale.

In addition to the above techniques, the microcontact and microfluidic patterning approaches described in the previous section can also be utilized as a method of non-contact cell patterning [Fig 1], albeit in an indirect manner as cells in solution are used to subsequently seed the surface after protein patterning. As mentioned previously, microcontact printing and microfluidic patterning can be used in order to pattern surfaces with proteins and other bioactive molecules. For microcontact printing, proteins that promote cellular attachment, such as laminin [38] and fibronectin [39], can be patterned onto surfaces while the remaining surface is functionally terminated with a non-adhesive group to inhibit cellular attachment, such as gold which has been coated in polyethylene glycol (PEG)-terminated alkanethiol-groups [38], in order to immobilize cells only in the locations defined by the protein. Using microfluidic devices to pattern proteins for cell attachment is very similar to the microcontact printing approach, however they vary in that proteins are introduced to the surface via flow through the microchannels in the microfluidic device [40]. Dike *et al.* used microcontact printing of proteins

for cellular attachment to investigate the effects of surface spreading on bovine endothelial cells seeded onto fibronectin and found that when the cells were seeded on 10 μm-wide lanes of fibronectin, they formed capillary tube-like structures and ceased proliferating after 72 hours [41]. It was also determined that when the endothelial cells were permitted to spread further on 30 μm-wide lanes, they continued to proliferate after 72 hours and did not form tube-like structures, highlighting the importance of cell-surface interactions on cellular differentiation. Using microfluidic protein patterning of laminin over microcontact patterned gradients of ephrinA5 Lang *et al.* examined the response of chick retinal ganglion cells to the gradients after seeding onto the lanes of laminin [42]. They observed that temporal populations of the ganglion cells produced axon extensions which all stopped at the same location within the gradient while the nasal population's axons continued to extend. In addition it was noted that all the axons grew further along shallow gradients and stopped earlier along steeper gradients, demonstrating the strength of the combinatorial microcontact printing and microfluidic patterning approach for quantifying cell response to gradients of immobilized chemoattractants.

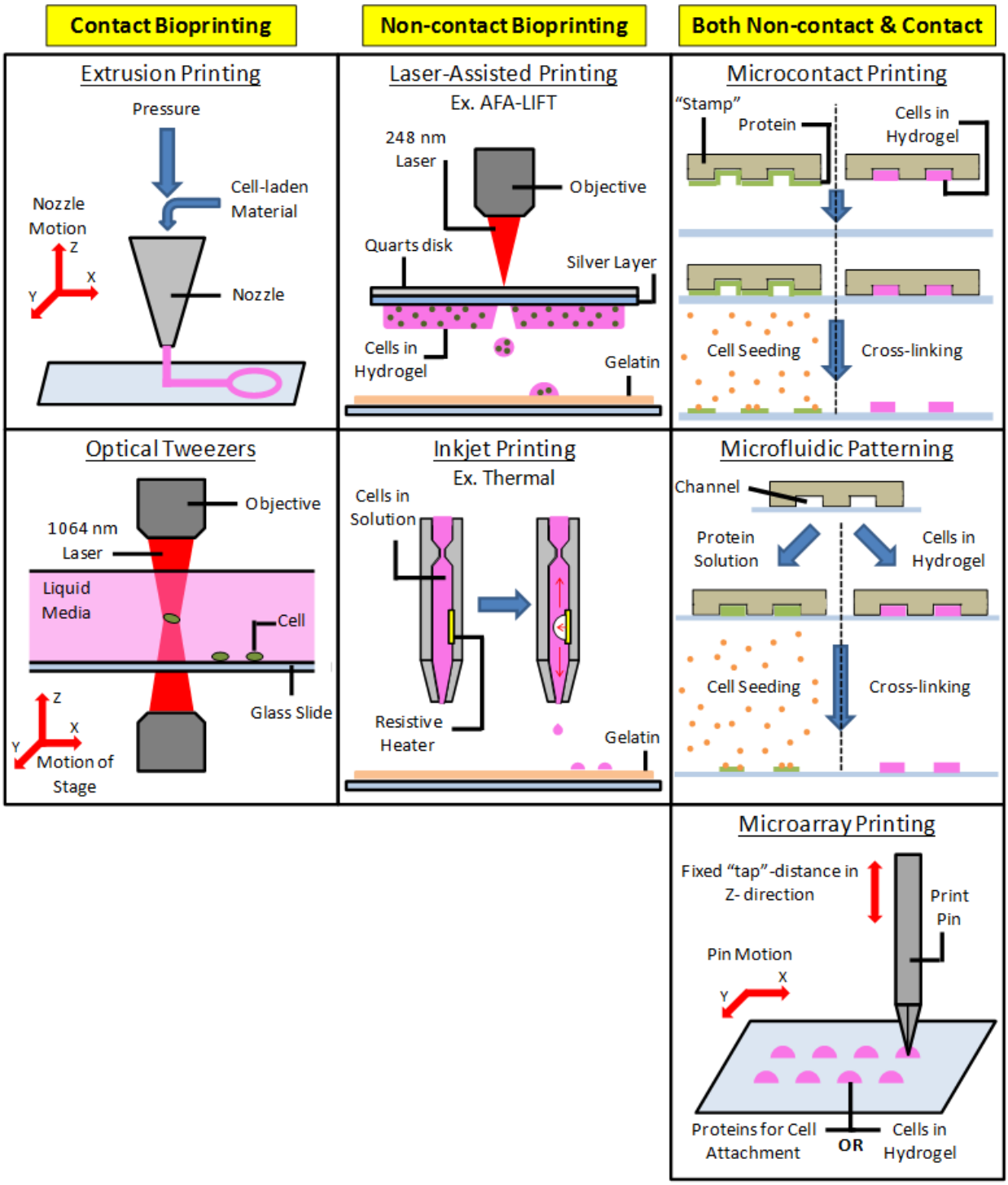

Figure 1. Summary of live-cell bioprinting methods. Contact techniques deliver the cells to the desired surface via direct interaction with the patterning apparatus. Non-contact methods require that cells and solutions travel to the surface over a distance using forces generated by the printing apparatus, such as pressure. Microcontact printing, microfluidic patterning, and microarray printing can be either contact or non-contact, depending on how they are employed.

Section 1.4. Current Trends in Bioprinting: A Focus on Tissue Engineering

In the last decade, tissue engineers have begun utilizing bioprinting to engineer biocompatible, cell-laden constructs, which support the growth and differentiation of the incorporated cells *in vitro*. The patterning of cells and biomaterials is intended to encourage the cells to assemble into a histoarchitecture very similar in form and function to that of natural tissues and organs [3]. More conventional tissue engineering approaches often involve seeding specific cell types onto either synthetic or decellularized natural matrices, followed by the directed cultivation of the incorporated cells in order to assemble the final, tissue-like structure [43]. While these approaches are responsible for substantial advancements in our understanding of tissue differentiation and self-assembly, they usually lack precision in the attachment and differentiation of the incorporated cells. Conventional techniques tend to be less effective when applied to more complex tissue systems containing multiple cell types with highly specific orientations [44]. This is due to the nature of the cell seeding process. Scaffolds are typically submerged in bulk solutions of cells in suspension, often leading to a non-specific, homogeneous deposition within the matrices, a condition which does not accurately represent their native positions *in vivo*. This phenomenon can result in poor control over the subsequent tissue growth and development [11].

The ability to pattern growth factors, proteins, live cells and even the scaffold-forming material itself is quite appealing in light of current fabrication methods, which can accurately control neither the positioning nor density of these materials within the construct. Bioprinters have the capability of patterning cells and bio-active molecules into fabricated 2D and 3D structures that can mimic the natural architecture of functional tissue. Sequential printing, cross-linking, and cultivation can generate a living scaffold by depositing cells and proteins within a

suitable, matrix-forming, hydrogel solution. While most bioprinting endeavors are currently focused on optimization and development of their respective patterning technologies, once matured, bioprinting is expected to enable the *in vitro*, bottom-up fabrication of organ and tissue-like constructs in a rapid and reproducible manner [13]. It is for these reasons that the majority of applied bioprinting studies have focused predominantly on enabling the fabrication of preliminary tissue-like constructs.

Examples of bioprinting being utilized for tissue engineering endeavors include the extrusion-based patterning performed by Duan *et al.* where aortic root sinus smooth muscle cells and aortic valve leaflet interstitial cells were encapsulated within alginate/gelatin hydrogel and patterned to form a living aortic valve conduit [45]. This effort represents an important step towards bioprinting of functional heart tissues as it demonstrates that multiple cell types can be patterned into a complex heterogeneous structure while maintaining cell viability. An example of non-contact tissue printing come from Micheal *et al.* who used a laser-assisted patterning approach to print cellularized skin-like constructs by patterning fibroblasts and keratinocytes on a Matriderm® substrate [46]. After patterning, the constructs were grafted onto mice using a dorsal skin fold chamber and observed for 11 days with the constructs exhibiting favorable characteristics such as collagen production and the presence of native blood vessels spreading toward the constructs. These results are promising as future applications of printed skin constructs could be used for humans to significantly improve the speed and quality of healing of burn-related injuries. Another example of non-contact bioprinting was used by Xu *et al.* with the development of a novel printing system which incorporates inkjet cell printing with electrospinning of fibers in an alternating deposition of cells and scaffolding materials for mechanically robust tissue constructs [47]. By layering rabbit elastic chondrocytes encapsulated

in a fibrin-collagen hydrogel with layers of electrospun polycaprolactone fibers, a cartilage-like construct was formed and evaluated both during *in vitro* cultivation and *in vivo* within a mouse model. It was determined that both the *in vivo* and *in vitro* constructs maintained cell viability and exhibited subsequent cartilage-specific ECM formation. This work represents a large step forward for bioprinted tissue constructs as it shows that not only can cells be patterned into a physiologically relevant organization, but also that the resulting construct can be tuned to better match the mechanical requirements of the native tissue.

Section 1.5. Bioprinting for Cell Signaling and Sensing Studies

The capability of emulating natural microenvironments is not only useful for the exploration of mammalian organs and tissues, it is also highly applicable to fundamental studies on cell signaling phenomena in both eukaryotic and prokaryotic microorganisms [48]. Cell behavior can be altered by signals received from physical interactions with their neighbors and extracellular matrix (ECM), as well as from soluble factors produced by other cells. Studying the characteristics and effects of cell-to-cell signaling in standard bulk cultures is often quite challenging. Standard bulk cultures allow little to no spatial control of cell or signaling factor distribution, which can cause an intractable situation where local signal strength and individual cell response cannot be readily correlated. In order to design an effective platform for the study of cell signaling phenomena, variables such as cell position, cell density, signal concentration and signal gradient formation must be well controlled. The same spatial control over cell and biomolecule deposition that makes bioprinting attractive to tissue engineers can be utilized in order to address these requirements. Bioprinting can be used to pattern all of the materials (i.e. signaling and attachment molecules) required for conducting highly controlled cell signaling

studies utilizing specifically formulated bio inks to ensure safe delivery and retention of these materials on the printed surface [49]. Reporter cells can be patterned and immobilized into extensive geometrically defined arrays, followed by the deposition of signaling molecules or cells by the same technique. As the signal diffuses away from the source, the response from the reporter cells can be easily observed and quantified as the signal gradient is established. In addition to printing soluble signaling factors, bio inks containing ECM components and other structural proteins can also be formulated and printed along with the cells of interest in order to evaluate the effects of their incorporation [50].

This same approach can also be applied to the development of high throughput fabrication methods for whole-cell based biosensors [51]. Biosensors utilizing immobilized cells have seen previous applications in the monitoring of environmental toxin or pathogen levels [52]. These cell-based sensors can provide benefits over traditional chemical based sensors in that they are readily capable of evaluating "group effects", including biological toxicity, mutagenicity, and pharmacological efficacy [20]. Additionally, they permit the resulting cellular phenomena to be measured via optical measurements [53] or extracellular electrical recordings [54]. A common challenge faced during the development of traditional molecular sensors, such as in enzyme-based biosensors, is the often costly and challenging amplification, isolation and immobilization process for the specific enzyme or other biomolecule of interest [5]. This process is critical to establish the sensors selectivity toward the desired analyte. However, these steps could be bypassed, as the cells that produce these molecules can themselves be utilized in a cell-based biosensor. This would ensure the safe delivery and retention of the sensing molecules to the surface while maintaining their functionality under normal physiological conditions [55]. Until recently, these cell-based biosensors have been limited in their methods of high-throughput

fabrication due to their reliance upon more traditional tissue culturing fabrication methods. This has greatly hindered their entry into common, practical application [56]. Through the rapid and precise patterning/immobilization of cells onto solid surfaces (e.g. glass [53], electrodes [54]), bioprinting represents a powerful tool in accelerating and miniaturizing the cell-based biosensor fabrication process, thereby significantly lowering the barrier to their routine use in the field [57]. **It is for these reasons I hypothesize that 2D, microarrayer-based, live cell bioprinting can enable the rapid development of well controlled microenvironments for the purpose of examining various diffusion-dependent phenomena *in vitro*, such as cellular signaling and sensing of small molecules, without the need for highly-specialized equipment or expertise.**

To test this hypothesis, first I will use microcontact printing to develop engineered substrates consisting of immobilized IgG antibodies and poly-L-lysine peptides to assist in the investigation of the intracellular events following FcγR-IgG ligation and signaling within mouse macrophages. Next I will utilize novel, microarrayer-based bioprinting to develop a widely adaptable process flow for cell-based biosensor development and use this approach to develop a proof-of-concept reactive oxygen species sensor. My final goal will be to use bioprinting to generate complex, yet well-defined, bacterial co-cultures to investigate the signaling-like interaction of diffusion-based mutualistic metabolite sharing.

References Cited

[1] M. Nakamura, S. Iwanaga, C. Henmi, K. Arai, and Y. Nishiyama, "Biomatrices and biomaterials for future developments of bioprinting and biofabrication.," *Biofabrication*, vol. 2, no. 1, p. 014110, Mar. 2010.

[2] F. Guillemot, V. Mironov, and M. Nakamura, "Bioprinting is coming of age: Report from the International Conference on Bioprinting and Biofabrication in Bordeaux (3B'09).," *Biofabrication*, vol. 2, no. 1, p. 010201, Mar. 2010.

[3] V. Mironov, V. Kasyanov, and R. Markwald, “Bioprinting: Directed Tissue Self-Assembly,” *Chem. Eng. Prog.*, vol. 103, no. 12, 2007.

[4] W. Hennink and G. D. Prestwich, “Hyaluronic acid-based clinical biomaterials derived for cell and molecule delivery in regenerative medicine,” *J. Control. Release*, vol. 155, no. 2, pp. 193–199, 2011.

[5] J. I. Rodríguez-Dévora, B. Zhang, D. Reyna, Z. Shi, and T. Xu, “High throughput miniature drug-screening platform using bioprinting technology.,” *Biofabrication*, vol. 4, no. 3, p. 035001, Sep. 2012.

[6] Y. Fang, J. P. Frampton, S. Raghavan, R. Sabahi-Kaviani, G. Luker, C. X. Deng, and S. Takayama, “Rapid generation of multiplexed cell cocultures using acoustic droplet ejection followed by aqueous two-phase exclusion patterning.,” *Tissue Eng. Part C. Methods*, vol. 18, no. 9, pp. 647–57, Sep. 2012.

[7] M. P. Lutolf, P. M. Gilbert, and H. M. Blau, “Designing materials to direct stem-cell fate,” *Nature*, vol. 462, no. 7272, pp. 433–41, Nov. 2009.

[8] V. Mironov, N. Reis, and B. Derby, “Review: bioprinting: a beginning,” *Tissue Eng.*, vol. 30, 2006.

[9] J. I. Rodríguez-Dévora, Z. Shi, and T. Xu, “Direct assembling methodologies for high-throughput bioscreening.,” *Biotechnol. J.*, vol. 6, no. 12, pp. 1454–65, Dec. 2011.

[10] K. Jakab, C. Norotte, B. Damon, F. Marga, A. Neagu, C. L. Besch-Williford, A. Kachurin, K. H. Church, H. Park, V. Mironov, R. Markwald, G. Vunjak-Novakovic, and G. Forgacs, “Tissue engineering by self-assembly of cells printed into topologically defined structures.,” *Tissue Eng. Part A*, vol. 14, no. 3, pp. 413–21, Mar. 2008.

[11] B. Guillotin and F. Guillemot, “Cell patterning technologies for organotypic tissue fabrication,” *Trends Biotechnol.*, vol. 29, no. 4, pp. 183–190, 2011.

[12] S. Khalil, J. Nam, and W. Sun, “Multi- nozzle deposition for construction of 3D biopolymer tissue scaffolds,” *Rapid Prototyp. J.*, vol. 11, no. 1, pp. 9–17, 2005.

[13] K. Jakab, C. Norotte, F. Marga, K. Murphy, G. Vunjak-Novakovic, and G. Forgacs, “Tissue engineering by self-assembly and bio-printing of living cells.,” *Biofabrication*, vol. 2, no. 2, p. 022001, Jun. 2010.

[14] C. James, R. Davis, and L. Kam, “Patterned protein layers on solid substrates by thin stamp microcontact printing,” *Langmuir*, vol. 7463, no. 13, pp. 741–744, 1998.

[15] I. Meyvantsson, J. W. Warrick, S. Hayes, A. Skoien, and D. J. Beebe, “Automated cell culture in high density tubeless microfluidic device arrays,” *Lab Chip*, vol. 8, no. 5, p. 717, 2008.

[16] W. S. Choi, M. Kim, S. Park, S. K. Lee, and T. Kim, "Patterning and transferring hydrogel-encapsulated bacterial cells for quantitative analysis of synthetically engineered genetic circuits.," *Biomaterials*, vol. 33, no. 2, pp. 624–33, Jan. 2012.

[17] S. Takayama, J. C. McDonald, E. Ostuni, M. N. Liang, P. J. Kenis, R. F. Ismagilov, and G. M. Whitesides, "Patterning cells and their environments using multiple laminar fluid flows in capillary networks.," *Proc. Natl. Acad. Sci. U. S. A.*, vol. 96, no. 10, pp. 5545–5548, 1999.

[18] J. H. Yeon and J.-K. Park, "Microfluidic cell culture systems and cellular analysis," *Biochip J.*, vol. 1, no. 1, pp. 17–27, 2007.

[19] R. Kane, "Patterning proteins and cells using soft lithography," *Biomaterials*, vol. 20, no. 23–24, pp. 2363–2376, 1999.

[20] T. G. Fernandes, M. M. Diogo, D. S. Clark, J. S. Dordick, and J. M. S. Cabral, "High-throughput cellular microarray platforms: applications in drug discovery, toxicology and stem cell research," *Trends Biotechnol.*, vol. 27, no. 6, pp. 342–349, 2009.

[21] M.-Y. Lee, R. A. Kumar, S. M. Sukumaran, M. G. Hogg, D. S. Clark, and J. S. Dordick, "Three-dimensional cellular microarray for high-throughput toxicology assays.," *Proc. Natl. Acad. Sci. U. S. A.*, vol. 105, no. 1, pp. 59–63, 2008.

[22] T. G. Fernandes, S. J. Kwon, M. Y. Lee, D. S. Clark, J. M. S. Cabral, and J. S. Dordick, "On-chip, cell-based microarray immunofluorescence assay for high-throughput analysis of target proteins," *Anal. Chem.*, vol. 80, no. 17, pp. 6633–6639, 2008.

[23] G. Weber and K. O. Greulich, "Manipulation of Cells, Organelles, and Genomes by Laser Microbeam and Optical Trap," in *International Review of Cytology*, 133rd ed., K. Jeon and M. Friedlander, Eds. London: Academic Press Limited, 1992, pp. 4–12.

[24] A. Faulkner and W. Shu, "Biological cell printing technologies Biological cell printing technologies," no. October, 2015.

[25] G. R. Kirkham, E. Britchford, T. Upton, J. Ware, G. M. Gibson, Y. Devaud, M. Ehrbar, M. Padgett, S. Allen, L. D. Buttery, and K. Shakesheff, "Precision Assembly of Complex Cellular Microenvironments using Holographic Optical Tweezers," *Sci. Rep.*, vol. 5, p. 8577, 2015.

[26] J. A. Barron, B. R. Ringeisen, H. Kim, B. J. Spargo, and D. B. Chrisey, "Application of laser printing to mammalian cells," *Thin Solid Films*, vol. 453, pp. 383–387, 2004.

[27] N. R. Schiele, D. T. Corr, Y. Huang, N. A. Raof, Y. Xie, and D. B. Chrisey, "Laser-based direct-write techniques for cell printing.," *Biofabrication*, vol. 2, no. 3, p. 032001, Sep. 2010.

[28] J. A. Barron, P. Wu, H. D. Ladouceur, and B. R. Ringeisen, “Biological Laser Printing: A Novel Technique for Creating Heterogeneous 3-dimensional Cell Patterns,” *Biomed. Microdevices*, vol. 6, no. 2, pp. 139–147, Jun. 2004.

[29] P. K. Wu and B. R. Ringeisen, “Development of human umbilical vein endothelial cell (HUVEC) and human umbilical vein smooth muscle cell (HUVSMC) branch/stem structures on hydrogel layers via biological laser printing (BioLP).,” *Biofabrication*, vol. 2, no. 1, p. 014111, Mar. 2010.

[30] T. Xu, J. Jin, C. Gregory, J. J. Hickman, and T. Boland, “Inkjet printing of viable mammalian cells,” *Biomaterials*, vol. 26, no. 1, pp. 93–99, 2005.

[31] R. E. Saunders, J. E. Gough, and B. Derby, “Delivery of human fibroblast cells by piezoelectric drop-on-demand inkjet printing,” *Biomaterials*, vol. 29, no. 2, pp. 193–203, 2008.

[32] P. Calvert and T. Boland, “Biopolymers and Cells,” in *Inkjet Technology for Digital Fabrication*, John Wiley & Sons, Ltd, 2012, pp. 275–305.

[33] K. Arai, S. Iwanaga, H. Toda, C. Genci, Y. Nishiyama, and M. Nakamura, “Three-dimensional inkjet biofabrication based on designed images.,” *Biofabrication*, vol. 3, no. 3, p. 034113, Sep. 2011.

[34] T. Xu, W. Zhao, J.-M. Zhu, M. Z. Albanna, J. J. Yoo, and A. Atala, “Complex heterogeneous tissue constructs containing multiple cell types prepared by inkjet printing technology,” *Biomaterials*, vol. 34, no. 1, pp. 130–139, 2013.

[35] B. Guillotin, A. Souquet, S. Catros, M. Duocastella, B. Pippenger, S. Bellance, R. Bareille, M. Rémy, L. Bordenave, J. Amédée, and F. Guillemot, “Laser assisted bioprinting of engineered tissue with high cell density and microscale organization,” *Biomaterials*, vol. 31, no. 28, pp. 7250–7256, 2010.

[36] J. Merrin, S. Leibler, and J. S. Chuang, “Printing multistrain bacterial patterns with a piezoelectric inkjet printer.,” *PLoS One*, vol. 2, no. 7, p. e663, Jan. 2007.

[37] C. Y. Chen, J. A. Barron, and B. R. Ringeisen, “Cell patterning without chemical surface modification: Cell–cell interactions between printed bovine aortic endothelial cells (BAEC) on a homogeneous cell-adherent hydrogel,” *Appl. Surf. Sci.*, vol. 252, no. 24, pp. 8641–8645, 2006.

[38] R. Singhvi, A. Kumar, G. P. Lopez, G. N. Stephanopoulos, D. I. C. Wang, G. M. Whitesides, and D. E. Ingber, “Engineering Cell Shape and Function,” pp. 696–698, 1994.

[39] M. Mrksich, L. E. Dike, J. Tien, D. E. Ingber, and G. M. Whitesides, "Using microcontact printing to pattern the attachment of mammalian cells to self-assembled monolayers of alkanethiolates on transparent films of gold and silver.," *Exp. Cell Res.*, vol. 235, no. 2, pp. 305–313, 1997.

[40] E. Delamarche, a. Bernard, H. Schmid, a. Bietsch, B. Michel, and H. Biebuyck, "Microfluidic networks for chemical patterning of substrate: Design and application to bioassays," *J. Am. Chem. Soc.*, vol. 120, no. 2, pp. 500–508, 1998.

[41] L. E. Dike, C. S. Chen, M. Mrksich, J. Tien, G. M. Whitesides, and D. E. Ingber, "Geometric control of switching between growth, apoptosis, and differentiation during angiogenesis using micropatterned substrates," *In Vitro Cell. Dev. Biol. Anim.*, vol. 35, no. 8, pp. 441–448, 1999.

[42] S. Lang, A. C. von Philipsborn, A. Bernard, F. Bonhoeffer, and M. Bastmeyer, "Growth cone response to ephrin gradients produced by microfluidic networks," *Anal. Bioanal. Chem.*, vol. 390, no. 3, pp. 809–816, 2008.

[43] P. Zorlutuna, N. E. Vrana, and A. Khademhosseini, "The expanding world of tissue engineering: the building blocks and new applications of tissue engineered constructs.," *IEEE Rev. Biomed. Eng.*, vol. 6, pp. 47–62, Jan. 2013.

[44] D. W. Hutmacher, M. Sittinger, and M. V Risbud, "Scaffold-based tissue engineering: rationale for computer-aided design and solid free-form fabrication systems," *Trends Biotechnol.*, vol. 22, no. 7, pp. 354–362, 2004.

[45] B. Duan, L. a. Hockaday, K. H. Kang, and J. T. Butcher, "3D Bioprinting of heterogeneous aortic valve conduits with alginate/gelatin hydrogels," *J. Biomed. Mater. Res. Part A*, vol. 101A, no. 5, pp. 1255–1264, 2013.

[46] S. Michael, H. Sorg, C.-T. Peck, L. Koch, A. Deiwick, B. Chichkov, P. M. Vogt, and K. Reimers, "Tissue engineered skin substitutes created by laser-assisted bioprinting form skin-like structures in the dorsal skin fold chamber in mice.," *PLoS One*, vol. 8, no. 3, p. e57741, 2013.

[47] T. Xu, K. W. Binder, M. Z. Albanna, D. Dice, W. Zhao, J. J. Yoo, and A. Atala, "Hybrid printing of mechanically and biologically improved constructs for cartilage tissue engineering applications," *Biofabrication*, vol. 5, no. 1, p. 015001, 2013.

[48] L. Bousse, "Whole cell biosensors," *Sensors Actuators B Chem.*, vol. 34, no. 1, pp. 270–275, 1996.

[49] J. A. Phillippi, E. Miller, L. Weiss, J. Huard, A. Waggoner, and P. Campbell, "Microenvironments engineered by inkjet bioprinting spatially direct adult stem cells toward muscle- and bone-like subpopulations.," *Stem Cells*, vol. 26, no. 1, pp. 127–34, Jan. 2008.

[50] P. G. Campbell and L. E. Weiss, “Tissue engineering with the aid of inkjet printers.,” *Expert Opin. Biol. Ther.*, vol. 7, no. 8, pp. 1123–7, Aug. 2007.

[51] P. Calvert, “Materials science. Printing cells.,” *Science*, vol. 318, no. 5848, pp. 208–9, Oct. 2007.

[52] P. Banerjee, D. Lenz, J. P. Robinson, J. L. Rickus, and A. K. Bhunia, “A novel and simple cell-based detection system with a collagen-encapsulated B-lymphocyte cell line as a biosensor for rapid detection of pathogens and toxins.,” *Lab. Invest.*, vol. 88, no. 2, pp. 196–206, Feb. 2008.

[53] F. Xu, T. Beyazoglu, A. E. Emre, E. Hefner, T. Manzur, U. Demirci, and S. Moon, “A high-throughput label-free cell-based biosensor (CBB) system.” Society of Photo-optical Instrumentation Engineers, 01-Apr-2010.

[54] C. R. Keese and I. Giaever, “A biosensor that monitors cell morphology with electrical fields,” *IEEE Eng. Med. Biol. Mag.*, vol. 13, no. 3, pp. 402–408, Jul. 1994.

[55] R. Chao Chang, “Biofabrication of three-dimensional liver cell-embedded tissue constructs for in vitro drug metabolism models,” Drexel, 2009.

[56] L. Zhou, G. Huang, S. Wang, J. Wu, W. G. Lee, Y. Chen, F. Xu, and T. Lu, “Advances in cell-based biosensors using three-dimensional cell-encapsulating hydrogels.,” *Biotechnol. J.*, vol. 6, no. 12, pp. 1466–76, Dec. 2011.

[57] F. Xu, J. Wu, S. Wang, N. G. Durmus, U. A. Gurkan, and U. Demirci, “Microengineering methods for cell-based microarrays and high-throughput drug-screening applications.,” *Biofabrication*, vol. 3, no. 3, p. 034101, Sep. 2011.

Chapter 2: Protein Patterning for Bacterial and Mammalian Cell Attachment

Section 2.1. Capturing Bacterial Cells with Patterned Molecules

As described in Chapter 1, both indirect and direct printing methods exist for immobilizing cells on surfaces in discreet patterns. Selection of the appropriate cell patterning approach required consideration of the intended applications to be pursued. Intentions of investigating diffusion-based bacterial communication and nutrient exchange over small distances, on the order of micrometers to millimeters, led to the development of a non-contact, microarrayer-based technique capable of indirectly patterning small populations of bacterial cells in two dimensions. The Bioforce NanoeNabler^{TM} (NeN) microarray printing system was selected due to its capabilities of patterning high-resolution depositions of solutions containing proteins using capillary action, producing spots with diameters between 1 and 10 μm under specific conditions [Fig 1]. In addition, the NeN is able to pattern arbitrary deposition geometries with sub-micrometer precision, making it an ideal platform for rapidly generating novel prints to investigate the effects of separation distance and population composition on intercellular phenomena. In light of the NeN's patterning capabilities, a technique to capture bacterial cells using immobilized antibodies was developed, optimized and qualitatively evaluated in terms of cell attachment to the antibody patterned regions.

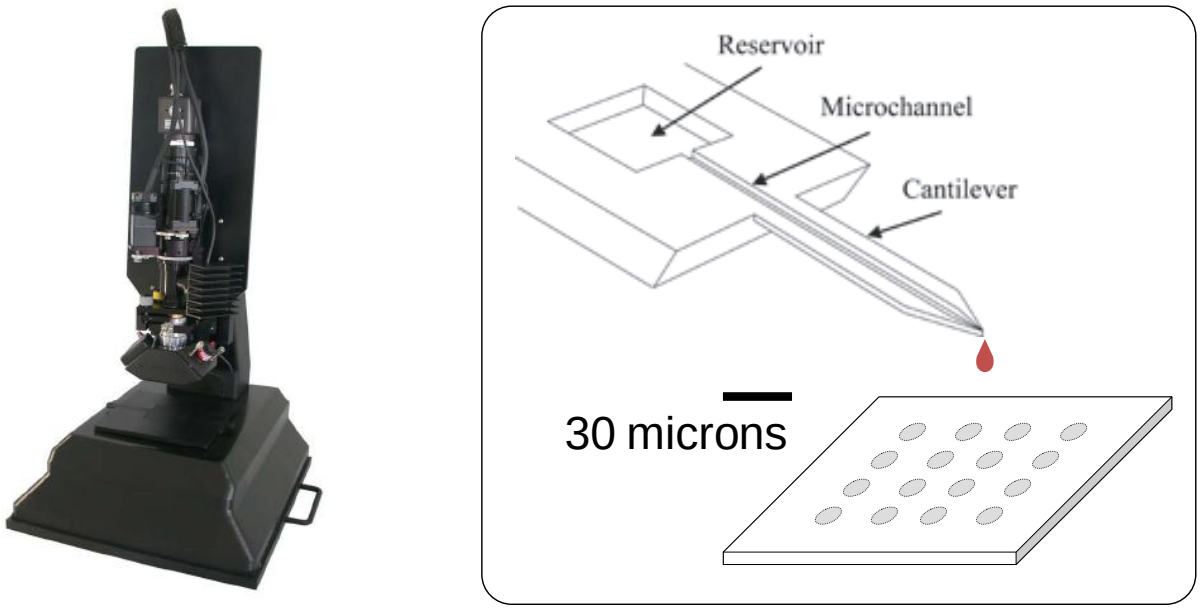

Figure 1. An image of the Bioforce NanoeNabler™ molecular printing system (Left) and an illustration of the silicon-based surface patterning tool used to deposit protein solutions onto solid surfaces (Right).

Initial experiments attempted to capture *S. typhi* pCR2.1 GFP cells engineered to express green fluorescent protein (GFP) onto rhodamine-labeled poly-L-lysine (PLL) peptides which were printed onto glass surfaces that had been functionalized with amino groups. PLL was chosen due to its polycationic structure, with the intent that it would interact and bind the negatively charged lipopolysaccharides present in the outer membrane of gram negative bacteria, such as *S. typhi*. Amino functionalization of the glass printing substrate with (3-aminopropyl)-triethoxysilane (APTES) was required in order to covalently attach the PLL to the surface via a condensation reaction between the surface-bound amino group and the free carboxylic group of the PLL. This functionalization was achieved by vapor phase deposition of APTES at 60°C for 1 hour. The printing solution consisted of rhodamine-labeled PLL mixed 1:1 with protein spotting buffer and was printed using a SPT-S-C10S surface patterning tool (SPT). The parameters of the

PLL deposition using the NeN included maintaining 70% relative humidity within the printing enclosure, with a SPT contact force threshold of 0.01 and dwell time of 0.1 seconds, resulting in spots approx. 5 μm in diameter when measured using fluorescence microscopy [Fig 2] showing rhodamine labeled PLL). After patterning of the amino surface with PLL using the NeN, the remainder of the surface was blocked using 10% bovine serum albumin (BSA) in phosphate buffered saline (PBS) to discourage cell attachment in the interstitial areas between the PLL depositions. Once surface blocking was complete, *S. typhi* cells suspended in PBS at a concentration of approx. 10^6 cfu/ml were introduced to the surface. The cells were allowed to sediment for 30 min and attach to the PLL via charge interactions between the positively charged lysine and the net negative charge of the bacterial membranes. However, after rinsing the surface three times with PBS it was observed that most of the cells were removed from the PLL deposition sites, suggesting that charge interactions were not sufficient to keep the cells immobilized to the surface (data not shown).

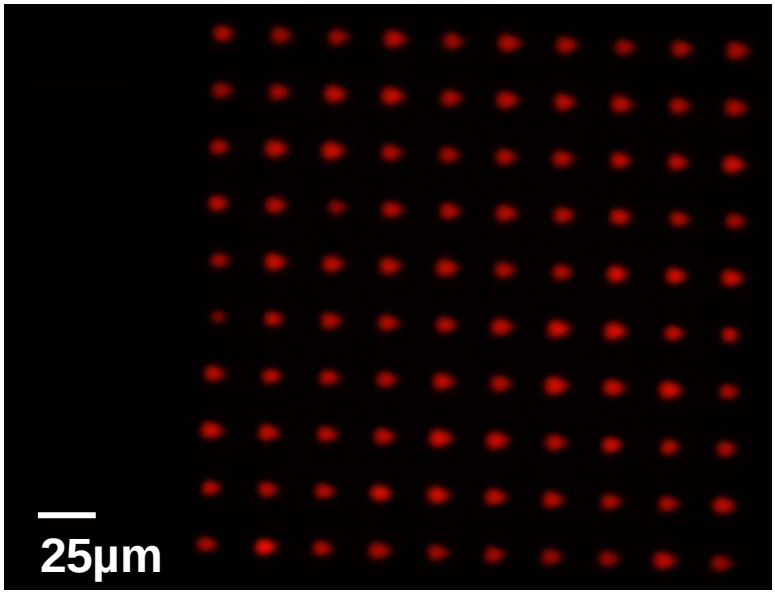

Figure 2. Fluorescence micrograph of rhodamine-labeled poly-L-lysine patterned and immobilized onto a (3-aminopropyl)-triethoxysilane functionalized glass surface using the NanoeNabler^{TM} molecular printer.

To promote strong attachment of cells to the surface, the relatively weak charge interaction of PLL was substituted for the high affinity binding of α-*Salmonella* antibodies. A tethering strategy was developed in order to attach the α-*Salmonella* antibodies to the surface in the optimum orientation to interact and bind to their epitope on the surface of *S. typhi* cells [Fig 3]. This was accomplished by using the NeN to print a solution containing 1:1 protein A (SpA) to protein spotting buffer onto the amino terminated surface, which becomes covalently attached via interaction between the amino group and the free carboxylic acid of the SpA. SpA is a protein which possesses five binding domains [1] with each having high affinity for the Fc region of certain IgG antibodies [2], allowing them to bind to the SpA in an orientation which faces the Fab region of the antibodies outward, ready to bind their epitopes. Following the patterning of SpA, the surface was blocked with solution of 1% BSA in PBS for 30 min, rinsed three times in PBS, and then incubated at room temperature with a solution containing 1% rabbit

α-salmonella IgG antibodies in PBS for 30 min, so that they may attach to the binding domains of the SpA. The surfaces were then rinsed three times in PBS and seeded with *S. typhi* cells suspended in PBS at a concentration of approx. 10^6 cfu/ml and allowed to bind for 30 min at room temperature to the immobilized antibodies. After cell seeding, the surface was again rinsed three times with PBS and imaged using fluorescence microscopy to qualitatively evaluate cell attachment.

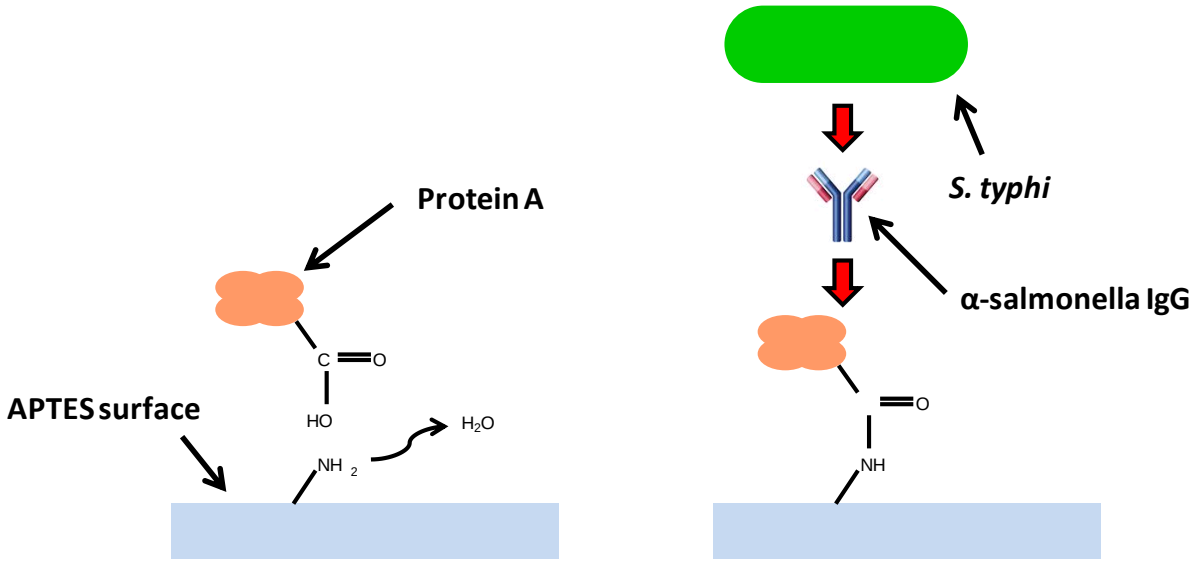

Figure 3. Illustration of the tethering strategy for indirect bacterial cell patterning using printed proteins.

Upon imaging it was observed that *S. typhi* cells remained bound to the patterned locations at high densities [Fig 3]. However, it was also observed that some cells were able to attach and remain bound to the blocked regions between the intended attachment sites, perhaps due to incomplete adsorption and binding of BSA to the APTES surface. This could be attributed to the hydrophilic nature of the APTES surface leading to only limited surface blocking, leading to partial IgG attachment to the blocked regions [3]. This indiscriminate

binding was unavoidable while using this protein patterning technique without extensive additional experimentation to optimize blocking conditions. It was also undesirable as our intended applications of investigating bacterial signaling and nutrient exchange required precise placement of the bacterial cells with all participants at known positions. At this point this indirect cell patterning approach was abandoned in favor of the development of a direct cell patterning strategy which is discussed in detail in the next chapter.

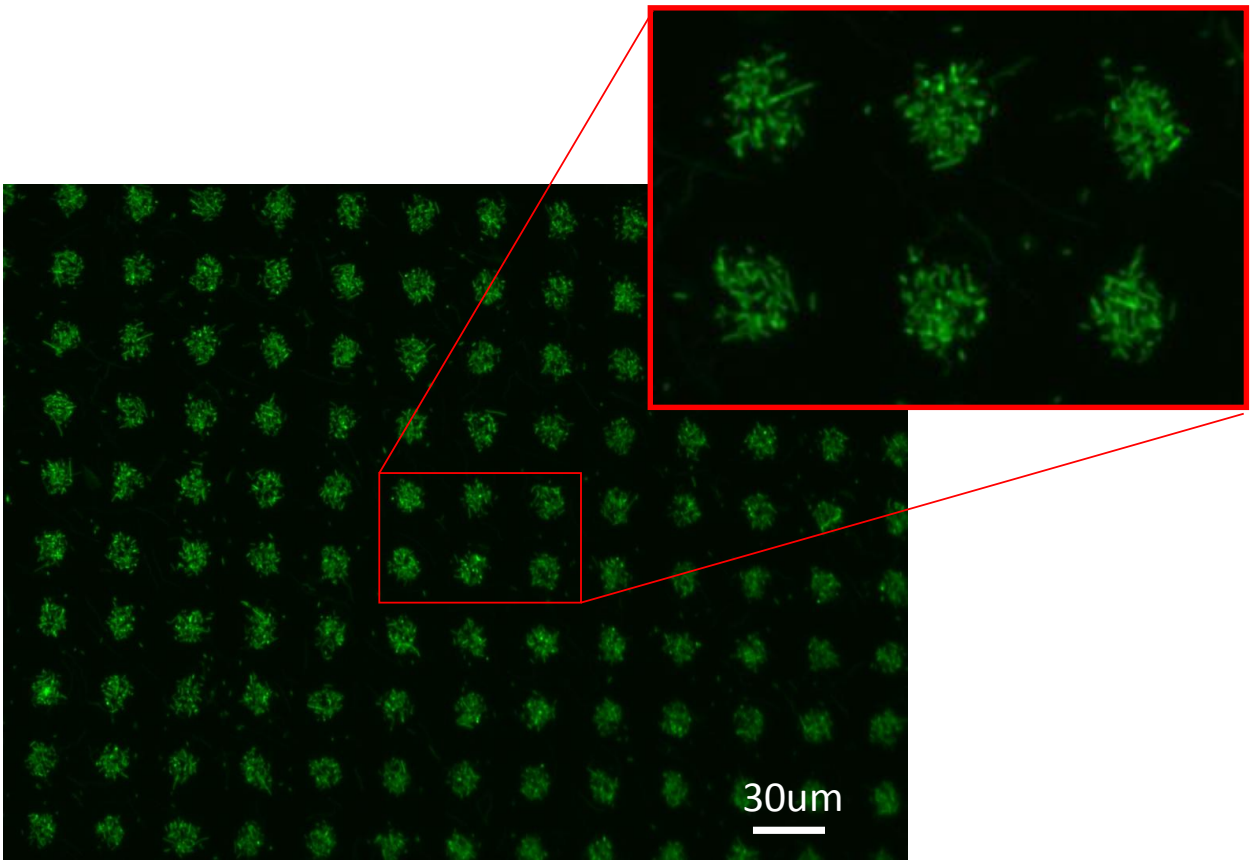

Figure 4. Fluorescence micrograph of *S. typhi* pCR2.1 GFP cells indirectly patterned onto a micropatterned surface. Image enlargement shows indiscriminate cell binding between patterned regions despite surface blocking with bovine serum albumin.

Section 2.2. Capturing Mammalian Cells with Patterned Molecules

The precise placement of cells is usually a desired outcome in regards to bioprinting applications. However, certain bioprinting applications not only do not require precise cell placement, but in fact rely upon cells settling upon non-patterned regions as well as the patterned locations. Specifically, studies designed to elucidate the mechanisms underlying certain cellular signaling events often benefit from cells interacting with surface-bound ligands, whose binding by cell surface receptors can generate an intracellular signaling cascade. The regions of the cell interacting with the portions of the surface lacking signal-inducing ligands can also be observed, and can serve as a control to identify the distinct intracellular events relating to receptor ligation [4]. This can permit the interrogation of intracellular events as they unfold, while allowing observation of individual regions within the cell in the context of signal-inducing interactions versus non-signal-inducing interactions when combined with confocal or total internal reflection fluorescence (TIRF) microscopy. By tagging specific proteins or cellular components with fluorescent markers, the investigator can determine which of these components are recruited specifically to the sites of signal-inducing ligand binding as well as the order and timing of their recruitment. Additionally, more information on the mechanisms of the signaling cascade can be gleaned by engineering the cells to express proteins with incomplete structure in order to evaluate which portions of the peptide are required for proper functioning. This can also help elucidate the specific function of the missing portion of the protein as it pertains to the signaling events and subsequent cell behavior.

The polymer lift-off method is another commonly used approach used to pattern spatially defined surfaces with specific proteins or other biomolecules to evaluate their interactions with cell surface receptors [5]. The polymer lift-off approach is less of a bioprinting

technique and more of a microfabrication technique as each surface is spatially defined using a combination of photolithography and etching. The surface, usually silicon or glass, is uniformly coated with polymer followed by coating with photoresist which is then patterned using photolithography to expose the polymer beneath. The polymer is then etched away, exposing the bare substrate below. After etching, the portions of the surface left exposed are subsequently coated using a solution containing biomolecules, followed by lift-off of the remaining polymer/photoresist to expose the remainder of the substrate for further coating. For studies involving receptor-mediated signaling, protein patterning for cell attachment via microcontact printing, polymer lift-off, microfluidic patterning, and microarray printing of signal-inducing ligands are ideal options despite the indiscriminate binding that can occur during the cell seeding step.

An example of a receptor-mediated signaling study utilizing patterned surface-bound ligands is the study performed by Wu *et al.* where lipid bilayers containing liganded lipids were defined using the polymer lift-off technique to directly observe the events that transpire at the cellular membrane upon interaction with cell surface receptors [6]. Specifically the signaling phenomenon under investigation was the antigen-mediated cross-linking of IgE to the Fcε receptor I on the surface of rat basophilic leukemia (RBL) mast cells. This was performed in order to visualize and characterize the formation of lipid rafts. By using spatially defined lipid bilayers that contain the epitope to the surface bound IgE-FcεRI complex of the RBL cells, in conjunction with fluorescently labeled cellular components, the timing and ordering of the redistribution of these components in response to ligation could be monitored. With patterned features which are smaller than the cells themselves (roughly 1μm in diameter), the investigators could simultaneously observe the portions of the cell which were interacting the ligands as well

as the regions of the cell which remained non-stimulated. This work demonstrates how surface modification for cell binding/signaling can act as a powerful tool for the analyses of receptor-mediated signaling responses, as well provide insights into their possible mechanism of function, in a way that non-spatially defined stimulation (e.g. the use of soluble antibodies) cannot. By avoiding complicating issues such as IgE-FcεRI complex internalization and providing a means with which to keep cells bound to the surface at fixed positions, surface modification provides a direct approach for investigating receptor-mediated signaling.

Section 2.3. Examination of the Role of PKC-epsilon in Phagocytosis

In light of the benefits of examining receptor-mediated signaling using spatially defined surfaces we began a collaborative research effort with Albany Medical College which focused upon the investigation of the role of protein kinase C-epsilon (PKC-ε) in macrophage phagocytosis. PKC-ε is a diacylglycerol sensitive kinase which possesses an actin-binding domain and is known to mediate the rate of phagocytosis in macrophages [7], however the exact mechanism of its role has not yet been fully characterized. Specifically, PKC-ε plays a role in -pseudopod extension, facilitating the spreading and invagination that is observed during phagocytosis [8]. PKC-ε has been implicated as an essential player in the context of a mammalian cell's physical interactions with its environment, including cell spreading, motility, cell-matrix and cell-cell interactions [9]. PKC-ε is also a known transformative oncogene [10], whose down-regulation can inhibit the metastatic phenotype in the transgenic mouse model of prostate adenocarcinoma [11].

The common structure of PKC isozymes consists of a catalytic and regulatory domain, which are connected via a flexible hinge region. The catalytic domains between PKC isoforms

are highly conserved, homologous structures which possess both an ATP binding site and substrate binding site which are critical for kinase activity [12]. The function of the hinged region is to permit the interaction between the catalytic and regulatory domains. The regulatory domain possesses a pseudosubstrate sequence that is able to bind to the active site in the catalytic domain. This intramolecular interaction causes the PKC to assume a reversible, inactive conformation. While the regulatory domain is required for the concentration of PKC-e during phagocytosis, the mechanism of concentration was unknown. Based on their pilot experiments, **it was hypothesized by our collaborator (Dr. Lennartz) that PKC-ε enters the phagosome on vesicles, which traffic from the Golgi on microtubules. Translocation on vesicles is dependent on the regulatory domain, while membrane fusion for pseudopod extension requires catalytic activity.**

Section 2.4. Development of IgG-modified Substrates for Inducement of "Frustrated Phagocytosis"

To visualize entry of PKC-e into the forming phagosome, a technique known as "frustrated phagocytosis" was employed [13]. Briefly, macrophages expressing fluorescent PKC-ε are sedimented onto IgG-coated surfaces, allowing their Fc receptors to engage the surface IgG. TIRF microscopy is used to detect the fluorescent protein as it approaches the plasma membrane. However, efforts to visualize this process were thwarted when the macrophages removed the IgG from the surface. Thus, strongly bound surface-IgG was needed to prevent internalization of the IgG-FcγR complex and surrounding membrane, as would normally occur during IgG-mediated phagocytosis. This requirement was met by using a surface-tethering strategy that culminated with matrix of (fluorescent) 3 μm IgG dots covalently

bound to a borosilicate glass substrate. This approach resulted in an optimal platform for observation of the events following IgG-FcγR ligation, while preventing IgG removal from the surface via membrane invagination and internalization. Regions of the surface that were not patterned with covalently-bound IgG were coated with covalently-bound PLL polymers, generating a polybasic surface that interacts non-specifically with cell membranes. Thus, when bone marrow derived macrophages (BMDM) interact with the surface, the IgG regions signal through the FcγR while the PLL acts as a non-signaling attachment molecule. The power of this approach is that, upon BMDM immobilization on the surface, regions of the cell that participate in receptor-mediated signaling can be observed alongside the regions of the cell which bind PLL only, providing an internal control. This tethering strategy relies entirely upon the formation of covalent bonds to attach the IgG to the surface preventing the antibodies from being removed from the surface by forces exerted by the macrophages undergoing phagocytosis.

Two other types of IgG-coated surfaces were also developed specifically for various experiments. These include IgG-coated glass cover-slips for patch-clamping experiments and IgG coated glass-bottomed PDMS wells for evaluation of whole-cell spreading and IgG-FcγR ligation across the entirety of the cell-surface interface. Glass-bottomed dishes 50 mm in diameter were used for fabrication of both IgG coated and IgG patterned glass-bottomed PDMS wells due to their compatibility with TIRF microscopy. PDMS slabs with dimensions of 28 mm x 28 mm x 3.5 mm were punched to form arrays of 4 x 5 wells 4 mm in diameter for IgG coated wells, or 2 x 2 wells 1 cm in diameter for the IgG patterned wells. Dividing a single glass-bottomed dish into multiple wells was preferable as it decreased costs associated with materials, and greatly decreased the number of cell required and reagent volumes required for individual

trials. Larger wells were required for IgG patterned surfaces so that the glass bottoms could be patterned via microcontact printing.

The tethering strategy was accomplished with aldehyde functionalization of the glass surfaces, followed by attachment of IgG antibodies using microcontact printing for patterned substrates, or incubation with a bulk IgG solution for surfaces coated completely by IgG. Briefly, all glass surfaces were initially prepared identically, beginning with a 3 minute O_2 plasma treatment to remove any surface contaminants. In the case of the surfaces partitioned with wells composed of PDMS (includes IgG coated wells and IgG printed wells), this was followed by the O_2 plasma treatment of the PDMS wells for 1 minute and 30 seconds to displace methyl-groups and promote subsequent bonding to the glass surfaces. Following plasma treatment, all surfaces were incubated at 60°C with the silane 11-(Triethoxysilyl) undecanal, which resulted in a monolayer of aldehyde groups covalently attached to the exposed glass surfaces. This incubation step also accomplishes the irreversible bonding of the PDMS wells to the glass surface in the cases of the coated glass-bottomed wells and the microcontact printed surfaces. For the aldehyde coated glass cover-slips and glass-bottomed PDMS wells, the final step required incubation with solution containing 25 μg/ml normal rabbit IgG in PBS (for coated cover-slips) or with 25 μg/ml normal rabbit IgG containing 25 ng/ml Alexa-546-labeled IgG in PBS (for coated glass-bottomed wells) for 1 hour at room temperature.

For the microcontact printed surfaces, the silane deposition and PDMS well-bonding steps were followed by the stamping/patterning of a solution containing 25 μg/ml Alexa-660-labeled IgG in PBS using a PDMS microstamp. The PDMS microstamp was fabricated using standard lithographic and etching techniques [14] to produce a master mold with arrays of 3μm diameter holes. Uncured PDMS was mixed at a 1:10 cross-linker-to-base ratio and used to fill

the master mold. The mold was then placed under vacuum for 15 minutes to remove bubbles and ensure all features of the mold were filled with PDMS. The PDMS was then cured at 60°C for 1 hour, at which point the PDMS microstamps were removed from the master, flipped face-up, and then cured for an additional 24 hours at 60°C to ensure complete cross-linking within the PDMS. Initial molding utilized a master mold fabricated from a single 5μm thick layer of SU-8 50 photoresist spun onto a 100 mm (4 in.) silicon wafer which was patterned using photolithography and developed, resulting in arrays of 3 μm holes. However, after the PDMS microstamps were demolded from the master and used for patterning, it was observed that the intended 3μm features did not result in uniform arrays of 3μm protein spots. This suggested that portions of the PDMS stamps were not demolding properly, with the pillars breaking off within the SU-8 holes. To address this, a second master was fabricated and treated with a vapor phase deposition of trichloro(1H,1H, 2H, 2H-perfluoro-octyl)silane at 60°C for 1 hour to form a non-adhesive layer to facilitate demolding of the PDMS after cross-linking.

While this approach did result in high fidelity PDMS stamps, after two uses the stamp fidelity began to degenerate, indicating that the pillars were still not demolding properly. To combat this, a new strategy was adopted for fabrication of the master. The second generation master was fabricated by using patterned Shipley 1813® photoresist, defined using standard photolithography and developing techniques [15], resulting in a 1 μm thick masking layer which was followed by reactive ion etching (RIE) of the exposed silicon substrate. Additionally, the mask was redesigned to maximize the size of the resulting arrays of patterned protein spots. By enlarging the arrays from 3 mm x 3 mm to 1 cm x 1 cm stamps could be cut from the molded PDMS which were large enough to cover nearly the entire area of the glass-bottom wells. The increased size of the patterned arrays of protein relative to the well bottom effectively maximized

the real estate available to bind cells during the cell seeding process, increasing the chances of encountering cells bound to both the printed protein and the PLL background. This new mask resulted in 5 μm deep features on the wafer substrate produced by the RIE, followed by stripping of the remaining Shipley 1813® photoresist to produce the final master. The silicon etched wafer was then treated with a vapor phase deposition of trichloro(1H,1H, 2H, 2H-perfluoro-octyl)silane at 60°C for 1 hour. Molding of the silicon etched master with PDMS resulted in high fidelity patterns, even after repeated uses.

Upon successful negative replication of the master mold using PDMS, microstamps with raised features consisting of 3μm diameter pillars were generated. The surfaces were then patterned by coating of the microstamp in fluorescently-labeled IgG and bringing the surface and stamp into contact for 30 minutes at room temp to permit protein transfer to the surface. Patterning of the aldehyde coated surfaces using the microstamps resulted in surfaces patterned with arrays of discrete 3μm dots consisting of fluorescently-labeled IgG. The micropatterned surfaces were then submerged in a solution containing 0.1 mg/ml PLL in PBS so that the interstitial sites between IgG dots would be modified with covalently bound PLL peptides. Following surface modification, all surfaces were rinsed 3X in PBS to ensure any proteins or peptides which remained adsorbed to the surfaces were removed before addition of cells.

Section 2.5. Results & Discussion of Indirect Mammalian Cell Patterning Studies

Through the use of our IgG-modified glass substrates, our collaborators at Albany Medical College were able to thoroughly examine the role of PKC-ε in macrophage phagocytosis. Using these surfaces, the Lennartz lab was able to demonstrated that PKC-ε is translocated via vesicles to the plasma membrane in response to FcγR-IgG binding. This

conclusion was based on PKC-e's col-localization with the transmembrane vesicle protein VAMP3 (vesicle-associated membrane protein 3) ([16] and failure to co-localize with Akt-PH [Fig 5], a fragment of protein kinase B that translocates from the cytosol to regions of IgG-FcR interaction [17]. Both PKC-ε-GFP and VAMP3-GFP appeared as distinct puncta, distinct from the pattern produced by Akt-PH-GFP.

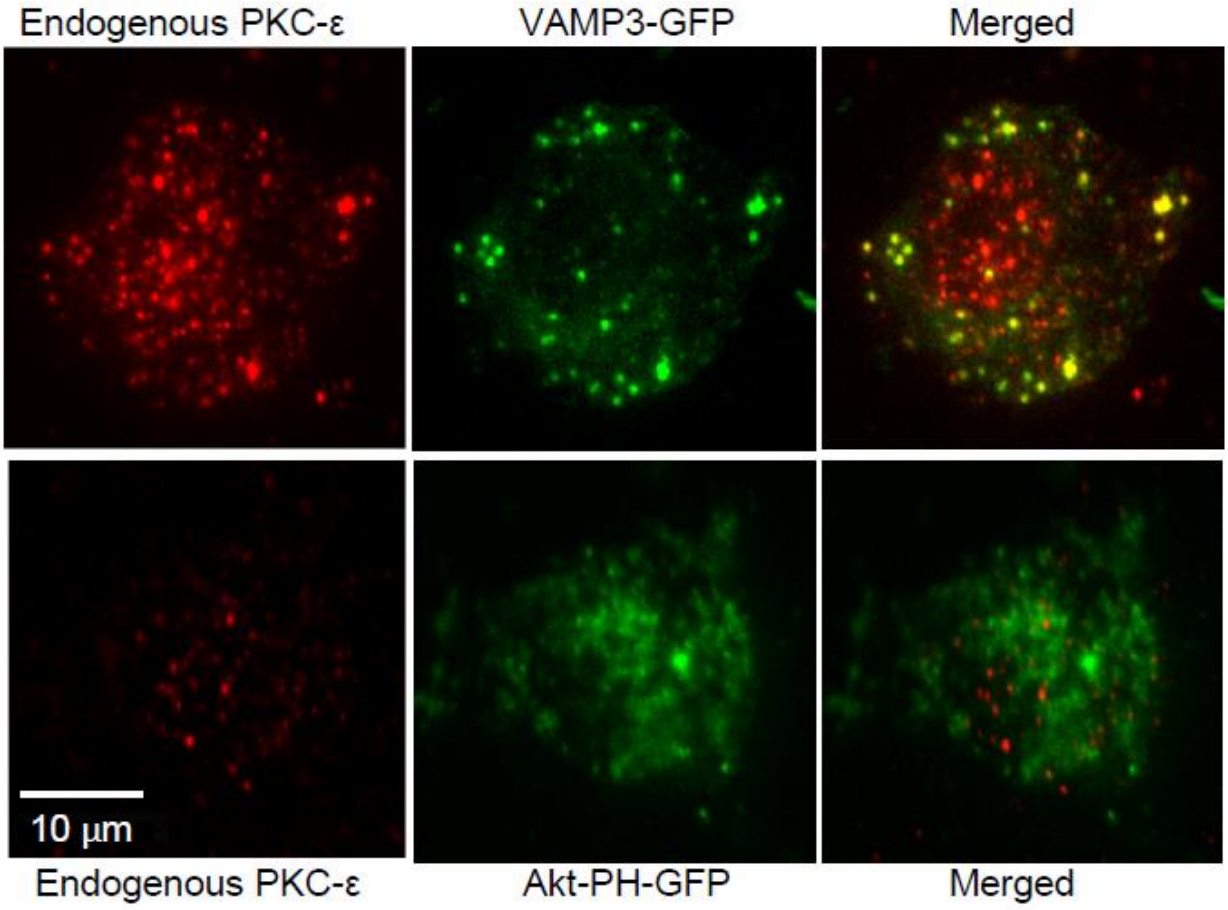

Figure 5. TIRF images demonstrating high co-localization of endogenous PKC-ε with transmembrane vesicle protein (VAMP3), but low co-localization with a cytosolic translocating protein, protein kinase B (Akt-PH-GFP). This suggests PKC-ε is translocated via vesicles to the plasma membrane during phagocytosis. Reproduced with permission from Dr. Lennartz, this work is currently under review at the Journal of Cell Biology.

Demonstration that PKC-ε is delivered only in response to IgG-FcγR ligation required the use of patterned IgG substrates with PLL deposited in the interstitial sites between IgG depositions. By using IgG dots with diameters of 3μm, BMDM that attached to the IgG dots during cell seeding would inevitably leave portions of the cell in contact with the covalently-bound IgG as well as the covalently-bound PLL background. PKC-ε-GFP puncta were found to accumulate at the portions of the cell membrane participating in IgG-FcγR ligation, and were absent from the regions in contact with PLL only [Fig 6]. Recruitment of PKC-ε-GFP vesicles to areas of IgG-FcγR ligation was observed to occur in a linear fashion, providing evidence at the PKC-ε-GFP vesicles travel to the phagosome on microtubules. Additionally, by using our IgG coated surfaces, our collaborators were able to elucidate the role of both the regulatory and catalytic domains of PKC-ε with respect to phagocytosis (results not shown). It should be noted that this is the first demonstration that a PKC can be delivered on a vesicle (the current paradigm is that PKC translocates from the cytosol to sites of receptor activation) and was accomplished because we were able to prevent the IgG from being internalized.

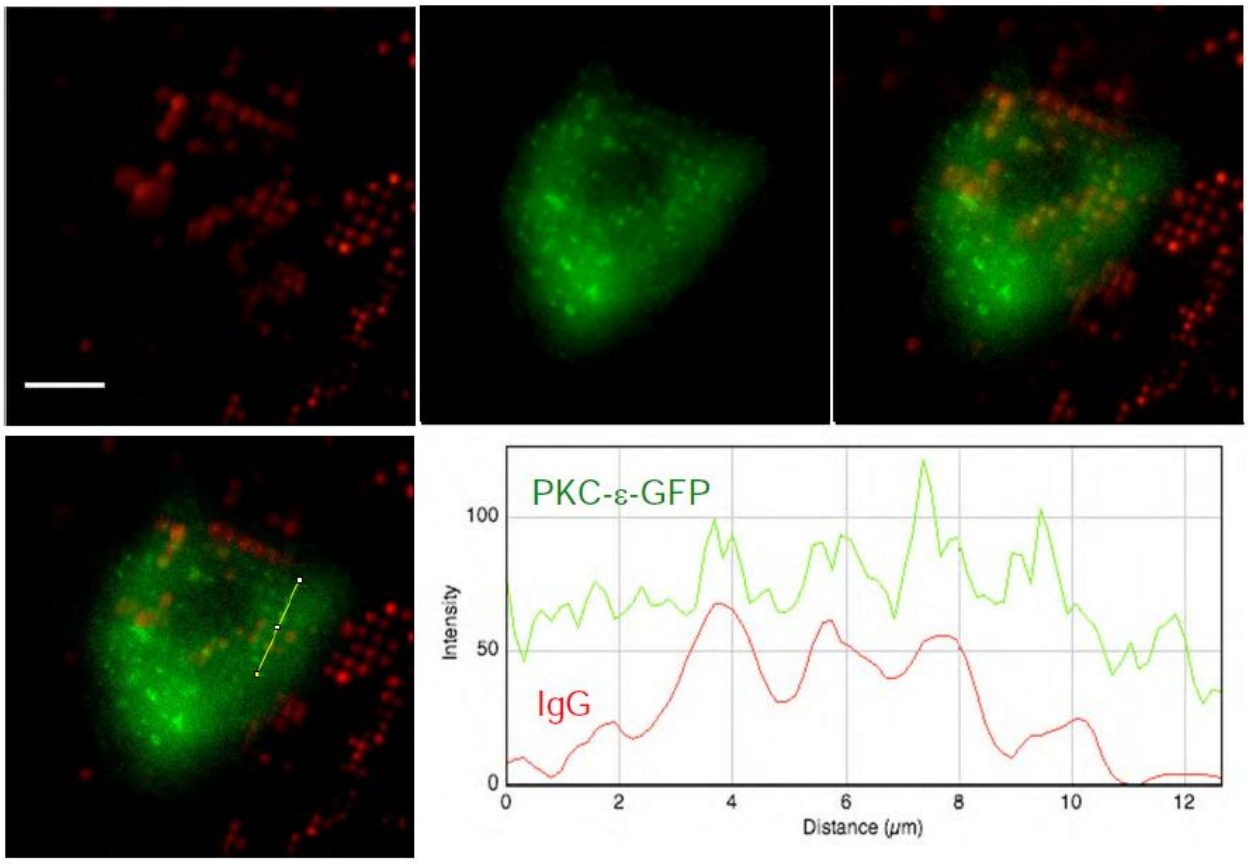

Figure 6. TIRF micrographs demonstrating that PKC-ε-GFP accumulates at sites of IgG-FcgR interaction. Images show a PKC-ε-GFP-expressing BMDM fixed 10 min after attachment to a surface patterned with microcontact printed Alexa660-IgG. The single IgG (Left) and GFP channels (Middle) with the merged image (Right) are presented. Line intensity profile along a line drawn through a row of Alexa546 IgG spots showing the correlation of peaks of GFP with IgG (Bottom). Scale bar = 10 μm. Reproduced with permission from Dr. Lennartz, this work is currently under review at the Journal of Cell Biology.

These results found by our collaborators highlight the utility of indirect cell patterning with respect to the examination of intracellular signaling phenomena and their underlying mechanisms. Without the ability to attach the macrophages to the surface directly with a covalent tethering strategy for IgG, specifically the silicon dioxide bound to the aldehyde silane, which was subsequently bound to the IgG, followed by ligation of the Fc region of IgG to the FcγR on the cell surface, detailed and time-dependent examination of frustrated phagocytosis

would not have been possible. If the IgG had simply been adsorbed to the glass substrate, the process of phagocytosis would have exerted sufficient force to remove the IgG during invagination, preventing the surface spreading associated with frustrated phagocytosis. TIRF microscopy would also not have been possible as the cell's phagocytic interaction with the surface would have been transient as macrophages are highly motile, making high-resolution imaging of the cell-substrate interface near impossible. Additionally, by utilizing patterned IgG surfaces with a PLL background, both signal-inducing attachment and non-signal-inducing attachment could be observed simultaneously. This resulted in a situation where both the experimental condition as well as the positive control scenario could be evaluated within a single cell.

Section 2.6. Materials, Reagents & Cell Culture

Bioforce NanoeNabler ™, SPT-S-C10S surface patterning tools, and protein spotting buffer (Bioforce Nanosciences, Ames, IA). Rhodamine-labeled poly-L-lysine (Nanocs, New York, NY). (3-aminopropyl)-triethoxysilane, trichloro(1H,1H, 2H, 2H-perfluoro-octyl)silane, bovine serum albumin, and protein A (Sigma-Aldrich, St. Louis, MO). 11-(Triethoxysilyl) undecanal (Gelest, Morrisville, PA). Phosphate buffered saline (National Diagnostics, Atlanta, GA). Rabbit α-*Salmonella* IgG antibodies (Thermo Fisher, Rockford, IL). 50mm Glass-bottomed dishes (Ted Pella, Redding, CA). SU-8 Photoresist (MicroChem, Westborough, MA). Shipley 1813® photoresist (Dow Chemical, Newark, DE) Polydimethylsiloxane (Dow Corning, Midland, MI). Rabbit IgG and Alexa Fluor 660 labeling kit (Life Technologies, Carlsbad, CA). *S. typhi* pCR2.1 GFP cells were cultured in tryptic soy broth (BD Diagnostic Systems, Sparks,

MD) for 24 hours at 37°C before centrifugation at 2000G and re-suspension in PBS for cell seeding onto patterned arrays.

Section 2.7. Conclusions on Protein Patterning for Indirect Cell Attachment

Protein patterning for cell attachment has many applications in the field of fundamental cell biology, exemplified by our collaborative effort outlined above, however many applications do require the precise placement of cells. In addition to issues regarding precise cell placement, these indirect, non-contact cell patterning approaches usually require many more cells than a direct cell printing process. This is due to the requirement of using cells suspended in solution to seed the surfaces during the cell attachment step of the sample preparation. Direct contact patterning processes, as well as certain non-contact techniques such as inkjet- and laser-based approaches, are able to deliver cells onto a surface discretely and with tunable cell densities. These densities can range from single cells to hundreds or thousands depending on the cell type and printing technology used. Utilization of fewer cells per individual experiment can benefit investigators greatly due to costs associated with maintaining larger or more numerous cell cultures. This benefit is even more meaningful for experiments involving primary cells isolated from patients or laboratory animals as the costs for these resources can become prohibitively high over the course of a long term study. Indirect, non-contact patterning approaches that require cell seeding are also typically limited to the patterning of a single cell type. While other cell types can be subsequently seeded onto the samples, the indiscriminant nature of their attachment can make intercellular interactions between the multiple cell types very challenging to observe due to variability in their relative positioning. While the incorporation of additional

attachment molecules can assist in capture of additional cell types, it does not guaranty that the cells will solely attach to those positions. Conversely, direct contact and non-contact patterning technologies that do not require cell seeding possess the capability of placing multiple cell types at specified proximities in either a parallel or serial manner. In order to take advantage of these benefits the focus shifted from developing multiple indirect, non-contact patterning techniques to the development of more versatile, microarrayer-based, direct contact cell printing technologies.

References Cited

[1] T. Moks, L. Abrahmsén, B. Nilsson, U. Hellman, J. Sjöquist, and M. Uhlén, "Staphylococcal protein A consists of five IgG-binding domains.," *Eur. J. Biochem.*, vol. 156, no. 3, pp. 637–643, 1986.

[2] a Forsgren and J. Sjöquist, "'Protein A' from S. aureus. I. Pseudo-immune reaction with human gamma-globulin.," *J. Immunol.*, vol. 97, pp. 822–827, 1966.

[3] Y. L. Jeyachandran, J. a. Mielczarski, E. Mielczarski, and B. Rai, "Efficiency of blocking of non-specific interaction of different proteins by BSA adsorbed on hydrophobic and hydrophilic surfaces," *J. Colloid Interface Sci.*, vol. 341, no. 1, pp. 136–142, 2010.

[4] J. J. Gooding, S. G. Parker, Y. Lu, and K. Gaus, "Molecularly engineered surfaces for cell biology: from static to dynamic surfaces.," *Langmuir*, vol. 30, no. 12, pp. 3290–302, 2014.

[5] A. J. Torres, M. Wu, D. Holowka, and B. Baird, "Nanobiotechnology and cell biology: micro- and nanofabricated surfaces to investigate receptor-mediated signaling.," *Annu. Rev. Biophys.*, vol. 37, no. November 2015, pp. 265–288, 2008.

[6] M. Wu, D. Holowka, H. G. Craighead, and B. Baird, "Visualization of plasma membrane compartmentalization with patterned lipid bilayers," *Proc. Natl. Acad. Sci. U. S. A.*, vol. 101, no. 38, pp. 13798–13803, 2004.

[7] E. C. Larsen, T. Ueyama, P. M. Brannock, Y. Shirai, N. Saito, C. Larsson, D. Loegering, P. B. Weber, and M. R. Lennartz, "A role for PKC-varepsilon in FcgammaR-mediated phagocytosis by RAW 264.7 cells," *J. Cell Biol.*, vol. 159, no. 6, pp. 939–944, 2002.

[8] T. R. Wood, R. Y. Chow, C. M. Hanes, X. Zhang, K. Kashiwagi, Y. Shirai, M. Trebak, D. J. Loegering, N. Saito, and M. R. Lennartz, "PKC-ε pseudosubstrate and catalytic activity are necessary for membrane delivery during IgG-mediated phagocytosis.," *J. Leukoc. Biol.*, vol. 94, no. 1, pp. 109–22, 2013.

[9] Y. Akita, "Protein kinase Cepsilon: multiple roles in the function of, and signaling mediated by, the cytoskeleton," *Febs J*, vol. 275, no. 16, pp. 3995–4004, 2008.

[10] M. a Gorin and Q. Pan, "Protein kinase Cε: an oncogene and emerging tumor biomarker," *Mol. Cancer*, vol. 8, no. 1, p. 9, 2009.

[11] B. Bin Hafeez, W. Zhong, J. Weichert, N. E. Dreckschmidt, M. S. Jamal, and A. K. Verma, "Genetic ablation of PKC epsilon inhibits prostate cancer development and metastasis in transgenic mouse model of prostate adenocarcinoma.," *Cancer Res.*, vol. 71, no. 6, pp. 2318–27, 2011.

[12] Z.-B. Xu, D. Chaudhary, S. Olland, S. Wolfrom, R. Czerwinski, K. Malakian, L. Lin, M. L. Stahl, D. Joseph-McCarthy, C. Benander, L. Fitz, R. Greco, W. S. Somers, and L. Mosyak, "Catalytic Domain Crystal Structure of Protein Kinase C-θ (PKCθ)," *J. Biol. Chem.*, vol. 279, no. 48, pp. 50401–50409, 2004.

[13] R. Takemura, P. E. Stenberg, D. F. Bainton, and Z. Werb, "Rapid redistribution of clathrin onto macrophage plasma membranes in response to Fc receptor-ligand interaction during frustrated phagocytosis," *J Cell Biol*, vol. 102, no. 1, pp. 55–69, 1986.

[14] A. P. Mosier, A. E. Kaloyeros, and N. C. Cady, "A novel microfluidic device for the in situ optical and mechanical analysis of bacterial biofilms," *J. Microbiol. Methods*, vol. 91, no. 1, pp. 198–204, 2012.

[15] T. Deng, H. Wu, S. T. Brittain, and G. M. Whitesides, "Prototyping of masks, masters, and stamps/molds for soft lithography using an office printer and photographic reduction," *Anal. Chem.*, vol. 72, no. 14, pp. 3176–3180, 2000.

[16] L. Bajno, X. R. Peng, A. D. Schreiber, H. P. Moore, W. S. Trimble, and S. Grinstein, "Focal exocytosis of VAMP3-containing vesicles at sites of phagosome formation," *J. Cell Biol.*, vol. 149, no. 3, pp. 697–705, 2000.

[17] M. Bohdanowicz, G. Cosío, J. M. Backer, and S. Grinstein, "Class I and class III phosphoinositide 3-kinases are required for actin polymerization that propels phagosomes," *J. Cell Biol.*, vol. 191, no. 5, pp. 999–1012, 2010.

Chapter 3: Development of Contact Cell Patterning Techniques

Section 3.1. Modification of the Nano eNabler Molecular Printing System

The Bioforce NanoeNabler ™ (NeN) is a contact-based microarray printer, designed to pattern DNA and protein solutions with silicon-based surface patterning tools (SPTs). The SPTs are designed to harness capillary action to deliver solutions containing various molecules into specified geometries onto solid surfaces. By examining the working principles of the silicon-based SPTs, we have successfully modified the NeN printing system to enable the patterning of viable cells onto a variety of solid and semi-solid surfaces. We have termed this technique "Quill Pen Lithography" (QPL). To facilitate cell printing we have developed larger, SU-8-based surface patterning tools (SU-8 SPTs) that possess the necessary dimensions to accommodate the passage of whole cells without clogging. These SPTs are fabricated solely out of SU-8 negative photoresist using standard lithographic exposure and development techniques. The process flow is such that the first SU-8 layer is spun onto the wafer and exposed to form the basal layer of the SPT, followed by a second resist layer that is exposed to form the reservoir and channel walls of the printing cantilever [Fig 1A]. These devices contain a base region that is connected to a microfluidic channel that is extended onto a 1.5 mm-long cantilever. Microfluidic channels ranged from 20-100 μm wide and 50-100 μm deep. The channels are connected to a 2 mm wide and 100 μm deep fluid reservoir. Microfluidic channels were left uncovered, or were coated with a thin (5 μm) capping layer that helps to prevent the evaporation of fluids within the channel. Schematic images of the devices are shown in [Fig 1B] with an image of a completed device shown in [Fig 1C]. Multiple cantilever variants were fabricated in order to test the effects of cantilever tip geometry, channel dimension and angle of printing approach on deposition size

and morphology [Fig 2]. Cantilevers were also fabricated with both open channels and enclosed channels. For the experiments reported here, only uncovered (open) channels were used.

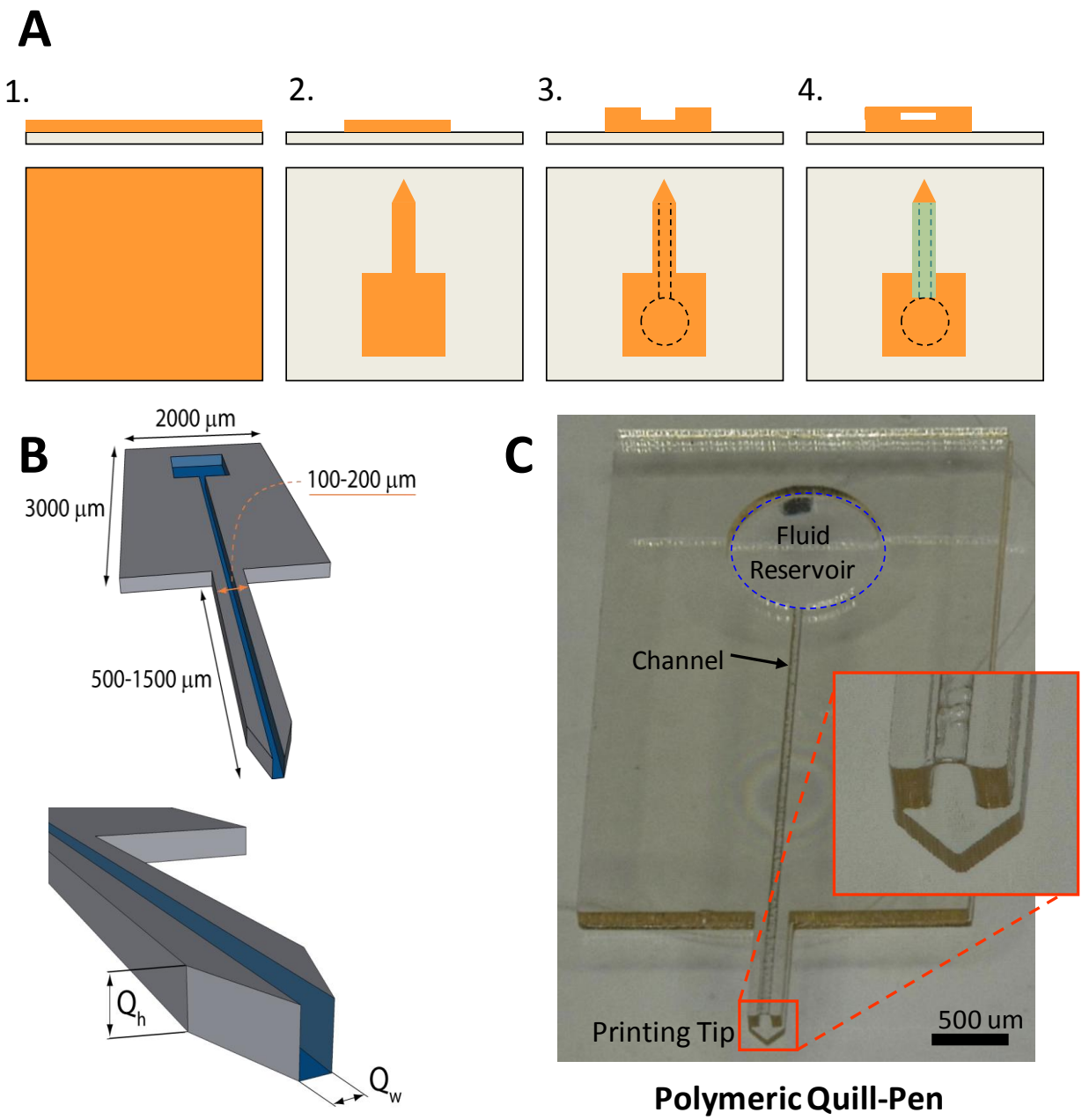

Figure 1. A. SU-8 SPT fabrication process. 1. SU-8 resist is spun onto the silicon wafer. 2. The first layer is patterned to form the device base. 3. Second layer is deposited and patterned to form the channel and reservior. 4. Optional short exposure over the channel to form a cover. **B.** Schematic illustration of the fabricated SU-8 SPTs showing the variable dimensions of the devices (Q_h= channel highet, and Q_w= channel width). **C.** Magnified photograph of a completed SU-8 SPT, shown with the optional channel covering.

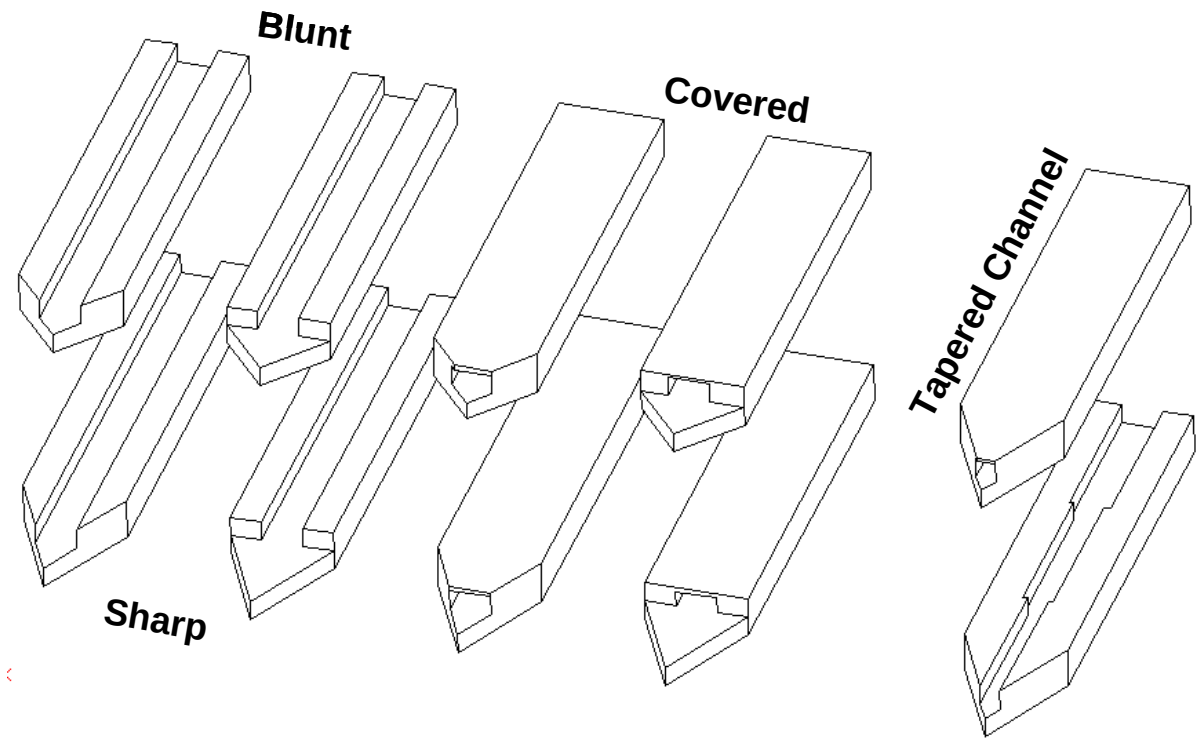

Figure 2. Illustrations showing some of the different tip geometries which were fabricated using the described process flow.

In addition to fabricating specialized cell printing SPTs, modifications were made to the NeN system to maintain printed cell viability and enhance printing versatility. The first modification made to the NeN system was to disable to the built-in humidity sensor in order to achieve a constant 85-90% relative humidity within the printing enclosure to prevent drying of the printed cells. During normal operation the humidity sensor functions to control the output of the NeN's humidifier by turning it off when the appropriate humidity has been reached, followed by reactivation once the relative humidity drops by 10%. This pause in the humidifier's functioning was found to be highly detrimental to printed mammalian cells, causing most of the cells to die rapidly by desiccation. By removing the humidity sensor the system is unable to deactivate the humidifier as it cannot sample the air within the enclosure, preventing any

unintentional interruption. The next modification was to increase the length of the SPT holder in order to facilitate printing onto the bottom of wells and plates without interfering with the motion of the SPT or printing stage. This was achieved by attaching a thin strip of nickel to the holder, thereby extending the reach of the holder while simultaneously allowing for easy manipulation of SPT's angle of approach to the surface. Due to the increased length of the SPT, it was necessary to adjust the field of view of the NeN's built in optics in order to properly focus on both the SPT and printing surface. This modification was performed by manually lowering the objective until the required focus was achieved.

Section 3.2. Nano eNabler Printing Optimization and Assessment of Viability

Several prototype SPTs were fabricated and tested iteratively under standardized conditions to determine the optimal print tip geometries for controlling spot width and eccentricity. Various printing substrates were also tested and patterned successfully, including glass, polystyrene, and agar-based gels. To initially characterize the printing performance, quill-pen devices were loaded with solutions containing 10 μm polystyrene beads, which were subsequently printed onto glass surfaces. The resulting spots were characterized for spot morphology in terms of deposition eccentricity [Fig 3] Four different tip geometries were tested; including blunt (L), intermediate (M) and sharp pointed tips (P), as well as rounded tips (R). The microfluidic channel within the quill-pen cantilevers tapered to a final width of 20, 50, or 100 μm for each tip geometry. The results of these experiments demonstrated that both tip geometry and channel width directly impact the size of the resulting printed droplets. Within a given tip geometry, devices with wider channels yielded larger spot sizes. For instance, the "M" geometry

produced 275 µm width spots with 100 µm wide channels, but approximately 125 µm width spots with both 20 and 50 µm wide channels. Furthermore, tip geometry alone affected spot size. The L, M, and R geometries produced average spot sizes of 250, 275, and 360 µm, respectively, when a 100 µm channel was used. These results have lead to the current generation of SU-8 SPTs, which are capable of producing spot diameters ranging from 400 µm to below 40 µm under specific conditions.

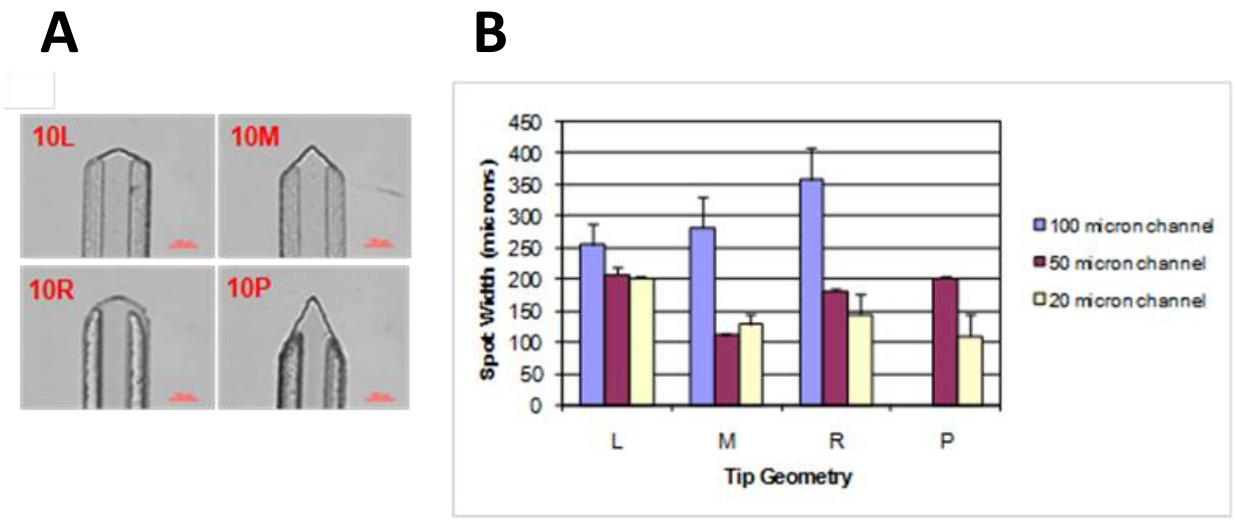

Figure 3. A. Brightfield micrographs of the various tip geometries which were fabricated and tested. Scale bars = 100 µm. **B.** Results of the tip evaluation in terms of the average spot width produced by the tip geometry. (The type 10P did not print reliably and has been excluded.)

Demonstration of our SU-8 SPT's ability to print whole cells was performed by successful patterning of both a bacterial and mammalian cell line. *E. coli* was selected as the model bacterial species and MTLn3 rat mammary tumor cells were selected as the representative mammalian cell line [Fig 4]. Successful printing of both cell types was readily achieved with the QPL technique, but maintaining their position and viability on solid surfaces proved challenging without a method of surface immobilization. Several immobilization techniques were tested,

including surface functionalization, alginate/CaCl2 cross-linking, and both standard Extracel™ and Extracel™ UV (Glycosan BioSystems, Alameda, CA). Cells suspended, printed and cross-linked in either Extracel™ formulation readily exhibited signs of viability after immobilization and incubation, while the other techniques proved insufficient at maintaining viability and pattern fidelity.

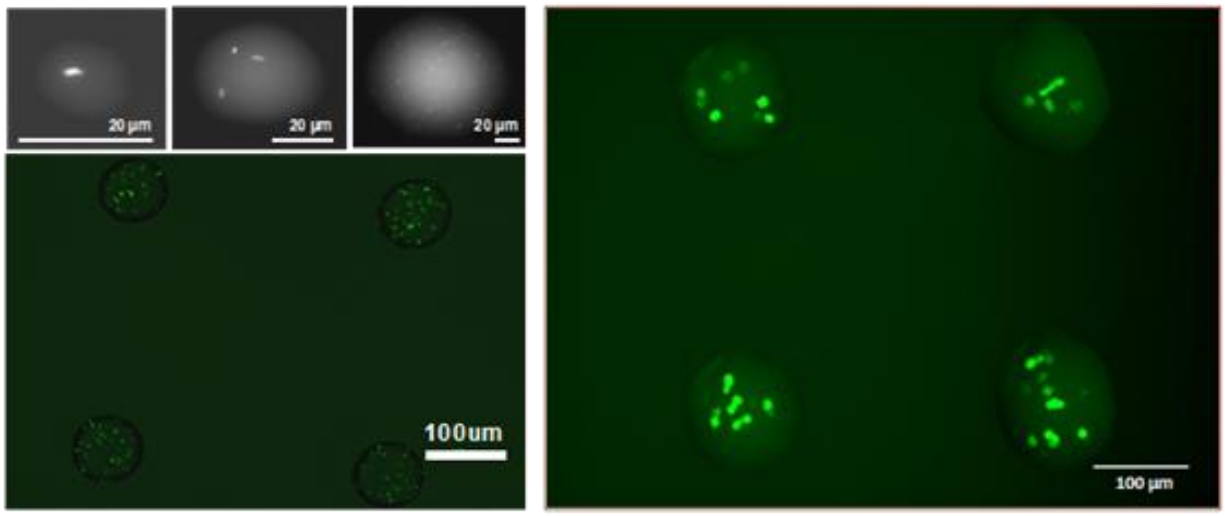

Figure 4. Demonstration of the tunability of spot size and cell density using QPL with green fluorescent protein (GFP) expressing *E. coli* (Top Left). A printed array of GFP expressing *E. coli* in phosphate buffered saline (PBS), onto a polystyrene surface (Bottom Left). A printed array of GFP expressing MTLn3 cells in PBS, onto a polystyrene surface (Right).

To test the effects of patterning with QPL on cell viability, human embryonic kidney cells (HEK 293) were printed and immobilized within a Extracel™ UV matrix and a mammalian cell viability assay was performed using calcein-AM and ethidium bromide homodimer-1 (Invitrogen, Carlsbad, CA) to fluorescently stain viable cells green and dead cells red so that counts could be taken. Viability of QPL printed HEK 293s was determined to be 91.7% ± 5.6% (±SD), while their viability after harvesting and after the bioink formulation were 93.3% ± 3.6%

and 90.7% ± 3.4% respectively, with no significant difference between any of the printing steps using an ordinary one-way ANOVA test, with a p value = 0.06984 [Fig 5]. This demonstrates that the QPL printing process had no appreciable effect on HEK 293 cell viability and that once an effective printing solution was incorporated, viable printing of numerous bacterial and mammalian cell species could be achieved. Successfully QPL patterned bacterial species included *E. coli*, *S. typhi*, *S. enterica*, *M. extorquens*, and *P. aeruginosa*, while printed mammalian cell types included rat MTLn3's breast cancer cells, mouse 3T3 embryonic fibroblasts, human HT1080 fibrosarcoma cells, mouse MH-S alveolar macrophages, human HEK 293 embryonic kidney cells, and mouse embryonic stem cells.

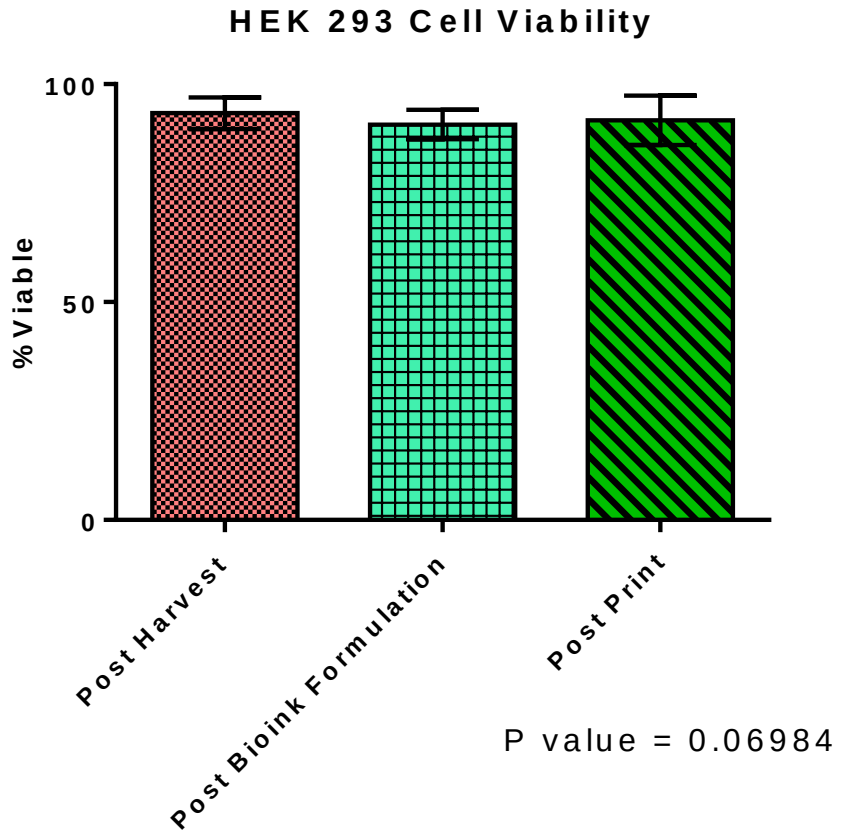

Figure 5. HEK 293 viability assay results showing percent viability at each major print process step. Results of an ordinary one-way ANOVA test demonstrated no significant difference in population means between the steps, suggesting the QPL printing process does not significantly impact cell viability.

Section 3.3. Modification of the Spotbot 3 Microarray Printing System

In light of the NeN's successful conversion from protein microarrayer to cell printer, we used our experience with the NeN to modify another contact-based microarrayer system, known as the Spotbot®3 Personal Microarrayer (SPA3) from Arrayit® Co., specifically for the rapid patterning of multiple bacterial species. The SPA3 is a pin printer with pins available which possess channels large enough (100-500 µm) to accommodate the patterning of whole cells without clogging. Similar to the NeN SPTs, the SPA3 pins function by utilizing capillary action

to deliver solutions to the printing substrate. The SPA3 is designed to pick printing solutions from one or multiple 384-well plates and it is capable of patterning up to thousands of different samples without interruption. While the NeN's strength is in its ability to pattern ad hoc geometries with precision, both manually and automatically, the SPA3's advantage rests with its ability to pattern many different solutions rapidly. As with the NeN, it was necessary to enhance the humidification system of the SPA3 in order to maintain a relative humidity of 85-90% during printing. This was accomplished by heating the water reservoir of the humidification system to enhance water vapor production. To achieve proper decontamination of the printing pins between sample loadings the standard rinsing buffer typically used in the SPA3's megasonic pin wash station was replaced with a solution of 70% ethanol. Substitution of the rinsing buffer was necessary to ensure that any cells which have managed to remain adherent to the pin after rinsing are effectively killed before moving on to the next sample for patterning. Finally, to permit the SPA3 system to pattern solutions into arbitrary patterns, as opposed to simple gridded arrays, a custom MatLab code [1] was used to produce the XML file used by the SPA3 instrument to determine which samples are patterned, where they are deposited, when the pins are washed, as well as the duration and the order each of these operations are performed.

Section 3.4. Spotbot 3 Printing Optimization and Assessment of Viability

Initial bacterial cell patterning with the SPA3 system was performed on thin (~1mm), planar substrates consisting of growth media and 2% agarose using the bacterial species *P. aeruginosa*. The printing solutions consisted solely of *P. aeruginosa* cells suspended in liquid growth media or PBS. These preliminary prints revealed that the weight of the printing pins

caused undesirable surface penetration of the gel during contact, leading to large pits at the center of the patterned bacterial microcolonies. To mitigate this surface damage two different pattering approaches were developed. The first approach involved immobilizing the bacteria to a glass surface via encapsulation within the Extracel™ UV hydrogel, followed by an overlay of growth media containing 0.7% agarose to both provide the cells with necessary nutrients and to prevent cell death from desiccation [Fig 6], while being thin enough (~1mm) to permit the diffusion of oxygen from the surface to the cells beneath. The second approach was to increase the agarose concentration of the original planar surfaces to 5%, which still resulted in minor indentation of the surface, but facilitated the patterning of cells on top of the gel rather than beneath. This allowed the cells to be grown in the same manner as in standard bulk cultures when they are spread and cultivated on agar plates, which was an important factor when printing microcolonies for the verification of the experimental bacterial growth model discussed in chapter 5.

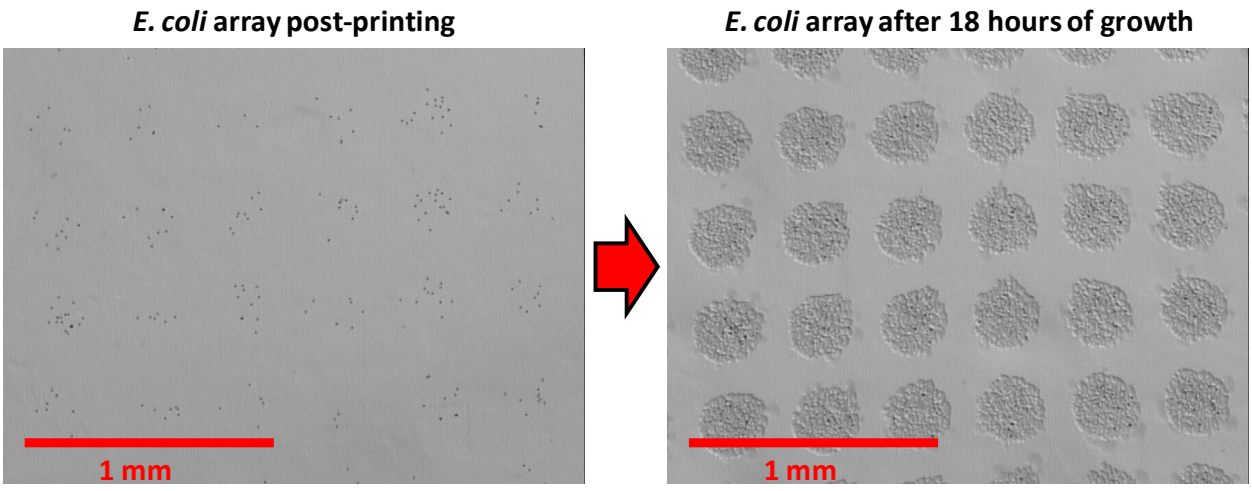

Figure 6. Micrographs of an *E. coli* array printed with the SPA3 and overlaid with growth media containing 0.7% agarose directly after printing (Left) and after 18 hours of incubation at 37°C (Right). Colonies were patterned with a solution containing latex beads (10 µm in diameter) to visualize colony locations directly after printing. Scale bars = 1 mm.

After qualitative observation of patterned bacterial cells it was noted that the number of cells within the resulting microcolonies was inconsistent and decreased over time as printing progressed. It was hypothesized that this decrease in the number of printed cells over time was caused by the sedimentation of cells out of solution within the sample wells over the course of printing. To correct for this, the viscosity of the printing solution was increased in order to keep the cells suspended uniformly throughout the solution and for longer periods of time. Agarose was selected as the viscosity enhancer of choice as it is both biocompatible and non-degradable by bacterial metabolic processes. Printing solutions containing 0.1% agarose improved spot uniformity in terms of cell number, however higher concentrations could not be reliably patterned due to clumping caused by agarose gelation, while lower concentrations did not dramatically improve printing performance.

All bacterial cells printed with the SPA3 system appeared to be viable after patterning onto compatible growth media. All printed species readily formed microcolonies after 24 hours with no apparent adverse effects. This qualitative observation in conjunction with the high viability recorded with HEK 293 cells printed using the NeN, we find it reasonable to presume most bacteria readily survive the SPA3 patterning process due to the similarity between the two printing processes. Successfully patterned bacterial species patterned with the SPA3 system include *P. aeruginos*a, *E. coli*, *S. epidermidis*, and *S. enterica*.

Section 3.5. Verification of Printed Cell Signaling

Maintenance of cell viability throughout the printing process is of utmost importance for most cell printing endeavors, however it is also highly critical to ensure that the printed cells also maintain their normal behavior and function. Our applications are centrally focused upon the examination and application of cellular signaling and sensing phenomena, therefore it was crucial to verify that cells printed with our microarrayer techniques were still capable of responding to signaling stimuli. To this end, the NeN system was used to pattern *E. coli* cells that have been transformed with components of the LasI/LasR and Rhll/RhlR quorum sensing (QS) systems, found in Pseudomonas Aeruginosa [2]. The *E. coli* pFNK 503 strain in this experiment is designed to respond to a specific acyl homoserine lactone (AHL) known as 3-oxododecanoyl-HSL (3OC12HSL) in order to up-regulate expression of the inserted reporter gene. The specific strain used for this experiment was engineered to express GFP as its reporter gene, allowing the QS response (gene expression) to be monitored with fluorescence microscopy.

To ensure that the printing process does not adversely affect the sensory ability of the *E. coli* we needed to verify that the cells could still respond to the presence of 3OC12HSL after patterning. To test this, we printed a line of 6 *E. coli* microcolonies onto solid media with a spacing of 1mm between each microcolony and allowed them to grow for 12 hours at 37°C. After incubation a solution containing exogenous 3OC12HSL was printed 1 mm from the first of the 6 printed microcolonies. Following the addition of 3OC12HSL, the surface was incubated again for 2 hours with images gathered every 30 minutes using fluorescence microscopy. The images revealed that the *E. coli* were responding to the 3OC12HSL diffusion gradient, with the earliest image showing the fluorescence response just beginning to emerge while the later images

showed the response increasing along the line of microcolonies over time [Fig 7]. This not only demonstrated the patterned cell's ability to sense the presence of the AHL, but it also verified that this technique is highly functional for diffusion-based sensing experiments.

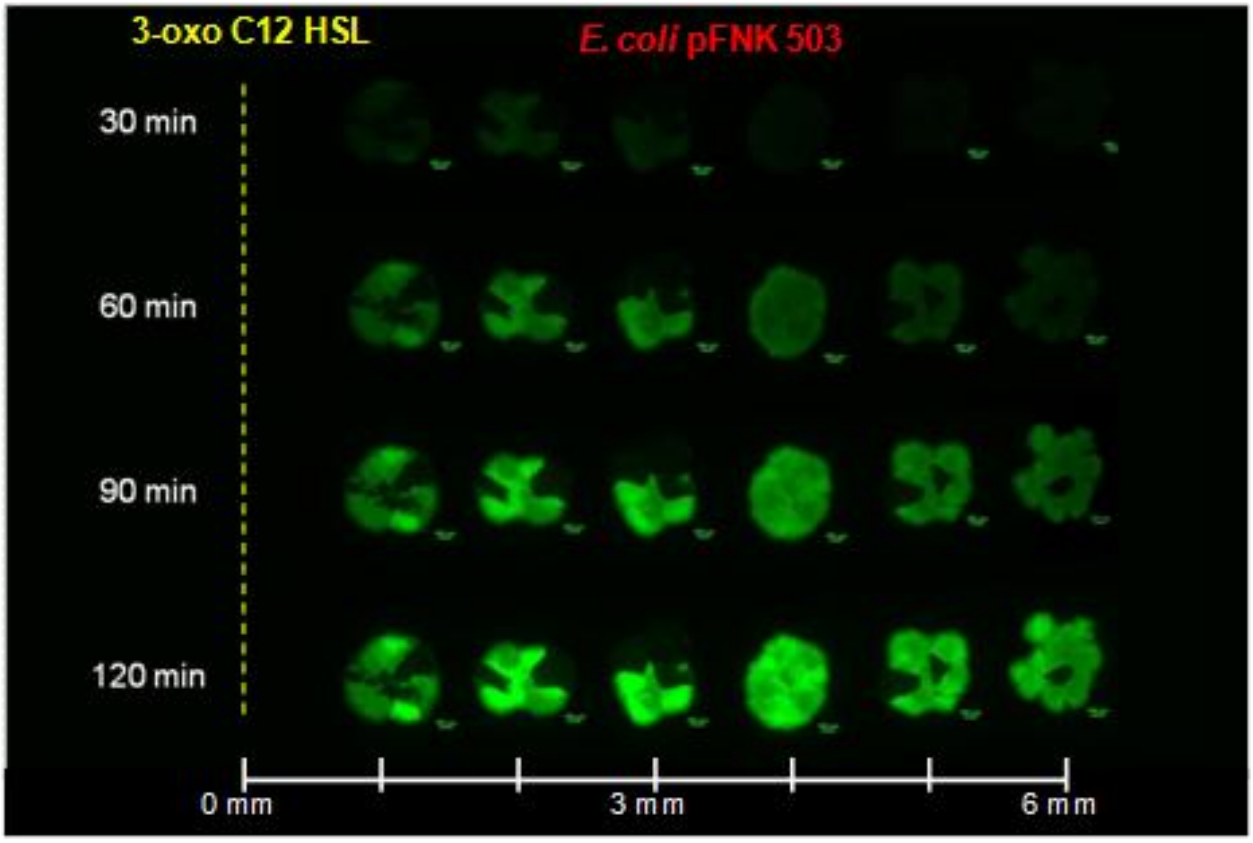

Figure 7. Fluorescent micrographs of the printed E. coli pFNK 503 colonies taken after 12 hours of growth and over the course of 2 hours after patterning of their exogenous AHL (3-oxo C12 HSL).

Next we verified that cells patterned with the SPA3 system would also maintain their ability to respond to the appropriate stimuli. This was tested by printing an artificial, obligate syntrophic consortium on to growth media which required both species to function normally for either of the two partner species to grow [3]. The two partner strains, *Salmonella enterica* serovar *Typhimurium* and an *E. coli* mutant auxotrophic for methionine, are required to exchange

nutrients in order to grow in environments lacking exogenous methionine and with lactose as the sole carbon source. To test whether the cell's ability to cross-feed was maintained after printing, these two species patterned with a separation distance of 1mm onto solid, agarose-based media which necessitated their interaction for growth the occur. The printed surfaces were incubated at 37°C for 120 hrs to provide enough time for the diffusion of necessary nutrients between the microcolonies. Brightfield images taken at 120 and 720 hours were qualitatively evaluated for the presence of growth to assess whether or not the syntrophic consortium was functioning as expected. The image comparison revealed that the species were in fact cross-feeding properly, even when printed at low cell densities, as visible growth was observed within 120 hours and continued for 30 days until the experiment was terminated [Fig 8]. While this diffusion-based cross-feeding does not involve the exchange of signaling molecules, it does possess many similarities with signaling/sensing events. Each cell type is producing a diffusible molecule which must travel to the receiving cell type, resulting in a measurable response, which in this case is the emergence of cell growth. Conservation of this "metabolite signaling" phenomena between the printed consortium partners demonstrated that the SPA3 printing process did not significantly interfere with the functioning of either species.

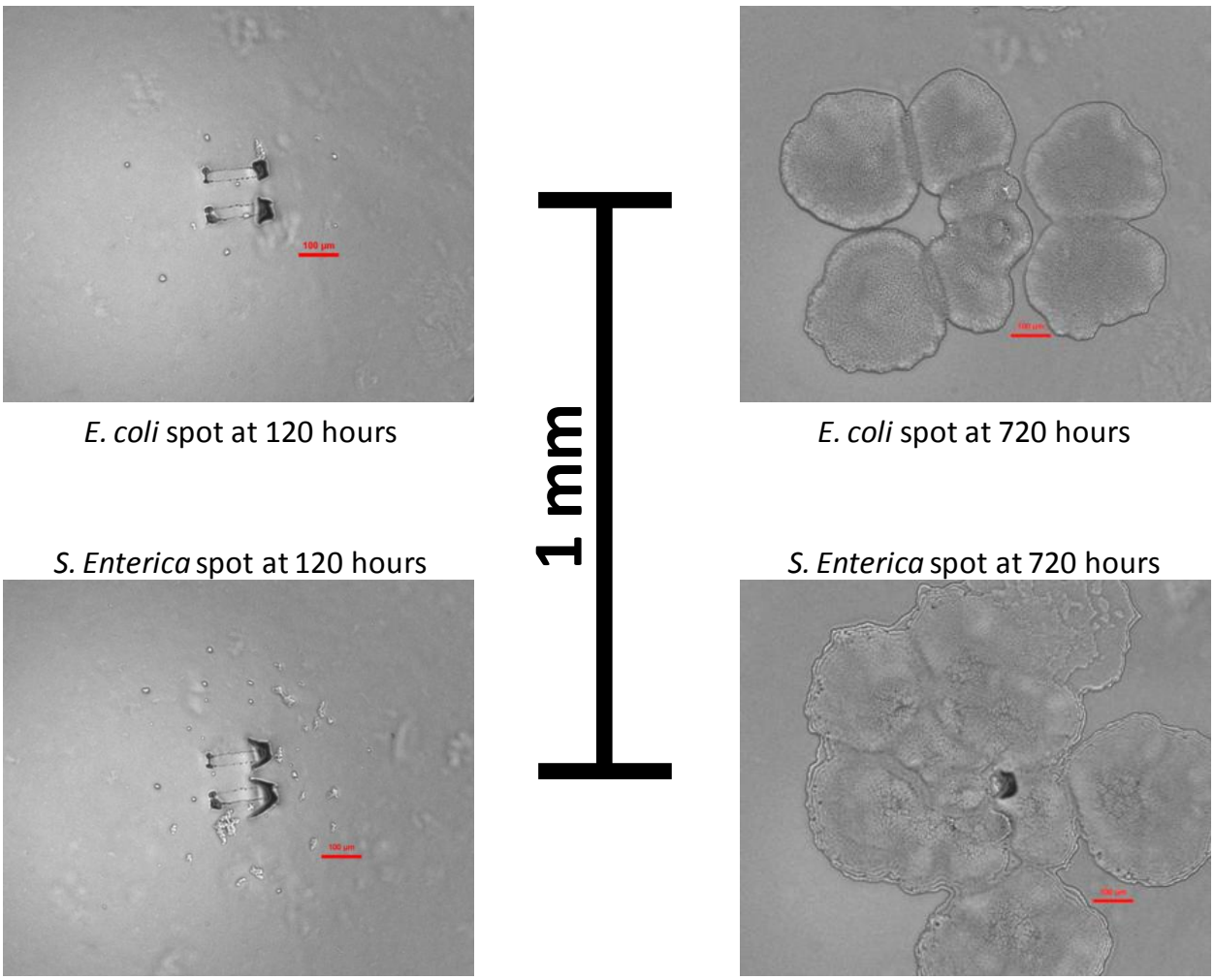

Figure 8. Brightfield micrographs taken of the cross-feeding consortium partner colonies at 120 and 720 hours separated by 1 mm distance. Scale bars = 100 μm.

References Cited

[1] M. L. Clarke, J. Y. Lee, D. V. Samarov, D. W. Allen, M. Litorja, R. Nossal, and J. Hwang, "Designing microarray phantoms for hyperspectral imaging validation," *Biomed. Opt. Express*, vol. 3, no. 6, p. 1291, 2012.

[2] K. Brenner, D. K. Karig, R. Weiss, and F. H. Arnold, "Engineered bidirectional communication mediates a consensus in a microbial biofilm consortium.," *Proc. Natl. Acad. Sci. U. S. A.*, vol. 104, no. 44, pp. 17300–4, Oct. 2007.

[3] W. Harcombe, "Novel Cooperation Experimentally Evolved Between Species," *Evolution (N. Y).*, vol. 64, no. 7, pp. 2166–2172, 2010.

Chapter 4: Direct Cell Patterning for the Development of a Reactive Oxygen Species Biosensor

(This work was performed in collaboration with Biotime Inc. and was published in the peer-reviewed, open-access journal "Biosensors" in 2014. Sections involving hydrogel formulation, characterization and evaluation with ADSCs were performed by Nate J. Doty of Biotime Inc.)

Section 4.1. Bioprinting for Biosensor Fabrication

Along with the tissue engineering applications discussed in Section 1.4, there are other, less explored, applications for bioprinting which require the precise positioning of cells and materials, including high-throughput drug screening platforms and fabrication of live-cell-based biosensors. By utilizing bioprinting to deposit microarrays of cells, drugs, toxins, or other analytes, rather than using bulk cell cultures, these screening and sensing platforms can be effectively miniaturized to the point where the necessary volumes of these materials are substantially less than what would be required to elicit a response from a bulk culture [1].

In addition to saving on material costs for reagents, patterning cells into arrays would allow for simple observation and tracking of individual cells throughout the trials, rather than attempting to deconvolute an individual cell's response from a larger population. Standard bulk cultures allow little to no spatial control of cell or signaling factor distribution, which can cause a situation where local signal strength and individual cell response cannot be readily correlated. In order to design an effective platform for the study of cell signaling and sensing phenomena, variables such as cell position, cell density, signal concentration and signal gradient formation should be well controlled. It is this same spatial control over cell and biomolecule deposition that makes bioprinting attractive to tissue engineers [2]. Signal or analyte gradients can be

established by patterning cells and bio-active molecules in specific geometries upon a planar surface that facilitates diffusion, resulting in a simplified, yet versatile platform to monitor the activity of the exposed cells. The use of bioprinting and real time monitoring of cellular physiology could also elucidate the mechanism of action of the drug, toxin or signal within the cells, if the proper measures are taken to monitor the resulting intracellular events upon exposure.

Bioprinting can directly facilitate the fabrication of cell-based biosensors. Biosensors are devices used for the detection of specific analytes or signals and are composed by 3 main components, the sensing element, the transducing element, and the reading element [3]. The purpose of the sensing element is to detect the presence and concentration of the analyte of interest, for example the use of an immobilized enzyme as a sensing element for the detection of its specific substrate molecule. The transducer is then responsible for translating the detection of the analyte performed by the sensing element into a signal which then can be interpreted by the reading element. The reading element is then needed to quantify the signal provided by the transducer in order to determine the concentration of analyte present within the system. An example of this is the conversion of the biochemical signal to an electronic one using a amperometric or potentiometric transducer which can then be detected using an ammeter or voltmeter as the reading element, respectively. Biosensors can utilize various biological materials as their sensing elements, including antibodies, oligonucleotides, and even live cells.

Cell-based biosensors have exceptional promise for applications in cytotoxicity screening due to their ability to sense the presence of toxins or stressors in the environment, while also demonstrating the bioavailability and cytotoxic effects of the toxins present [4]–[8]. Cell-based biosensors have the potential to give researchers quantitative data on the

concentrations of available toxicant within the cellular environment as well as the deleterious effects the toxicant may have on the cell's physiology [9]. An example of a eukaryotic cell-based sensor which has been used to detect the presence of toxic analytes is the cardiomyocyte-based sensor developed by Wang *et al.* to detect the presence and concentration of the marine toxins saxitoxin (STX) and brevetoxin (PbTX-2) [10]. This sensor utilizes cardiomyocyte cells coupled to electrodes in order to monitor the transmembrane potential of the cells at both the resting state and after exposure to marine toxins. Both STX and PbTX-2 will affect the cells Na+ channels, which in turn will affect the cell's transmembrane potential. In this way the effects of STX and PbTX-2 can be measured in order to detect and quantify the presence of either toxin, as well as discriminate between the two. An example of a bacterial cell-based biosensor is the *E. coli*-based sensor developed by Qureshi *et al.* for the purpose of examining the potential toxicity of various sized Fe_3O_4 nanoparticles (NPs) [11]. By immobilizing *E. coli* cells onto the surface of gold electrodes, capacitance measurements could be taken in order to determine if the bacterial cell membranes were compromised due to NP interactions. This sensor was able to detect the presence of NP exposure as well as quantify the effects of NPs of various sizes and concentrations on the integrity of the bacterial cell membranes. This represents a versatile and non-invasive method for the determination of NP toxicity in bacteria, which could provide insights as to how these particles could affect higher organisms.

Section 4.2. Role of Reactive Oxygen Species in Cell Physiology

Reactive oxygen species (ROS) is a term used to classify reactive oxygen ions, which can cause irreparable damage to cells and their processes by reacting with the cellular DNA, proteins

and other biomolecules, altering their structure, and interfering with their normal functions. While the redox equilibrium within cells is critical in maintaining homeostasis, the presence of ROS can alter the redox potential within the cell, causing normal cellular processes to break down, eventually leading to apoptosis. ROS are produced during normal cellular metabolic processes, generally within organelles such as mitochondria, but are typically deactivated through interactions with enzymes such as catalases. These interactions lead to the conversion of the ROS into harmless O_2 and H_2O. Unfortunately, these enzymes are not completely effective, and some ROS damage to cellular DNA, lipids, and proteins does occur.

ROS are critically important, but not incredibly well-understood molecules in biological systems. All ROS molecules contain oxygen in a more reactive form than its more common, relatively inert, O_2 state. These molecules, such as peroxide (O_2^{2-}) and superoxide (O^{2-}), are normal byproducts of healthy cell metabolism and have important roles in intracellular signaling pathways such as the activation of NFκB/rel family transcription factors [12] and regulating the cell's redox equilibrium [13]. But ROS can become detrimental to cells if their concentrations increase beyond homeostatic levels due to environmental stresses, such as short-wave UV exposure, by reacting with proteins, lipids, DNA and other biomolecules and altering or inhibiting their proper functioning. It is commonly thought that ROS are directly responsible for many health issues in humans, including the phenomenon of aging [14]. Therefore, understanding the mechanisms of these molecules in both their signaling and toxicological roles are of great importance, not just for fundamental biological research, but for the possible treatment and inhibition of the aging process and its associated, degenerative diseases.

Section 4.3. Techniques for ROS Detection and Evaluation

Since the presence of ROS within the cell are known to contribute significantly to the redox equilibrium of the cytoplasm [13], it would stand to reason that monitoring the cell's redox potential would allow investigators to garner a better understanding of their roles as signaling molecules and toxins. However, this is often accomplished by monitoring the concentration ratios of specific redox molecules such as the glutathione/glutathione-disulfide [15] or the reduced/oxidized thioredoxin ratios [16]. Unfortunately, these assays (often involving selective chromatography or mass spectrometry) are usually highly destructive and inherently inaccurate as the reduced and oxidized species must be removed from the cells, separated and preserved in order to achieve accurate measurements of these molecules, which is often an issue as most often these tests are performed in an oxidizing environment (i.e. air) [17]. Since these methods of evaluation require the destruction of the organism, the spatial and temporal resolution of these assays are inherently extremely limited [18].

Another method of measuring ROS concentrations and activity utilizes fluorescent probes in order to monitor the presence and activity of ROS both in vitro and in vivo. Fluorescent probes such as 9-[2-(3-carboxy-9,10-dimethyl)anthryl]-6-hydroxy-3H-xanthen-3-1 (DMAX) have been shown to have high sensitivity and selectivity toward singlet oxygen ($^1O_2$), while remaining unresponsive toward other reactive species such as H_2O_2, O^{2-}., and NO [19]. Probes such as these are appealing as they may allow access to the observation and quantification of cellular ROS in a way that mass spectrometry and chromatography cannot, by providing a way to monitor ROS activity spatially and temporarily. While these types of probe assays are promising for ROS sensing, they do suffer from at least one major drawback, they must be

administered to the cells exogenously as they cannot be synthesized by the cells themselves due to their complex chemistries and must be synthesized in a laboratory setting.

In response to this limitation of the more common fluorescence probes, probes such as redox sensitive green fluorescent protein (roGFP) have been developed in order to permit for the genetic encoding of these probes within cells so that they may be expressed similarly to the widely utilized, non-redox sensitive, Aequorea victoria GFP. These roGFP probes may not possess the high selectivity of the laboratory synthesized probes, however they do allow for the localization of these probes into specific sites of ROS activity interest such as the cytoplasm or mitochondria [20]. These indictors possess specific mutations which expose 2 surface cysteines at positions 147 and 204 on the peptide, which can participate in disulfide bonds under oxidizing conditions. When these disulfides are formed the conformation of the roGFP molecule is altered in such a way that it shifts its excitation peak from 405 nm (oxidized) to 488 nm (reduced), the ratio of which can indicate the extent of oxidation while canceling out the amount of indicator and the absolute optical sensitivity. An example of the utilization of these probes has demonstrated the real-time visualization of the redox response of the probes under physiological redox changes during superoxide bursts from macrophage cells in response to pathogens [18]. **We hypothesize that roGFP producing cells can be readily incorporated into a live-cell-based, optical biosensor for the detection of ROS in liquid environments using our QPL bioprinting technique.**

Section 4.4. Development of a Live-Cell Based ROS Biosensor

4.4.1. Hydrogel Matrix Formulation and Printing Matrix Preparation

Thiolated hyaluronan (Glycosil®, 1% w/v), thiolated porcine gelatin (Gelin-S®, 1% w/v) and polyethylene glycol diacrylate (PEGDA) MW 3400 (Extralink®) were obtained from BioTime Inc. (Alameda, CA, USA). Irgacure® 2959 was from BASF (Southfield, MI, USA). Polyethylene glycol (PEG) norbornene was derived from 4-arm PEG (MW 20,000) and was synthesized as previously described [21]. To form gels in 24-well tissue culture plates, all components (Glycosil, Gelin-S, and 1% w/v PEG norbornene) were reconstituted in 0.05% w/v Irgacure 2959 and mixed in a 2:2:1 volumetric ratio. The final concentrations (w/v) of Glycosil, Gelin-S, PEG norbornene, and Irgacure 2959 are 0.4%, 0.4%, 0.2%, and 0.05%, respectively. UV cross-linking was performed using a handheld compact UV lamp (365 nm, 4 W, 115 V, 0.16 A, Cat no. UVL-21; UVP, Upland, CA, USA). Oscillatory shear measurements of the elastic modulus, G′, and the viscous modulus, G″, were obtained at room temperature using a Bohlin CVO rheometer (Malvern Instruments, Worcestershire, UK). Cells at the appropriate concentrations were mixed with the cross-linker in a 1:9 volumetric ratio and subsequently mixed with Glycosil and Gelin-S solutions and gelled as described above. For Bioprinting, the hydrogel mixture (HyStem-C/PEGnor) was prepared as described above but with PEG-norbornene at 5% w/v initial concentration (1% w/v final concentration). The HyStem-C/PEGnor solution was then mixed with the cell-suspension at a 3:1 ratio to produce the final printing solution.

4.4.2. Cell Culture

For initial hydrogel biocompatibility experiments, adipose derived stem cells (ADSCs) were used. ADSCs were isolated from human tumescent lipoaspiration samples as previously described [22] [38]. Briefly, stromal vascular fraction (SVF) was prepared from human lipoaspirate. The adherent cellular fraction (adipose derived stem cells) was isolated by incubating the SVF incubated overnight at 37 °C/5% CO2 in control medium (Dulbecco's modified Eagle's Medium (DMEM), 10% fetal bovine serum (FBS), 1% antibiotic/antimycotic solution) on plastic tissue culture plates. Following incubation, the plates were washed well with 1× PBS. The remaining adherent cell population (adipose derived stem cells (ADSCs)) were cultured at 37 °C/5% CO2 in non-inductive control medium at sub-confluent levels.

For cell printing experiments, a variety of cell types were used, including fibroblasts, macrophages, and stem cells. NIH-3T3 murine fibroblasts were grown in DMEM medium containing 10% fetal bovine serum (FBS), 2 mM L-glutamine, and 1% penicillin streptomycin. Murine alveolar macrophages (MHS) cells were transfected with the pEGFP-N1 plasmid to allow constitutive expression of roGFP-R12 within the cytosol, while their media was supplemented with G418 antibiotic to maintain the plasmid. The resultant MHS-roGFP-R12 cells were grown in RPMI-1640 medium (Gibco®) supplemented with 10% FBS, 0.05 mM 2-mercaptoethanol, and 1 mg/mL G418 antibiotic. CCE mouse embryonic stem cells (mESCs) (StemCell Technologies, Vancouver, Canada) were grown on gelatin-coated tissue culture flasks in a maintenance medium consisting of Dulbecco's Modified Eagle's Medium (DMEM with 4.5 g/L D-glucose), supplemented with 15% (v/v) fetal bovine serum (FBS, StemCell Technology), 100 U/mL penicillin, 100 µg/mL streptomycin, 0.1 mM non-essential amino acids, 10 ng/mL murine recombinant leukemia inhibitory factor (StemCell Technology), 0.1 mM

monothioglycerol, 2 mM L-glutamine, and 1 mM sodium pyruvate (Sigma-Aldrich) [23]–[25]. All cell types were incubated overnight at 37 °C/5% CO2. Cells were harvested at 70–80% confluency, centrifuged at 3,000×g for 5 min, and re-suspended in fresh growth media via vortexing to generate a suspension of single cells.

4.4.3. Cell Printing

Qualitative confirmation of our ability to pattern viable eukaryotic cells was performed by subsequent patterning, incubation and observation of printed NIH-3T3 fibroblasts. The SU-8 SPTs selected for this experiment possessed channel widths of 100 µm and were treated with UV/ozone for 30 min to enhance the hydrophilic nature of the printing channel. After treatment, the SU-8 SPT was loaded with 2 µL of the cell/hydrogel mixture containing NIH-3T3 cells and used to pattern a glass cover-slip with a 5 × 5 array consisting of columns and rows with 500 µm spacing. After the printing process, cell-patterned cover-slips were sealed in a dish and exposed to long-wave, 365 nm UV lamp for 2 min to cross-link the HyStem-C/PEGnor hydrogel and immobilize the patterned cells. The cover-slip was then submerged in fresh media and incubated at 37 °C/5% CO2 until imaging was performed. Media was replaced every 24 h to maintain cell health. Bright-field imaging was performed at 18, 32, 54, 78, 100, and 194 h after patterning in order to monitor cell proliferation.

4.4.4. Examination of 3D Growth in Cell Deposits

Mouse embryonic stem cells (mESCs) were patterned and fluorescently stained in order to visualize their growth within the three dimensional (3D) microenvironment of the cross-linked droplet. The Invitrogen LIVE/DEAD® Viability/Cytotoxicity kit (calcein AM and ethidium homodimer-1) for mammalian cells was used for cell staining (Carlsbad, CA, USA). These stains were selected to both visualize cells during confocal microscopy, as well as qualitatively assess the viability of the patterned mESCs. The mESCs were suspended in HyStem-C/PEGnor and printed using UV/ozone treated SU-8 SPTs onto the bottom of a glass bottom dish (WillCo Wells B.V., Amsterdam, NL, USA) in a 5 × 5 array (500 μm spacings). The patterned dish was then sealed and exposed to UV light for 2 min, to cross-link the HyStem-C/PEGnor hydrogel and immobilize the patterned cells. The cell array was then submerged in fresh media and incubated for 72 h at 37 °C/5% CO2, with media being refreshed every 24 h. At hour 72 confocal laser scanning microscopy (Leica SP-5, Leica Microsystems) was performed to gather three-dimensional information on the cell growth occurring within the printed spots.

4.4.5. Development of a Living ROS Sensor

MHS-roGFP-R12 was developed essentially as described by Melillo et al. [26]. MHS-roGFP-R12 cell-laden hydrogel mixture was loaded into UV/ozone treated SU-8 SPTs and deposited in a 5 × 5 array (500 μm spacings) onto the bottom of a glass bottom dish (WillCo Wells B.V.). The patterned dish was then sealed and UV-cross-linked for 2 min to immobilize cell deposits. After exposure, the dish was opened and the cell array was rinsed three times with 1× HBSS buffer (Gibco®), after which fresh media was added to the dish, submerging the

printed array. The added media lacked any FBS to prevent neutralization of ROS in solution during the detection trials. Following addition of media, the dish was mounted on a confocal laser scanning microscope (Leica SP5, Leica Microsystems) and the cell array was imaged by fixing the emission wavelength at 515 nm while the excitation wavelength was toggled between 405 and 488 nm, to quantify oxidization and reduction fluorescence shifts, respectively. After base-line images were gathered at 1 min intervals for 5 min, the cells were exposed to 500 µM of hydrogen peroxide and imaged at 1 min intervals for a period of 8 min. Cells were then exposed to 10 mM of Dithiothreitol (DTT) in order to neutralize oxidizing activity and return cellular roGFP to a fully reduced state, followed by imaging at 1 min intervals for 4 min. Results gathered from individual cells were quantified using Leica LAS image processing software and plotted to determine if shifts in roGFP excitation would directly correspond to the addition of oxidizers and reducers to the environment.

4.5. Results

4.5.1. Hydrogel Matrix Formulation and Optimization

Initial bioprinting experiments with HyStem®-C showed that we did not have the requisite temporal control of gelation for bioprinting on glass cover-slips using the modified SPT in the Nano eNabler device. More specifically, HyStem-C gelled too slowly after spotting. This constraint required close attention to maintenance of chamber humidity; in addition, spotting experiments were slowed since we were required to wait for gelation before adding media. Another limitation was the hydrogel's spontaneous cross-linking. Since cross-linking typically

occurs via the Michael Addition reaction between the hydrogel thiols and the PEGDA acrylates, the reaction gels in 10–20 min and can potentially clog the SPT channels mid-experiment. The solution was to substitute the polyethylene glycol (PEG)-diacrylate cross-linker with PEG-norbornene [21], which can be photo-coupled to thiol-containing molecules using radical-initiated “thiol-ene” chemistry [27]. Specifically, radically initiated thiyl radicals form from the cysteines of the thiolated hyaluronic acid (Glycosil) and porcine gelatin (Gelin-S) components in the presence of photoinitiator (Irgacure 2959) and ultraviolet light. The thiyl groups couple through the alkene bond of the norbornene adducts on the ends of four-armed PEG molecule [Fig 1].

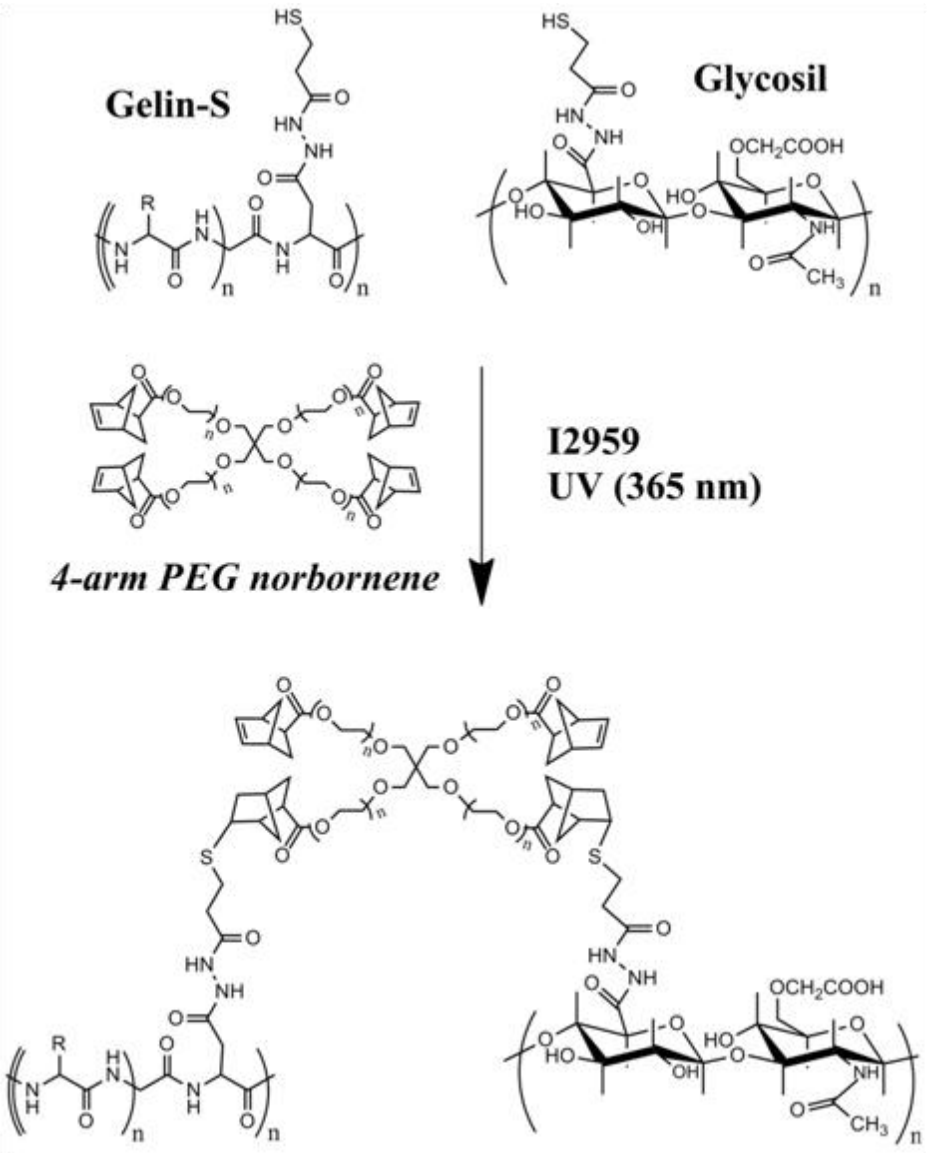

Figure 1. Radically-mediated thiol-ene photopolymerization using thiolated hyaluronic acid, porcine gelatin, 4-arm PEG norbornene, and Irgacure 2959 (I2959).

Using thiol-ene chemistry, hydrogels were formed within thirty seconds and attained a shear elastic modulus (G′) of up to 550 Pa after 15 min with only a final concentration of 0.2% w/v PEG norbornene [Fig 2A]. The gelation occurred at every ratio of thiols and alkenes (from thiol:alkene molar ratios of 31 down to 1.94 depending on the PEG norbornene concentration

used [Fig 2B]. Importantly, gel stiffness could also be modulated with increasing concentration of PEG norbornene to a shear elastic modulus greater than 2 kPa [Fig 2C]. The optimized Irgacure 2959 concentration is 0.05% [Fig 2C]. Therefore, photoinitiated thiol-ene chemistry enabled rapid gelation of thiolated hyaluronon/gelatin hydrogels, thus providing a matrix that is well-suited for bioprinting.

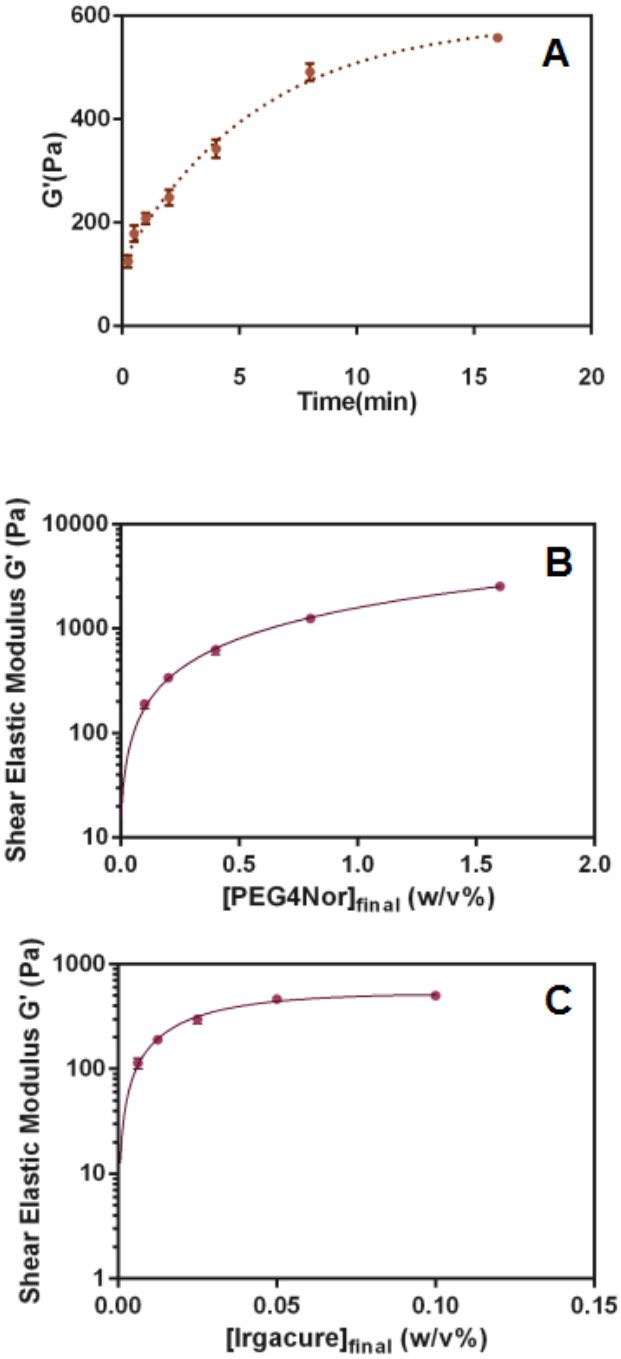

Figure 2. Rheometry experiments for shear elastic modulus (G′) of hydrogel networks formed with Glycosil, Gelin-S, at different ultraviolet light exposure times and substrate concentrations. (**A**) Time course with final concentration 0.2% w/v PEG norbornene and UV illumination for up to 15 min. (**B**) PEG norbornene dose response (final concentrations listed) with UV illumination for 3 minutes at each concentration. (**C**) Irgacure 2959 dose response with hydrogels prepared with PEG norbornene (0.2% final concentration) and UV illuminated for 3 min at each concentration.

4.5.2. Biocompatibility of the HyStem-C/PEG Norbornene Hydrogels

Biocompatibility of the HyStem-C/PEG norbornene hydrogels was explored using human adipose-derived stem cells (ADSCs) isolated from human lipoaspirates. Human ADSCs were chosen for these experiments due to their clinical potential (e.g., for tissue engineering and cell therapy [28], [29]). ADSCs were cultured on top of either HyStem-C/PEG norbornene or HyStem-C hydrogels (the latter as a control). The proliferation rates between cells at two different cell numbers was similar for both hydrogels after one week [Fig 3], indicating that neither the UV exposure nor presence of PEG norbornene and Irgacure 2959 presented cytotoxicity issues at the UV intensities used.

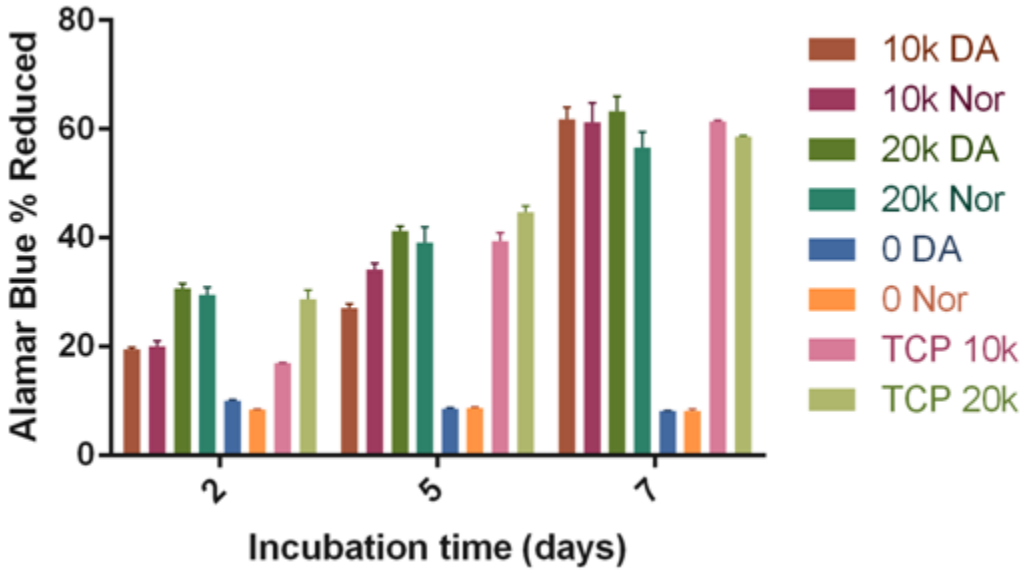

Figure 3. Alamar Blue percent reduction for ADSCs on HyStem-C crosslinked with either PEGDA (Extralink) or PEG norbornene and grown in 2D. The figure legend nomenclature shows number of cells/well (0; 10 K, 10,000; 20 K, 20,000) followed by type of crosslinker (DA, Extralink; Nor, PEG norbornene). TCP indicates tissue culture plastic controls at different cell numbers.

4.5.3. Cell Proliferation after Printing

For cell printing experiments, we first attempted printing of a robust fibroblast line, namely NIH-3T3 cells. NIH-3T3 cells were printed in the HyStem-C/PEG norbornene hydrogel and imaged at several time points during their growth, starting at 18 h and ending at 192 h, when the cells began to overgrow the surface [Fig 4]. Directly after patterning, cells possessed a rounded morphology, similar to that displayed by unattached cells suspended in solution. However, images at 18 h show cells beginning to spread and form long pseudopodia, indicative of cell attachment to either the glass surface or the 3D HyStem-C/PEGnor matrix [Fig 4]. As growth progressed through 32 h, cells began proliferating, and at 100 h started to escape from the printed matrix and spread across the glass substrate. By 192 h the cells had completely over-grown the entire array area (4 mm2), obscuring the array and discouraging further imaging. At 192 h the original depositions remained visible, due to the higher density of cells within the 3D matrix, as compared to the confluent cells growing on the interstitial, two dimensional glass surface.

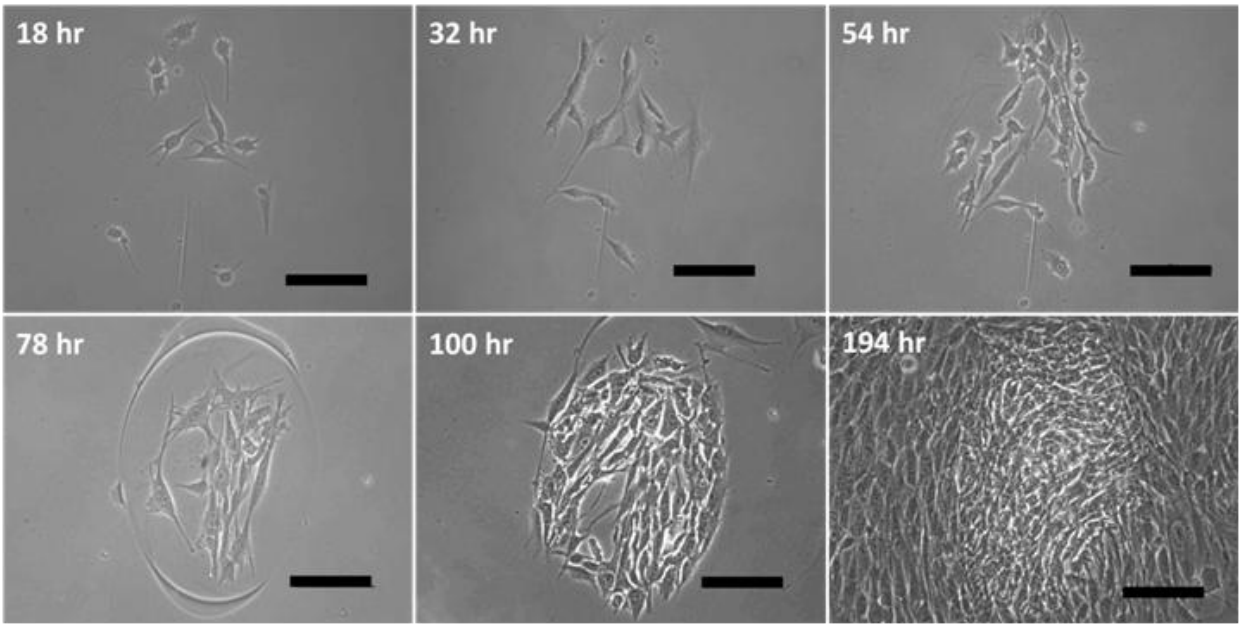

Figure 4. Demonstration of NIH/3T3 cell growth within printed spots over 8 days, images at hour 18, 32, and 54 show the consistent progression of the same spot. Scale bar = 100 μm.

4.5.4. The 3D Nature of the Printed Cell Matrix

To assess the 3D nature of printed spots of cells in HyStem-C/PEG norbornene, and further assess biocompatibility with other cell lines, we printed mouse embryonic stem cells (mESCs). Patterned mESCs were subjected to live/dead staining. After staining, confocal laser scanning microscopy was used to reveal the cell positions within the printed matrix material by producing an optical cross-section of the deposition from the compiled image planes [Fig 5]. Examination of the deposition cross-section confirms that the cells growing within the matrix reach a height of approximately 20–25 μm from the glass surface. Like many eukaryotic cells, the average mESC cell possesses a diameter of roughly 10 μm, suggesting that the growth within the microenvironment of the printed matrix is two to three cell layers in height, which is indicative of 3D cell growth. Additionally, none of the cells within the examined deposition were

positive for ethidium homodimer-1 (which stains the nucleus red for dead cells), demonstrating that high survivability of mESCs was maintained when submitted to our patterning process.

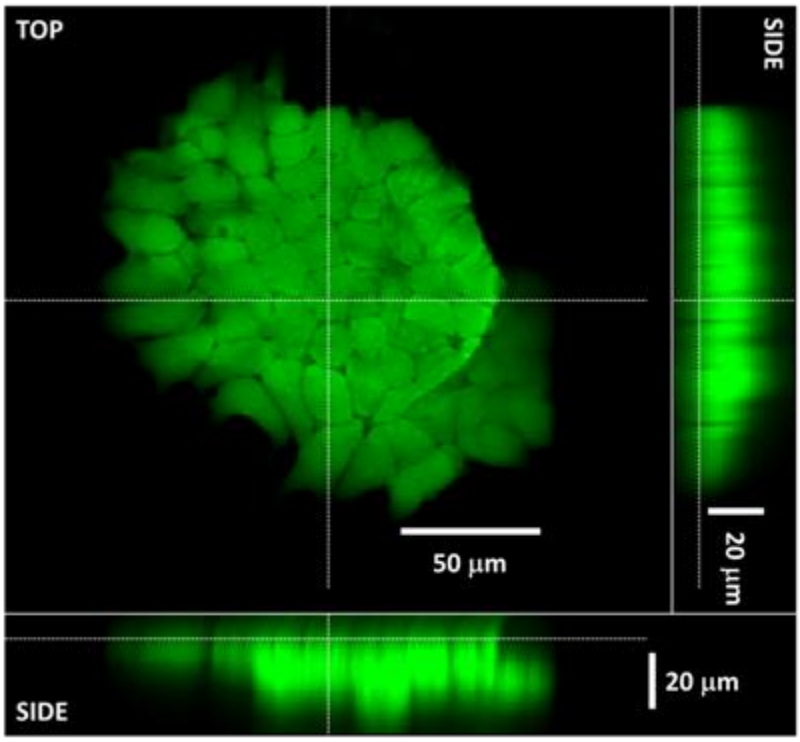

Figure 5. Demonstration of viable mESC patterning into discrete, 3D spots via live/dead staining and confocal laser scanning microscopy. Image cross-section suggests cells are distributed in the Z-direction, in addition to the XY-plane.

4.5.5. Verification of Living ROS Sensor Function

The ROS sensing capability of the printed MHS-roGFP-R12 cells was tested by exposing the cell array to oxidizing agent (hydrogen peroxide), followed by exposure to reducing agent (DTT). Cell response was quantified by selecting three separate cells within a single printed spot for observation. Utilizing confocal scanning laser microscopy in conjunction with Leica LAS

image processing software, the resulting intensity at 515 nm was measured for each cell at 1 min intervals during exposure. The MHS-roGFP-R12 cells demonstrate maximum fluorescence emission at 515 nm when excited by 405 nm, if the roGFP-R12 protein is in the oxidized form. Likewise, they demonstrate maximum excitation at 488 nm when in the reduced state. Thus, by exciting cells at both 405 and 488 nm wavelengths and then taking the ratio of resulting emission at 515 nm (for both excitation wavelengths), one can deduce the relative state (oxidized vs. reduced) for the roGFP-R12 protein [30]. Ratiometric comparison of oxidized to reduced roGFP-R12 was performed for each of three cells, individually, which were then averaged together in order to quantify the overall response from the spot as a whole [Fig 6]. Examining these data reveals that the printed cells were able to respond to both oxidizing and reducing environments rapidly and effectively. Results from all three cells demonstrate an oxidative response directly upon addition of hydrogen peroxide (minute 5), which increases toward a maximal level until a reductive response is elicited immediately upon addition of reductive DTT (minute 13). This result confirms the proper functioning of the patterned MHS-roGFP-R12 cells, as well as the capability to print a functioning and reversible live-cell-based ROS sensor.

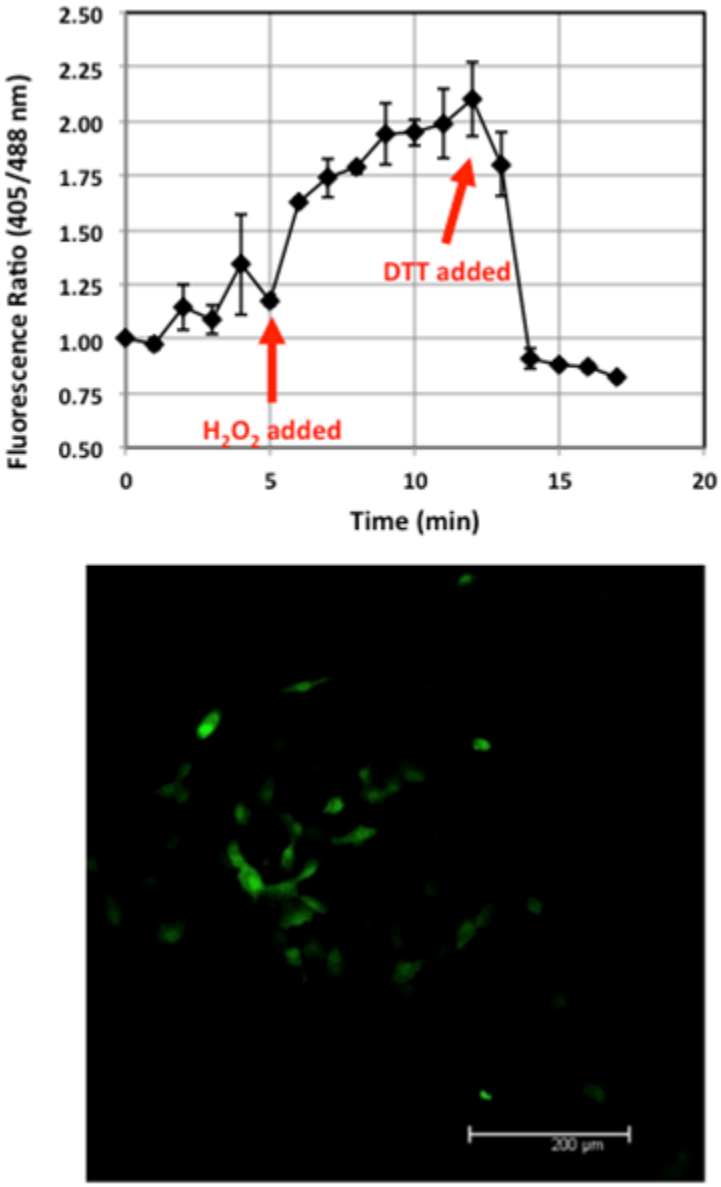

Figure 6. Living biosensor function is verified by plotting the ratio of 405 nm (oxidized) fluorescence intensity over the 488 nm (reduced) intensity (Top). Fluorescence micrograph of a representative printed spot of MHS-roGFP-R12 cells (Bottom). Scale bar = 200 µm.

4.6. Discussion

Current bioprinting technologies are most commonly used to engineer and fabricate cell-based constructs for tissue engineering applications [31]. Some techniques, such as inkjet

bioprinting, have been used to develop high-throughput drug screening platforms [1], however comparatively little has been done toward the development of cell-based biosensors using bioprinting. A potential barrier to bioprinting for cell-based biosensor fabrication is the acquisition of specialized equipment and the experience required in order to use said equipment to reliably pattern viable cells. We have successfully modified a bench-top micro-patterning system, and in turn developed a novel method for printing live eukaryotic cells, a method we have entitled quill pen lithography (QPL). In addition, we have modified a biocompatible hyaluronic acid based hydrogel, HyStem-C, to include a new cross-linker (PEGnor) which provides the requisite spatial-temporal control for bioprinting applications. The resulting HyStem-C/PEG norbornene hydrogels were shown to be biocompatible with human derived adipose-derived stem cells, which demonstrate the possible utility for future tissue engineering applications. We also showed that the elastic modulus of these hydrogels was dynamically tunable across a range of 550 Pa to >2 kPa, which is within a range of several human tissues [32].

Cell printing experiments demonstrated that mammalian cells (NIH-3T3) could both survive the printing process and proliferate during long-term culture. Cells remained within the printed spots until later time points (>100 h) but eventually escaped the 3D hydrogel matrix. Importantly, our experiments with mESCs printed in HyStem-C/PEG norbornene survived printing (as determined by live/dead staining) and grew both vertically and laterally within the matrix, as confocal microscopy showed cells growing throughout the height of the spot (>20 μm). Our results demonstrate that HyStem-C/PEG norbornene matrices are suitable for 3D cellular organization, and the utility of our cell printing method for producing small, 3D cell cultures.

Using our printing approach, we have also developed a functional, living ROS biosensor by immobilizing cells that express a redox sensitive, fluorescent protein to a surface which permits easy observation and quantification of the intensity shifts which occur upon changes in environmental redox levels. The success of our 3D bioprinting approach for cell-based biosensing indicates that the QPL technique is a viable alternative to other bioprinting strategies for the development of 2D platforms for studying both cell sensing and signaling phenomena. While this sensor was a proof of concept device, the same fabrication technique can used to develop similar, more sophisticated devices with the capability of monitoring intracellular redox activity. By incorporating cells that have been engineered to express roGFP at a specific location, (e.g., in the mitochondria or cell membrane) redox events which occur at the organelle can be monitored and quantified, potentially elucidating ROS signaling mechanisms or their cytotoxic effects. In addition to observing the redox activity of ROS in a controlled environment, this living sensor could be used conversely to perform high-throughput screening of a variety of antioxidants for counteracting the presence or activity of these ROS molecules in vitro. More advanced applications of such a sensor could also include evaluating the proximity effects of ROS production from natural sources, such as senescent cells [33] on the physiology of nearby, healthy cells.

Finally, our results demonstrate that micro-printing tools already useful for the fabrication of protein and DNA-based biosensors, in this case the NeN, can be repurposed as viable cell printers for the development of cell-based sensors. This would be especially useful for groups who utilize these tools on a regular basis as the required modifications can be performed rapidly (in minutes) and without specialized tools or knowledge. The only additional components

needed to transform the NeN into an effective cell printer are the SU-8 SPTs described here that possess the necessary dimensions to transfer whole cells onto solid and semi-solid surfaces.

4.7. Conclusions on Bioprinting for Sensor Fabrication

We have developed a novel, direct cell-patterning technique using a modified protein microarray printing system in conjunction with a specialized surface patterning tool and hydrogel specifically formulated to immobilize cells in a highly biocompatible and cytocompatible 3D matrix. Viable cell printing using QPL was verified by monitoring the resulting cell growth and morphology after patterning via microscopy, as well through qualitative viability staining. The 3D nature of the cross-linked cell depositions was revealed via optical cross-sectioning using confocal laser scanning microscopy, demonstrating that each spot is actually a 3D microenvironment in which the cells are not restricted to motility solely in the XY-plane, but are also able to move in the Z-plane. The utility of QPL bioprinting was demonstrated by fabricating a live-cell-based biosensor that is capable of monitoring changes in redox activity within an engineered in vitro environment.

References Cited

[1] J. I. Rodríguez-Dévora, B. Zhang, D. Reyna, Z. Shi, and T. Xu, "High throughput miniature drug-screening platform using bioprinting technology.," *Biofabrication*, vol. 4, no. 3, p. 035001, Sep. 2012.

[2] B. Derby, "Bioprinting: inkjet printing proteins and hybrid cell-containing materials and structures," *J. Mater. Chem.*, vol. 18, no. 47, p. 5717, 2008.

[3] A. Turner, G. Wilson, and I. Kaube, *Biosensors: Fundamentals and Applications*, 1st ed., vol. 33. Oxford, UK: Oxford University Press, 1987.

[4] R. Kubisch, U. Bohrn, M. Fleischer, and E. Stütz, “Cell-based sensor system using L6 cells for broad band continuous pollutant monitoring in aquatic environments,” *Sensors*, vol. 12, no. 3, pp. 3370–3393, 2012.

[5] M. N. M. Arip, L. Y. Heng, M. Ahmad, and S. Ujang, “A cell-based potentiometric biosensor using the fungus Lentinus sajor-caju for permethrin determination in treated wood,” *Talanta*, vol. 116, pp. 776–781, 2013.

[6] D. Jiang, J. Ji, lu an, X. Sun, Y. Zhang, G. Zhang, and L. Tang, “Mast cell-based electrochemical biosensor for quantification of the major shrimp allergen Pen a 1 (tropomyosin),” *Biosens. Bioelectron.*, vol. 50, pp. 150–156, 2013.

[7] W. L. Shing, L. Y. Heng, and S. Surif, “Performance of a cyanobacteria whole cell-based fluorescence biosensor for heavy metal and pesticide detection.,” *Sensors (Basel).*, vol. 13, no. 5, pp. 6394–6404, 2013.

[8] F. Cortés-Salazar, S. Beggah, J. R. van der Meer, and H. H. Girault, “Electrochemical As(III) whole-cell based biochip sensor,” *Biosens. Bioelectron.*, vol. 47, pp. 237–242, 2013.

[9] S. Belkin, “Microbial whole-cell sensing systems of environmental pollutants,” *Current Opinion in Microbiology*, vol. 6, no. 3. pp. 206–212, 2003.

[10] Q. Wang, J. Fang, D. Cao, H. Li, K. Su, N. Hu, and P. Wang, “An improved functional assay for rapid detection of marine toxins, saxitoxin and brevetoxin using a portable cardiomyocyte-based potential biosensor,” *Biosens. Bioelectron.*, vol. 72, pp. 10–17, 2015.

[11] A. Qureshi, A. Pandey, R. S. Chouhan, Y. Gurbuz, and J. H. Niazi, “Whole-cell based label-free capacitive biosensor for rapid nanosize-dependent toxicity detection,” *Biosens. Bioelectron.*, vol. 67, pp. 100–106, 2015.

[12] K. Hensley, K. a Robinson, S. P. Gabbita, S. Salsman, and R. a Floyd, “Reactive oxygen species, cell signaling, and cell injury,” *Free Radic. Biol. Med.*, vol. 28, no. 10, pp. 1456–1462, 2000.

[13] J. M. Gutteridge and J. Mitchell, “Redox imbalance in the critically ill.,” *Br. Med. Bull.*, vol. 55, no. 1, pp. 49–75, 1999.

[14] E. R. Stadtman and B. S. Berlett, “Reactive oxygen-mediated protein oxidation in aging and disease,” *Chemical Research in Toxicology*, vol. 10, no. 5. pp. 485–494, 1997.

[15] D. J. Reed, J. R. Babson, P. W. Beatty, A. E. Brodie, W. W. Ellis, and D. W. Potter, “High-performance liquid chromatography analysis of nanomole levels of glutathione, glutathione disulfide, and related thiols and disulfides,” *Anal. Biochem.*, vol. 106, no. 1, pp. 55–62, 1980.

[16] B. D'Autréaux and M. B. Toledano, "ROS as signalling molecules: mechanisms that generate specificity in ROS homeostasis," *Nat. Rev. Mol. Cell Biol.*, vol. 8, no. 10, pp. 813–824, 2007.

[17] C. C. Winterbourn, "Reconciling the chemistry and biology of reactive oxygen species.," *Nat. Chem. Biol.*, vol. 4, no. 5, pp. 278–286, 2008.

[18] C. T. Dooley, T. M. Dore, G. T. Hanson, W. C. Jackson, S. J. Remington, and R. Y. Tsien, "Imaging dynamic redox changes in mammalian cells with green fluorescent protein indicators," *J. Biol. Chem.*, vol. 279, no. 21, pp. 22284–22293, 2004.

[19] N. Soh, "Recent advances in fluorescent probes for the detection of reactive oxygen species," *Anal. Bioanal. Chem.*, vol. 386, no. 3, pp. 532–543, 2006.

[20] G. T. Hanson, R. Aggeler, D. Oglesbee, M. Cannon, R. A. Capaldi, R. Y. Tsien, and S. J. Remington, "Investigating Mitochondrial Redox Potential with Redox-sensitive Green Fluorescent Protein Indicators," *J. Biol. Chem.*, vol. 279, no. 13, pp. 13044–13053, 2004.

[21] B. D. Fairbanks, M. P. Schwartz, A. E. Halevi, C. R. Nuttelman, C. N. Bowman, and K. S. Anseth, "A versatile synthetic extracellular matrix mimic via thiol-norbornene photopolymerization," *Adv. Mater.*, vol. 21, no. 48, pp. 5005–5010, 2009.

[22] P. a Zuk, M. Zhu, H. Mizuno, J. Huang, J. W. Futrell, a J. Katz, P. Benhaim, H. P. Lorenz, and M. H. Hedrick, "Multilineage cells from human adipose tissue: implications for cell-based therapies.," *Tissue Eng.*, vol. 7, no. 2, pp. 211–28, 2001.

[23] E. Robertson, a Bradley, M. Kuehn, and M. Evans, "Germ-line transmission of genes introduced into cultured pluripotential cells by retroviral vector.," *Nature*, vol. 323, no. 6087, pp. 445–448, 1986.

[24] G. Keller, M. Kennedy, T. Papayannopoulou, and M. V Wiles, "Hematopoietic commitment during embryonic stem cell differentiation in culture.," *Mol. Cell. Biol.*, vol. 13, no. 1, pp. 473–486, 1993.

[25] M. R. Zonca, P. S. Yune, C. L. Heldt, G. Belfort, and Y. Xie, "High-Throughput screening of substrate chemistry for embryonic stem cell attachment, expansion, and maintaining pluripotency," *Macromol. Biosci.*, vol. 13, no. 2, pp. 177–190, 2013.

[26] A. A. Melillo, C. S. Bakshi, and J. A. Melendez, "Francisella tularensis antioxidants harness reactive oxygen species to restrict macrophage signaling and cytokine production," *J. Biol. Chem.*, vol. 285, no. 36, pp. 27553–27560, 2010.

[27] C. E. Hoyle and C. N. Bowman, "Thiol-ene click chemistry," *Angewandte Chemie - International Edition*, vol. 49, no. 9. pp. 1540–1573, 2010.

[28] A. Schäffler and C. Büchler, “Concise review: adipose tissue-derived stromal cells - basic and clinical implications for novel cell-based therapies.,” *Stem Cells*, vol. 25, no. 4, pp. 818–827, 2007.

[29] A. I. Caplan, “Adult mesenchymal stem cells for tissue engineering versus regenerative medicine,” *Journal of Cellular Physiology*, vol. 213, no. 2. pp. 341–347, 2007.

[30] C. R. Arias-Barreiro, K. Okazaki, A. Koutsaftis, S. H. Inayat-Hussain, A. Tani, M. Katsuhara, K. Kimbara, and I. C. Mori, “A bacterial biosensor for oxidative stress using the constitutively expressed redox-sensitive protein roGFP2,” *Sensors*, vol. 10, no. 7, pp. 6290–6306, 2010.

[31] V. Mironov, N. Reis, and B. Derby, “Review: bioprinting: a beginning,” *Tissue Eng.*, vol. 30, 2006.

[32] C. T. McKee, J. a Last, P. Russell, and C. J. Murphy, “Indentation versus tensile measurements of Young’s modulus for soft biological tissues.,” *Tissue Eng. Part B. Rev.*, vol. 17, no. 3, pp. 155–164, 2011.

[33] A. Takahashi, N. Ohtani, K. Yamakoshi, S. Iida, H. Tahara, K. Nakayama, K. I. Nakayama, T. Ide, H. Saya, and E. Hara, “Mitogenic signalling and the p16INK4a-Rb pathway cooperate to enforce irreversible cellular senescence.,” *Nat. Cell Biol.*, vol. 8, no. 11, pp. 1291–1297, 2006.

Chapter 5: Establishing microbial communities via bioprinting for the experimental validation of a predictive bacterial growth model

Section 5.1. Bridging the Gap between Simulation and Experiment

The observation and characterization of bacterial interactions within complex populations, consisting of multiple species or strains, are important for understanding fundamental cellular behavior and the impacts that these interactions have on the surrounding environment at every ecosystem-scale. In addition to the importance of understanding complex microbial interactions within their natural context, synthetic bacterial consortiums have many potential industrial applications, ranging from novel drug development to revolutionizing bioremediation efforts [1]. Despite the importance of these interactions on the resulting ecology within all existing ecosystems and their impacts on humans, little is well understood about these microbial processes due to the challenges of observing these types of events in well controlled, laboratory microenvironments [2]. Traditional cell culturing methods often fall short of maintaining the necessary control over the spatial distribution of cells and diffusible molecules. This can make studying microbial interactions which depend upon the formation of concentration gradients, such as diffusion-based metabolite-sharing [3], [4], chemotaxis [5], [6], and quorum sensing [7], [8], a challenge to execute in the laboratory, especially on the micro-scale [9].

In recent years, groups interested in quantifying these interactions have begun developing computational models to predict cell behavior under specific conditions [2], [10], [11]; however the same culturing limitations which prevent them from directly observing the behavior *in vitro*

can also prevent them from validating the predictions of their platforms experimentally. Some researchers focus on modeling homogenous, well-mixed environments or environments with populations patterned on the macro-scale as these types of conditions are more readily replicated using liquid cultures such as chemostats and batch reactors [2], [10], [12] or macro-scale plating techniques [2], [13]. These approaches often use simplifying assumptions, such as a uniform distribution of nutrients or organisms within the system, which may not accurately predict growth rates or cellular behavior when spatiotemporal dynamics are prevalent and often do not reflect the heterogeneity found in most natural ecosystems [14], [15]. Models which consider interactions with respect to time and space can provide a more complete picture of cellular interactions within diverse communities and across non-uniform environments [16], [17]. Under normal circumstances it is not uncommon for researchers to perform iterative tests, while refining parameters, in order to produce a range of predictions to identify possible trends. This is normally performed by including theoretical calculations of dynamic cellular interactions based on the diffusion and availability of nutrients, toxins, signaling molecules, etc. The predictions are then considered reasonable if deemed biologically feasible when compared to data from literature, which can be challenging if the culturing conditions are not precisely reported to ensure reproducibility [18], or until experimental results can be produced to directly substantiate or refute the hypotheses [19].

Computation of Microbial Ecosystems in Time and Space (COMETS) is an experimental bacterial growth model which strives to predict dynamic microbial behavior at all ecosystem levels, ranging from single cells to the biosphere, specifically with respect to their spatiotemporal dependencies. By utilizing the intracellular metabolic stoichiometry generated from the microbe's complete genome in combination with a dynamic flux balance analysis (dFBA)

algorithm, COMETS is able to link internal metabolism with dynamic external biogeochemistry to predict changes in microbial biomass [16]. By including a spatial lattice within the model, COMETS is capable of predicting the spatiotemporal, diffusion-based interactions between multiple bacterial species. It can accomplish this by tracking the flux of metabolic by-products produced and excreted by one species, the resulting changes in nutrient availability within the environment caused by diffusion, and the subsequent utilization of the metabolite by other bacterial species to maximize their biomass. Previously COMETS has been shown to accurately predict the effects of inter-species nutrient competition within complex environments on the macro-scale (approx. 2 mm diameter colonies, separated by 10 mm distance), termed "the eclipse dilemma" [16].

This work builds upon the previous study by extending COMETS' simulations to the micro-scale where the colonies examined were approx. 3-fold smaller and the separation distance was decreased by 5-fold,in order to validate COMETS predictions as they approach closer to the cellular level. Additionally, another form of competition will be evaluated both within COMETS and in the laboratory to determine how the presence of conspecific competitors outside the path of metabolite exchange can interfere with diffusion of nutrients between cooperators. Herein we demonstrate the utility of bioprinting for computational model validation by comparing growth data from micro-patterned colonies to predictions made by the COMETS software platform. Bioprinting is a term which refers to a collection of printing technologies used to pattern live cells and biomaterials in defined geometries for a number of applications, ranging from tissue engineering [20], [21] to biosensor development [22]. A common trait shared by the inkjet- [23], [24], extrusion- [25], microarrayer- [26] and laser-based [27] bioprinting technologies is the ability to deposit cells, nutrients, soluble signals, toxins and polymers onto

solid surfaces. **We hypothesized that direct cell patterning could be used to establish structured microbial communities confined by geometry and nutrient availability in order to evaluate the interaction effects across species within controlled environments.** In turn, this would result in an experimentation platform for extending experimental recapitulation of complex bacterial growth models with spatiotemporal capabilities to the micrometer scale.

Section 5.2. Bioprinting for COMETS Validation

5.2.1. Materials and Reagents

The Arrayit Spotbot® 3 (Telechem, Sunnyvale, CA) microarray printer was used for all micro-scale bacterial printing experiments. All cell culturing materials were purchased from Sigma-Aldrich (St. Louis, MO), with the exception of lysogeny broth Lennox (LB) agar used for the initial plating which was purchased from BD Difco (Sparks, MD). Agarose for surface fabrication and printing solution formulation was purchased from Bioline (London, UK). Phosphate buffered saline (PBS) was purchased from National Diagnostics (Atlanta, GA). Ethanol for print pin decontamination was purchased from Decon Laboratories (King of Prussia, PA).

5.2.2. Culturing and Printing Solution Preparation

The artificial mutualistic consortium consisted of *Salmonella enterica* serovar Typhimurium WH212 and *Escherichia coli* WH224 which constitutively express yellow

fluorescent protein (YFP) and cyan fluorescent protein (CFP), respectively. *S. enterica* WH212, an evolved methionine overproducer, cannot metabolize lactose and must rely upon acetate generated by *Escherichia coli* WH224, which is a metB knockout mutant, and must rely on upon the *S. enterica* for its acquisition. Preparation of these cell lines into a functioning syntrophic pairing is described in [29]. Competition experiments included the wild type (WT) *S. enterica* WH100 as a non-cooperative, cheater population. All cells were cultured in their respective defined growth media, consisting of Hypho defined media (2.92 mM lactose, 7.26 mM K_2HPO_4, 0.88 mM NaH_2PO_4, 1.89 mM $(NH_4)_2SO_4$, 0.41 mM $MgSO_4$, and 1 mL of Delaney's metal mix [16] with glucose substituted for lactose for *S. enterica* cultures and 10 mM methionine included for *E. coli* cultures. Colonies were picked from lysogeny broth Lennox plates and used to inoculate 7 mL liquid cultures consisting of their defined media, which were then incubated for 24 hrs at 37°C. After 24 hrs, the cultures were spun down and re-suspended in 1 ml of fresh defined media and 100 µL of each culture was transferred to a fresh 7 mL liquid culture and incubated for 12 hrs at 37°C to ensure the cells would be in the exponential growth phase when harvested for patterning. Before patterning, cells were spun-down and re-suspended in 100 µL of defined media with 0.1% agarose added. Agarose was included to increase solution viscosity to minimize spreading of the patterned spots, as well as to prevent sedimentation of cells during printing.

5.2.3. Printing Surface Preparation

Planar gel printing surfaces were formed by evenly casting a molten solution of consortium media (lactose +, methionine -, glucose -) with 5% agarose onto sterilized glass

microscope slides. The solution was allowed to cool until completely solidified, and then the surfaces were stored at 4°C until required. Before printing, the surfaces were removed from storage and allowed to reach room temperature. Using sterile tweezers, each agarose slab was flipped so that the planar side previously contacting the glass surface was positioned face-up. Each surface was allowed to partially dry in a closed Petri dish for 20 min before patterning to prevent droplet spreading due to water present on the gel surface caused by syneresis. Each slab was then cut into fifths (15mm x 25mm x 1mm) in order to form the final printing surfaces.

5.2.4. Cell Printing

Prior to cell patterning, unique printing geometries and sample keys were designed in Microsoft Paint and Notepad, respectively. This was followed by decontamination of the interior of the printing enclosure with 70% ethanol. After printing solution preparation, each solution was vortexed for 30 sec and 3 µL of each solution was loaded into a specific well of a 384-well plate, as defined by the sample key. After the SPA3's enclosure humidity reached 90% relative humidity, both the 384-well plate and the agarose printing surfaces were placed at their specified locations within the enclosure. During printing, each pin wash cycle was programmed to occur after 3 spots were patterned and between all solution changes. The wash cycle was programmed with a duration of 3 sec for washing and 1 sec for drying for the first two steps, followed by a 10 second wash and 5 second dry for the final step. Each print was programmed to use a pin dwell time of 3 sec to draw solution from the sample well and a 0.5 sec dwell time for the pin when contacting the agarose substrate to deposit cells.

5.2.5. Culturing for Observation

Before cell patterning, carrier dishes were prepared by filling Petri dishes with molten 2% agarose in diH_2O. The dishes were allowed to cool and dry overnight at 4°C before being sealed and stored at 4°C until needed. After patterning, each surface was sealed into a carrier plate using parafilm to prevent surface drying and allow for easy handling of the patterned surfaces over the duration of the incubation and observation period. Carrier plates were incubated at 37°C between all imaging steps. Fluorescent microscopy was performed using a Nikon Eclipse 80i microscope equipped with a QImaging QICAM Fast 1394 digital camera using a FITC filter at 48 hr intervals to track changes in biomass. During imaging the carrier plates were opened under flame to prevent interference with the microscope objective and to provide clear images under sterile conditions. After each imaging period, a Pasteur pipette was used to deposit drops of sterile diH_2O into the carrier plates to replace water lost due to evaporation upon the surface's exposure to ambient air during imaging.

5.2.6. Image Evaluation

Images gathered during the observation period were analyzed using NIS-Elements AR 4.11 software (Nikon Instrument Inc., Melville, NY). All micrographs were captured using identical camera settings and exposure times for each species to maintain consistency between all experiments and time points. Intensity measurements were taken from the colonies by using the thresholding, smoothing and cleaning functions to remove all background pixels below a specific intensity. The threshold intensity was chosen for each individual sample by manual adjustment until all cell fluorescence was highlighted, while including as little background as

possible. The fluorescence intensity of the highlighted pixels (those containing cells) were added together to determine the total sum intensity for each colony. The background intensity per pixel for bare surface was also recorded using an ROI, averaged and subtracted from each highlighted pixel to ensure all measured fluorescence intensity came from the cells only.

5.2.7. Conversion from Intensity to Cell Density

Measurements of fluorescence intensity were converted to estimates of biomass by imaging printed micro-colonies which were grown for 96 to 144 hours, which was followed by their removal from the surface and subsequent plating for colony forming unit (CFU) counts. Four separate surfaces consisting of each species respective defined media were patterned with twenty individual micro-colonies. After growth, three random micro-colonies from each surface were imaged using fluorescence microscopy so that average intensity measurements could be recorded. Each surface was then placed within a 50 ml conical centrifuge tube, along with 1 ml of PBS, and vortexed for 10 min in order to reclaim the printed cells from the surface. Cells suspended in PBS were removed from the tube and used to perform a ten-fold serial dilution. Each dilution was then plated onto a LB plate and incubated for 24 hours in order for colonies to form. After 24 hours CFU counts were performed, which permitted calculation of the average number of cells in the original, individual micro-colonies.

5.2.8. COMETS Modeling Parameters

COMETS modeling and parameter selection was performed by Professor William R. Harcombe (University of Minnesota, College of Biological Sciences)

5.3. Results

5.3.1. Printed Consortium Controls

Testing an experimental bacterial growth model which predicts biomass changes due to interspecies cross-feeding required selection of a mutualistic consortium composed of well-characterized and genetically sequenced participants. An artificial consortium was selected, consisting of *S. enterica* and an *E. coli* mutant auxotrophic for the amino acid methionine. Each consortium partner is reliant upon metabolites generated by the other when present on consortium media, which lacks methionine and with lactose present as the sole available carbon-source. To confirm proper functioning of the consortium post-printing, each species was printed onto consortium media both in isolation and co-deposited with partner colonies separated by a 2 mm, center-to-center distance. *E. coli* did not display any observable growth after 240 hours in isolation (data not shown), while *S. enterica* did display slight growth in isolation conditions which was quantified in terms of fluorescence intensity and included in the control graph. When patterned at a separation distance of 2 mm, both partners exhibited observable growth (quantified via increasing fluorescence intensity) for 240 hours [Fig 1]. Background growth exhibited by *S. enterica* was dependent upon the addition of lactose within the media as only media with no

carbon-source present prevented *S. enterica* growth in isolation (data not shown). This suggests either impurities in the lactose or a slight ability *S. enterica* to metabolize lactose underlie for this observation. To account for this isolated growth in future experiments, all *in vitro* data for *S. enterica* were normalized by subtraction of the change in intensity measured in the negative control. It should be noted that the fluorescence emission produced by the CFP expressed by the *E. coli* was less intense than that of the YFP expressed by the *S. enterica*, resulting in the differences observed between growth curves for *E. coli* and *S. enterica*.

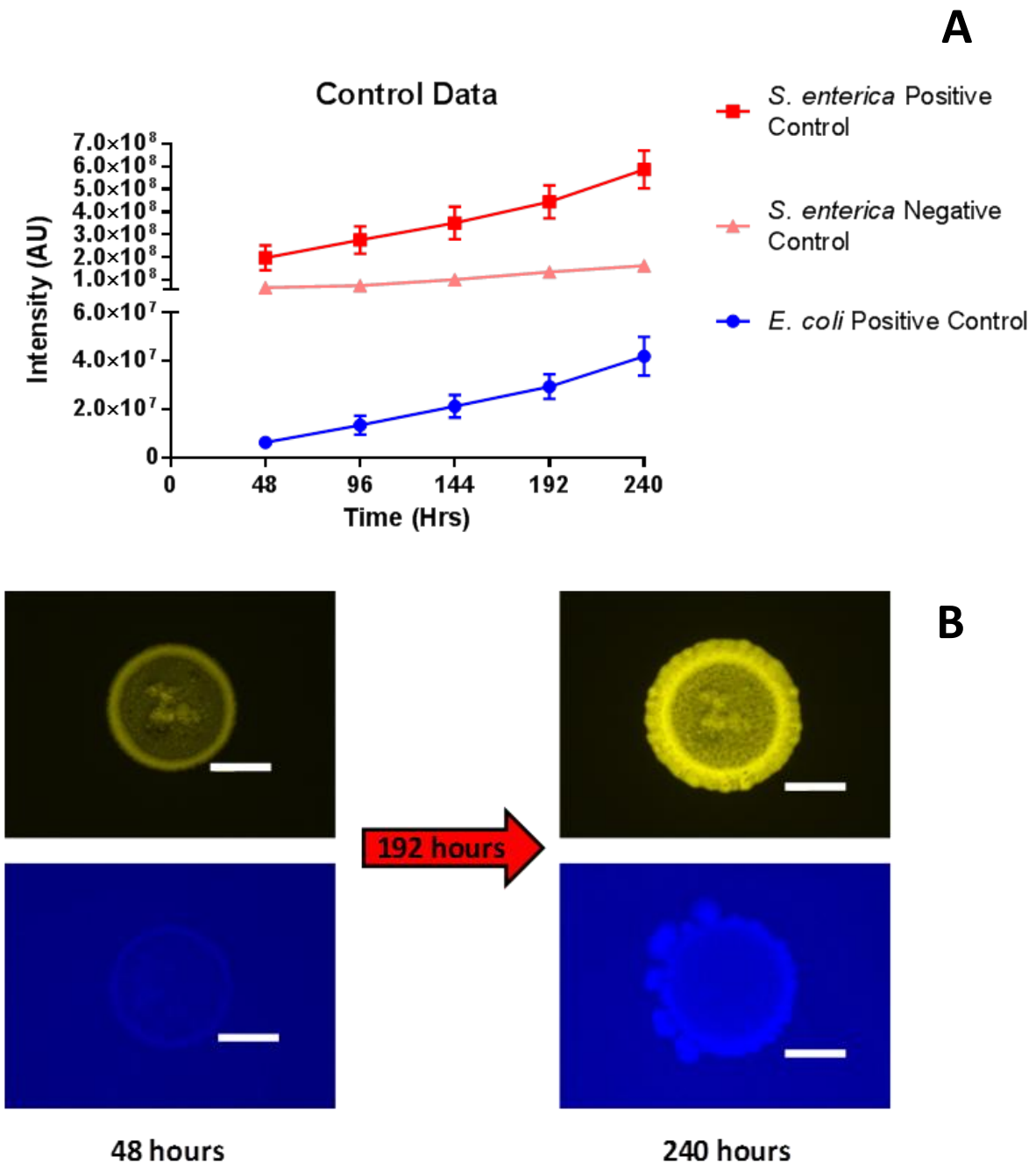

Figure 1. A) Printed consortium controls. Positive controls consisted of cross-feeding partners patterned 2 mm from one another, while negative controls consisted of cross-feeding partners patterned in isolation *S. enterica* growth recorded during the negative control was subtracted from all subsequent results. Negative control for *E. coli* exhibited no measurable growth (data not shown). Error bars represent standard deviation. **B)** Representative micrographs of *S. enterica* (above) and *E. coli* (below) positive controls at 48 hours and 240 hours of growth. Scale bars = 300 µm.

5.3.2. Relating Colony Fluorescence Intensity to Cell Number

In order to verify that colony florescence intensity is directly related to colony biomass a separate experiment was performed to generate CFU counts from the patterned consortium partners. After cell printing and incubation, 3 of the 20 printed colonies were randomly selected from each surface and imaged using fluorescence microscopy so that average colony intensity could be recorded. CFU counts were then performed after the printed colonies were reclaimed from the surfaces via thorough washing. When each sample was plotted as average intensity against the cell number recorded during the CFU count a general trend of increasing intensity resulting in increasing cell density was observed [Fig 2]. These results demonstrated that colony fluorescence intensity is a reasonable measure of biomass as colony cell density is inherently related to colony biomass as the mass of each cell is a direct contributor to the overall mass of the colony.

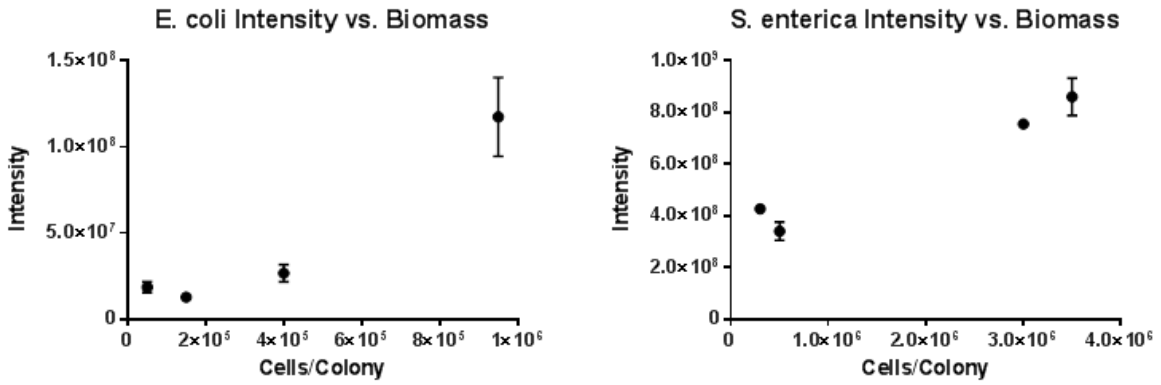

Figure 2. Plots of average colony fluorescence intensity recorded 96 to 144 hours after printing and the number of cells per printed colony calculated after performing CFU counts on each sample. Each point represents the average intensity of 3 random colonies from the 20 colonies patterned on each sample. Error bars represent standard deviation.

5.3.3. COMETS Predictions of Distance Dependency and Experimental Validation

After performing control experiments, the COMETS model was used to predict the distance dependent growth rates of the consortium partners, *E. coli* and *S. enterica*. The "V-formation" printing geometry used to test the distance dependence of the cross-feeding interaction is illustrated in [Fig 3]. Briefly, *S. enterica* micro-colonies were patterned in a straight line with a spacing of 5 mm (center-to-center), while the *E. coli* were patterned at an angle which resulted in an increasing separation distance of 500 μm between each of the *S. enterica* and *E. coli* micro-colony pairings, with the distance of separation ranging from 1 mm to 3.5 mm (center-to-center). The 5 mm spacing between the patterned micro-colony pairs was chosen in order to limit diffusion from transporting metabolites between the individual parings. At increasing spatial separations, the model suggested that the cross-feeding interaction possesses a strong, linear distance-dependency [Fig 4]. Previously, macro-scale plating techniques were used to qualitatively evaluate this interaction which validated COMETS predictions on the macro-scale [16]. In order to validate the COMETS prediction of distance-dependence on the micro-scale, bioprinting was used to pattern the consortium partners at increasing distances in a tightly controlled microenvironment.

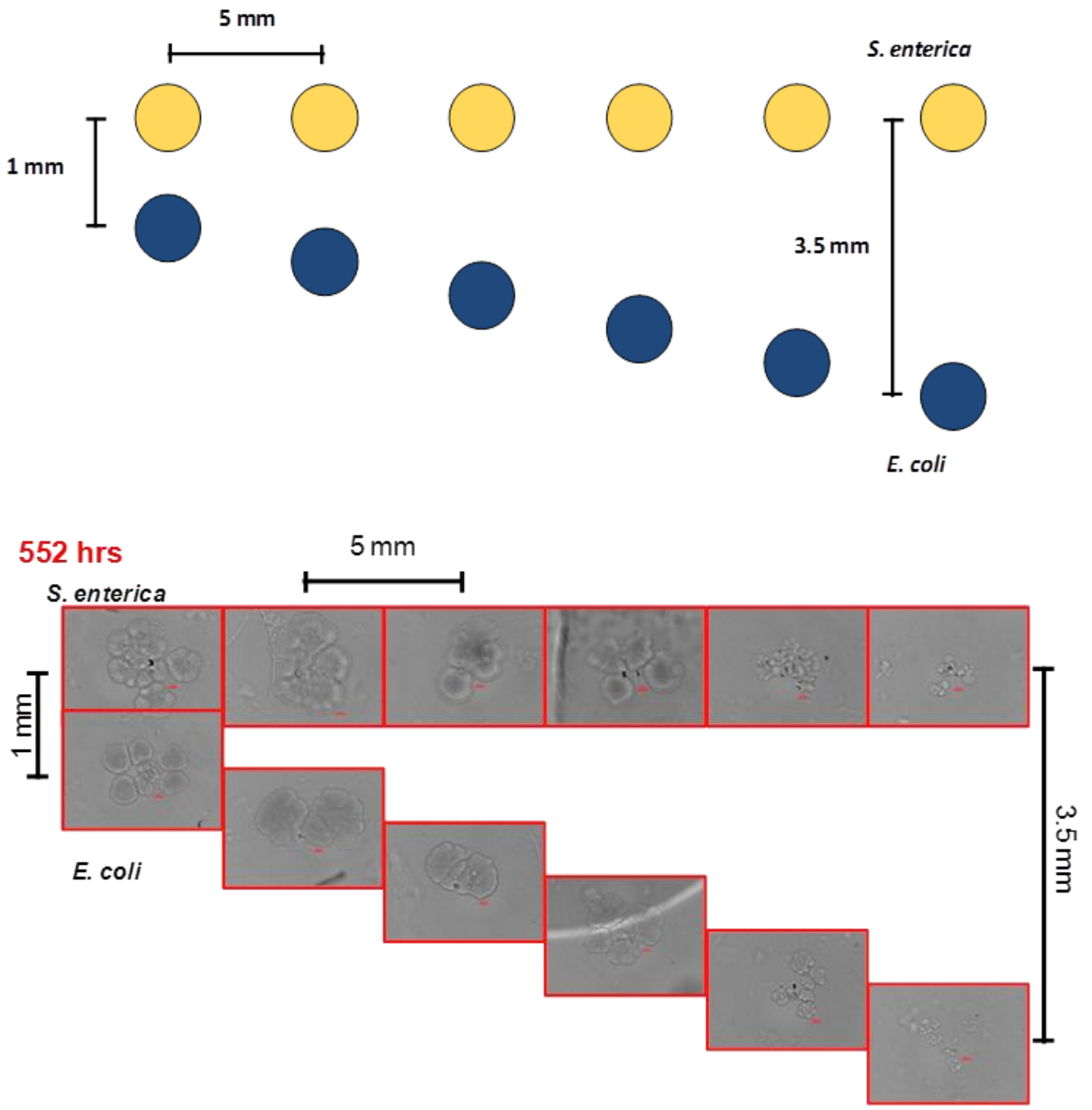

Figure 3. Illustration of the V-formation printing geometry used to test COMETS predictions of distance-dependent cross-feeding (above). Brightfield micrographs showing cross-feeding partners after 552 hours of growth as separation distance is increased (below). Colonies are separated by distances ranging from 1 mm to 3.5 mm, center-to-center.

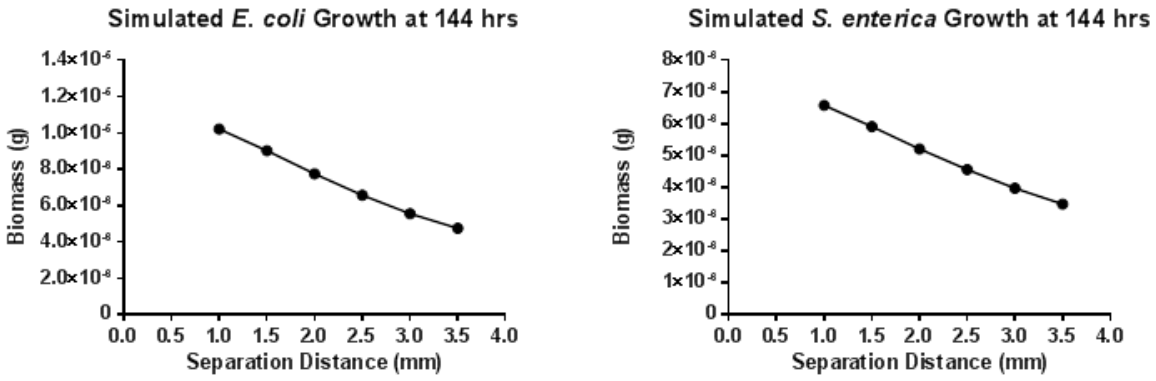

Figure 4. COMETS predictions of biomass accumulation for each species over the course of 144 hours based on colony proximity.

Experimental growth trends were compared to COMETS simulation data generated using a diffusion coefficient of $5x10^{-6}$ cm^2/sec. This diffusion coefficient was chosen under the assumption that the molecules would diffuse through a 5% agarose gel at a lower rate than they would within aqueous solutions. Reported diffusion coefficients for acetate and methionine in aqueous solutions are $9.5x10^{-6}$ cm^2/sec [30] and $1.1x10^{-5}$ cm^2/sec [31], respectively. Further, the diffusion coefficient of $5x10^{-6}$ cm^2/sec was chosen as the previous macro-scale plating experiments were found to be predicted with high accuracy when compared to simulations generated with this value [16].

Fluorescence micrographs gathered after 144 hours of growth were analyzed to quantify micro-colony fluorescence in arbitrary units. Measurements of total intensity were taken from the patterned colonies in order to compare changes in colony intensity to the changes in biomass simulated by COMETS [Fig 5]. Each colony was measured relative to the colony separated by the shortest distance, 1 mm between cross-feeding partners, in order to calculate the percentage of relative growth as separation distance increased for each species, with each *in vitro* colony

compared to its *in silico* counterpart [Fig 6A]. Interestingly, when the diffusion coefficient for acetate was lowered to $1x10^{-6}$ cm^2/sec the predicted *S. enterica* growth trend became less linear and appeared to better reflect the *in vitro* growth values [Fig 6B].

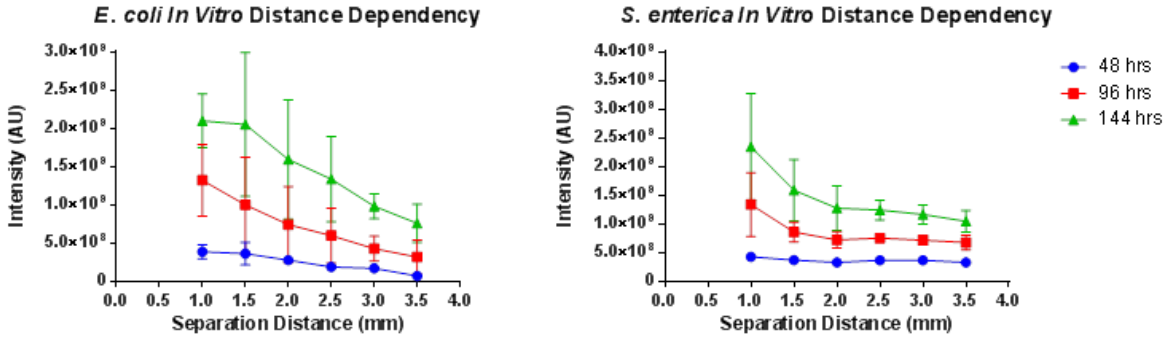

Figure 5. Fluorescence intensity measurements gathered from the consortium colonies patterned in the V-formation from 48 hours to 144 hours post-printing. Error bars represent standard deviation.

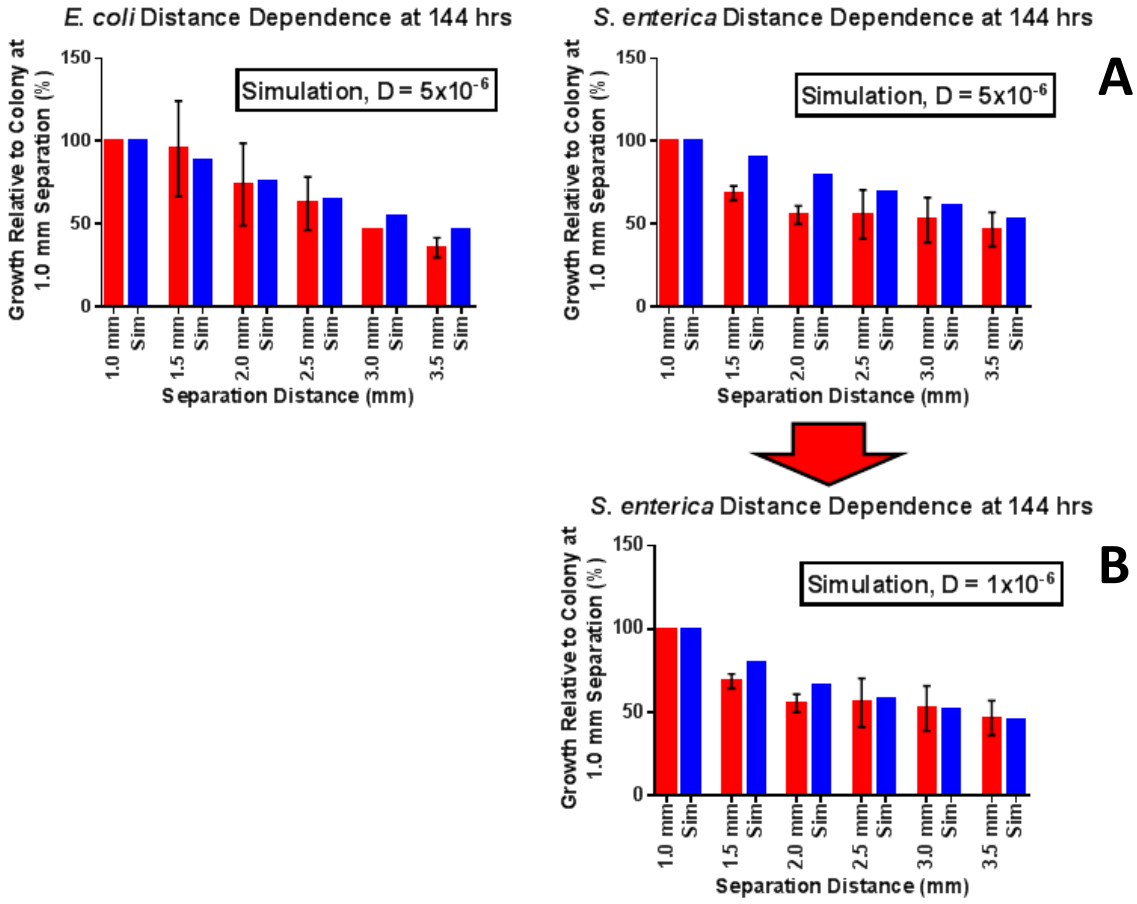

Figure 6. A) Comparison of *in silico* and *in vitro* distance dependence growth ratios at 144 hours for both cross-feeding partners. Growth percentages are relative to the colonies separated by 1 mm distance. **B)** When the diffusion coefficient for acetate is lowered within COMETS from $5x10^{-6}$ cm^2/sec to $1x10^{-6}$ cm^2/sec the resulting *in* silico ratios are closer to the *in vitro* ratios. Error bars represent standard deviation.

5.3.4. Prediction and Validation of Eclipse Dilemma Scenarios

Due to the pervasiveness of complex mutualistic interactions between multiple species in natural ecosystems, we have selected printing geometries which place either a competitor or an additional cooperator inside and outside the path of nutrient exchange between the obligate syntrophic strains. Similar scenarios were previously investigated on the macro-scale, with the resulting growth of one of the partners compared to COMETS simulations, which were found to

correctly predicted the experimental outcomes [16]. In the current work, bioprinting was used to determine if COMETS could correctly predict the experimental outcomes of these types of complex competition scenarios as the scale is shifted closer to the cellular level. Each printed scenario consisted of both of the consortium partners, *E. coli* WH224 and *S. enterica* WH212, along with either the WT *S. enterica* WH100 as an interspecific competitor or an additional *S. enterica* WH212 spot as a conspecific competitor. Here the additional *S. enterica* WH212 YFP colonies are referred to as conspecific competitors as they will compete for the focal *S. enterica* colony's diffusible carbon-source, but participate in methionine exchange with *E. coli*. An illustrated layout and representative micrographs of the micro-scale printed samples are shown in [Fig 7]. The WT *S. enterica* WH100 functions as an interspecific competitor as it will compete for both diffusible metabolites while contributing nothing in exchange to the consortium partners. This scenario has been termed the "eclipse dilemma", as the intervening colonies interfere with the direct exchange of nutrients between the consortium partners by either utilizing one or both metabolites, yet may also aid growth of the other species [16].

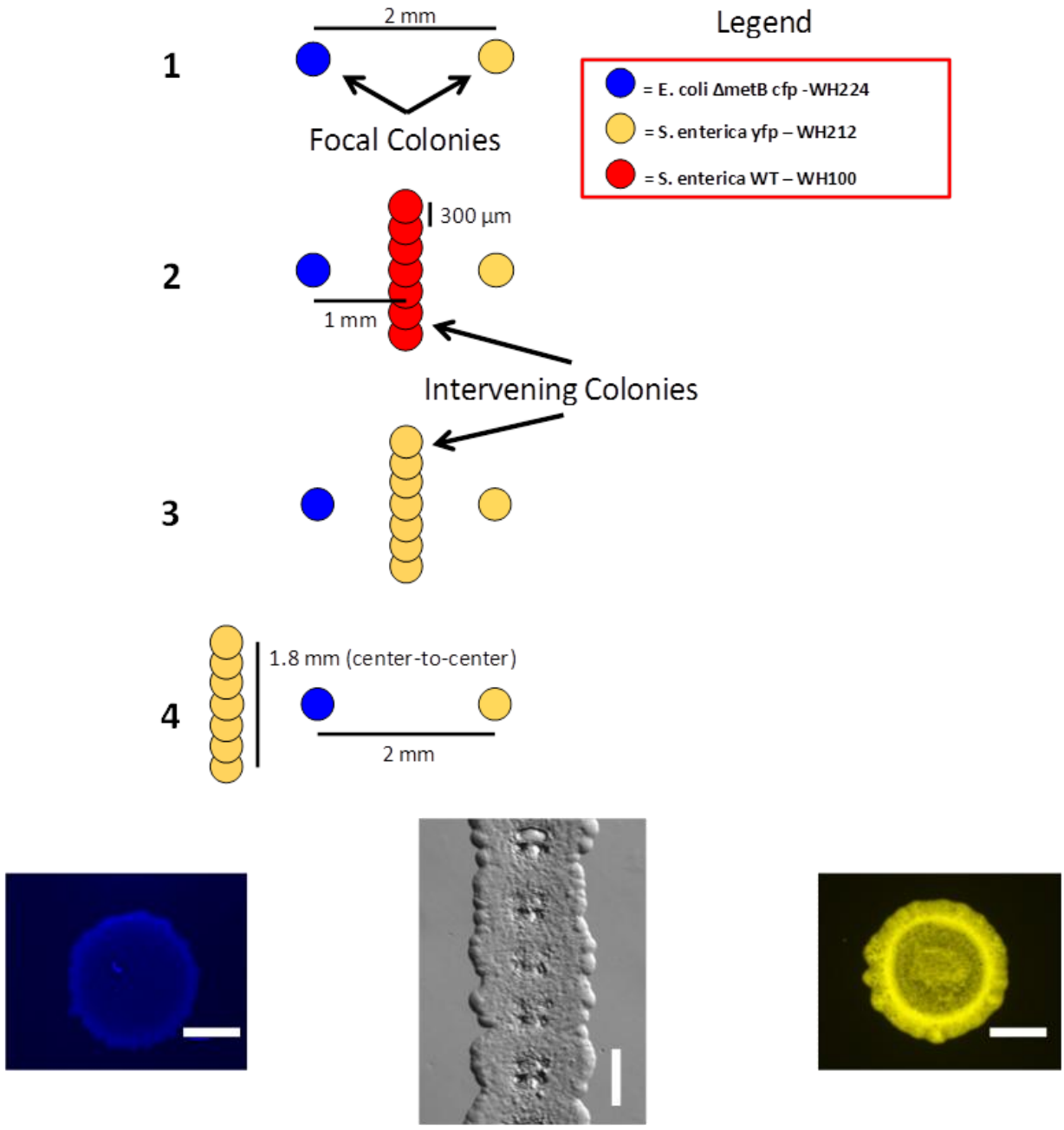

Figure 7. Illustration of the "eclipse-dilemma" colony geometry (above). Each scenario was patterned on a separate surface with a fixed 2 mm separation between the focal consortium colonies. Representative micrographs of printed samples taken from Scenario 2, showing *E. coli* WH224, WT *S.enterica* WH100, and *S. enterica* WH212 from left to right (below). Scale bars = 300 µm.

Initial trials examining the eclipse dilemma employed smaller, single deposition intervening colonies. However, after fluorescence analysis was performed it became evident that

the single colonies were not sufficient to appreciably interfere with cross-feeding between the focal colonies over the course of the experiment, resulting in only minor differences in average fluorescence between the scenarios (data not shown). A plausible explanation for this is that the diffusion of metabolites around the single intervening colony eventually caused the collapse of the depleted region or "metabolite shadow" which had formed initially due to the nutrient usage of the single intervening colony. As diffusion is a continuous process characterized by molecules moving from regions of high to low concentration due to random motion, the formation of an additional concentration gradient between the metabolites diffusing past the intervening colony and the depleted region was likely the driving force behind the collapse [Fig 8]. This gradient may have driven the diffusion of the metabolites back into the inter-colony space over time, decreasing the overall effect of shadowing. To enhance the shadowing effects of the intervening colonies, the surface area of the colonies along with the number of resident cells was increased in subsequent trials by patterning a line of seven overlapping colonies. This patterning method resulted in contiguous intervening colony "walls" approximately 2.5 mm in length, which were large enough to prevent the collapse of the metabolite shadowing due to the effects of continuous diffusion.

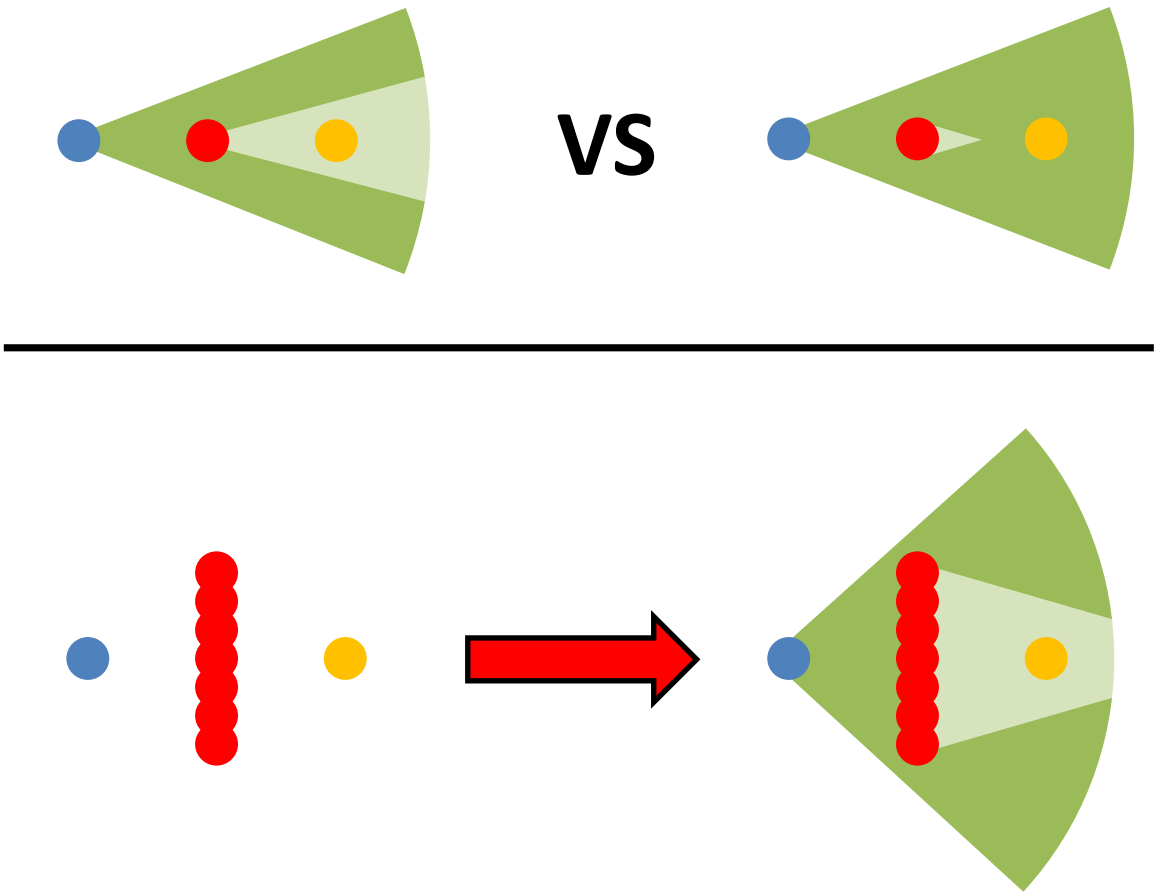

Figure 8. Illustrative explanation for using the "wall colony" formation instead of a single intervening colony. Metabolite shadowing caused by a single colony will likely become less effective over time as diffusion will drive metabolites from the regions of higher concentration into the lower concentration shadowed region (above). Incorporation of a larger colony that is the same length as the diffusion path between cross-feeding partners should prevent collapse of the shadowed region over the duration of the experiments.

COMETS predicted that the utilization of metabolites by the intervening competitors or conspecific competitors would result in a shadowing effect where one or both of the consortium colonies would suffer a decreased growth rate due to the strain on the available supply of nutrients [Fig 9A]. Specifically, the scenario 2 geometry was expected to result in decreased growth rates for both consortium partners as the *S. enterica* WT was predicted to strain cross-feeding relative to scenario 1 by utilizing both metabolites without reciprocation. In the scenario 3 geometry, the intervening colony was composed of conspecific competitors. In this scenario, it

was predicted that the *E. coli* growth rate would be enhanced while the distal *S. enterica* colony would suffer decreased growth very similar to scenario 2. The scenario 4 geometry was investigated here for the first time and predicted to result in enhanced growth for the *E. coli* as they would receive excess methionine. Despite an increase in acetate production due to a larger *E. coli* colony in this scenario, the *S. enterica* was predicted to suffer decreased growth when compared to scenario 1, but was also predicted to experience more growth than in either scenario 2 or 3. The COMETS simulation indicated that the presence of so many cooperating competitors would precipitate the formation of an acetate "diffusion sink" due to the rapid utilization of acetate by the colonies despite their placement outside the path of metabolite exchange. It was predicted that this region would consistently possess a lower acetate concentration than the region between the *E. coli* and the focal *S. enterica* colony, resulting in a back-flow of acetate toward the cooperating competitor colonies. The scenario 1 geometry was included as a control under which no metabolite competition would transpire. Growth of patterned colonies was observed for 240 hours, with fluorescence micrographs gathered at 48 hour time intervals to measure intensity changes as biomass increased [Fig 9B].

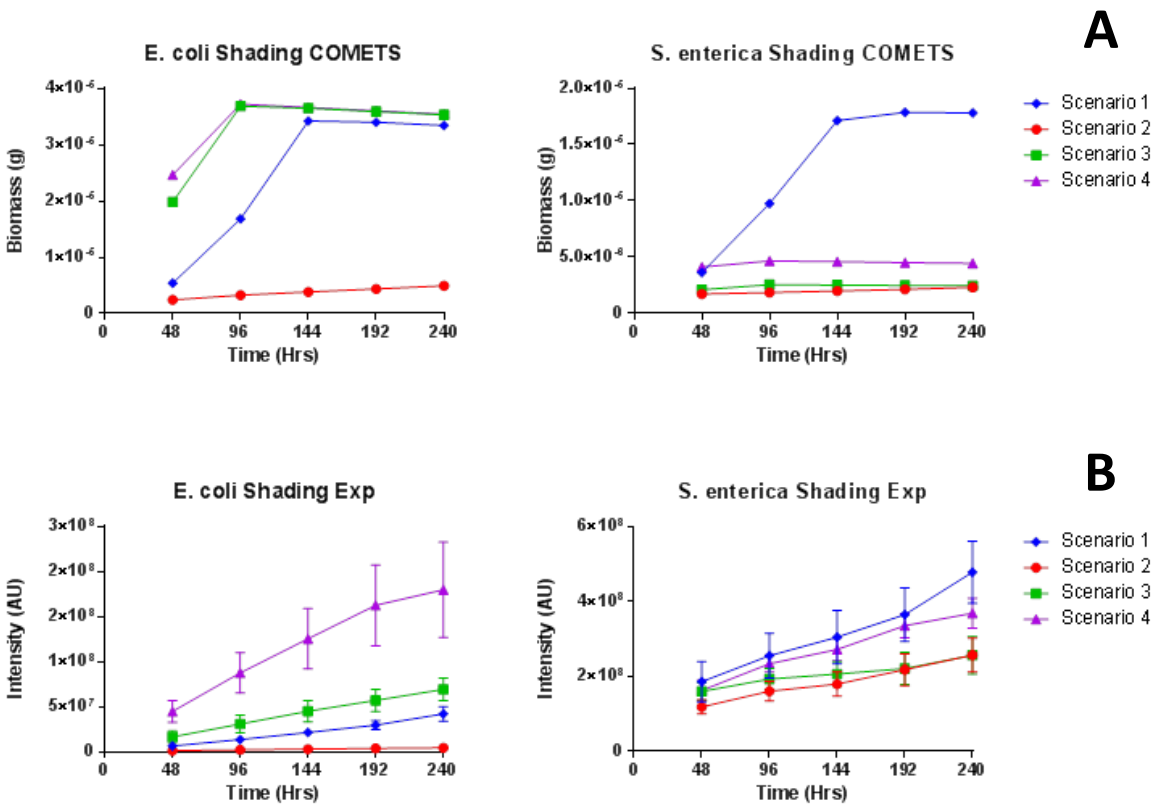

Figure 9. A) COMETS model predictions of biomass accumulation over 240 hours under the eclipse scenario for both consortium partners. **B)** Measure of total fluorescence intensity for the consortium colonies over 240 hours under the eclipse scenario. Error bars represent standard deviation.

For the eclipse dilemma trials each focal colony was evaluated relative to the growth of the colony of the corresponding species in scenario 1. Comparison of COMETS predictions of micro-colony biomass to the *in vitro* fluorescence data from the eclipse scenarios exhibits agreement between the growth trends at the 240 hour time point, with COMETS able to accurately predict the overall order of growth ratios as they occurred upon the patterned surfaces [Fig 10A]. But while the trends of the *in silico* and *in vitro* growth ratios are similar, the overall ratios themselves do not agree as well as the distance-dependence data in the previous section. During the distance dependence trials, the diffusion coefficients used to generate COMETS predictions of biomass were identified as a parameter which significantly affected the simulation

outcome. Thus, the COMETS simulation of the eclipse scenarios was modified by lowering the diffusion coefficients from $5x10^{-6}$ cm^2/sec for both metabolites to $1x10^{-6}$ cm^2/sec for methionine and $5x10^{-7}$ cm^2/sec for acetate [Fig 10B]. While adjustment of the diffusion coefficients did bring the *in vitro* and *in silico* results closer together, it did not completely correct all inconsistencies. This suggests that on the micro-scale COMETS' predictions become less accurate as the experimental scenarios become more complex, with respect to the relatively simple, micro-scale distance dependence experiment. When the outcomes of the macro-scale eclipse scenario trials are compared to those of the micro-scale experiments, the importance of scale becomes apparent in regards to predicting the behavior of microbial interactions. When similar scenarios were patterned using a macro-scale plating technique (with the exception of scenario 4, which was examined here for the first time), COMETS was able to correctly predict the trends and magnitudes of the biomass ratios [16]. When the eclipse dilemma was investigated on the micro-scale, COMETS was able to correctly predict the trends for all scenarios, save for *E. coli* in scenario 4, but was unable to correctly predict the magnitude of growth in the majority of scenarios with respect to scenario 1 . Comparison of the macro- and micro-scale results demonstrates the requirement of investigating microbial interactions on multiple scales in order to validate the predictions of bacterial growth models which simulate complex spatiotemporal interactions [Fig 11].

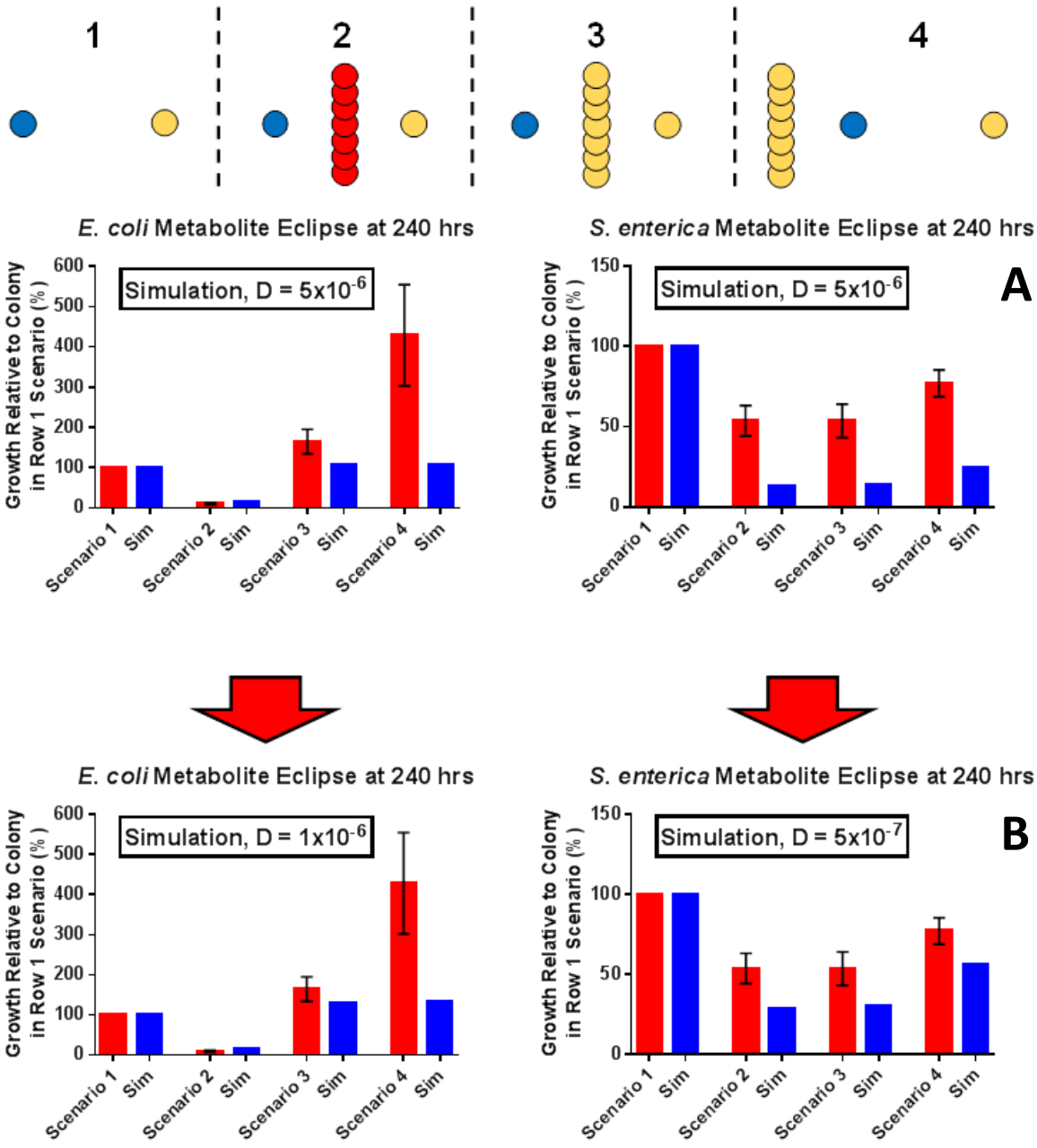

Figure 10. A) Comparison of *in silico* and *in vitro* eclipse dilemma data at 240 hours relative to the growth of the focal colony of the corresponding species in scenario 1. Red bars and blue bars denote *in vitro* and *in silico* scenarios, respectively. **B)** Adjustment of the metabolite diffusion coefficients used by COMETS to generate biomass predictions resulted in only partial correction, suggesting other modeling parameters may require refinement to more accurately predict the microbial interactions at the micro-scale. Error bars represent standard deviation.

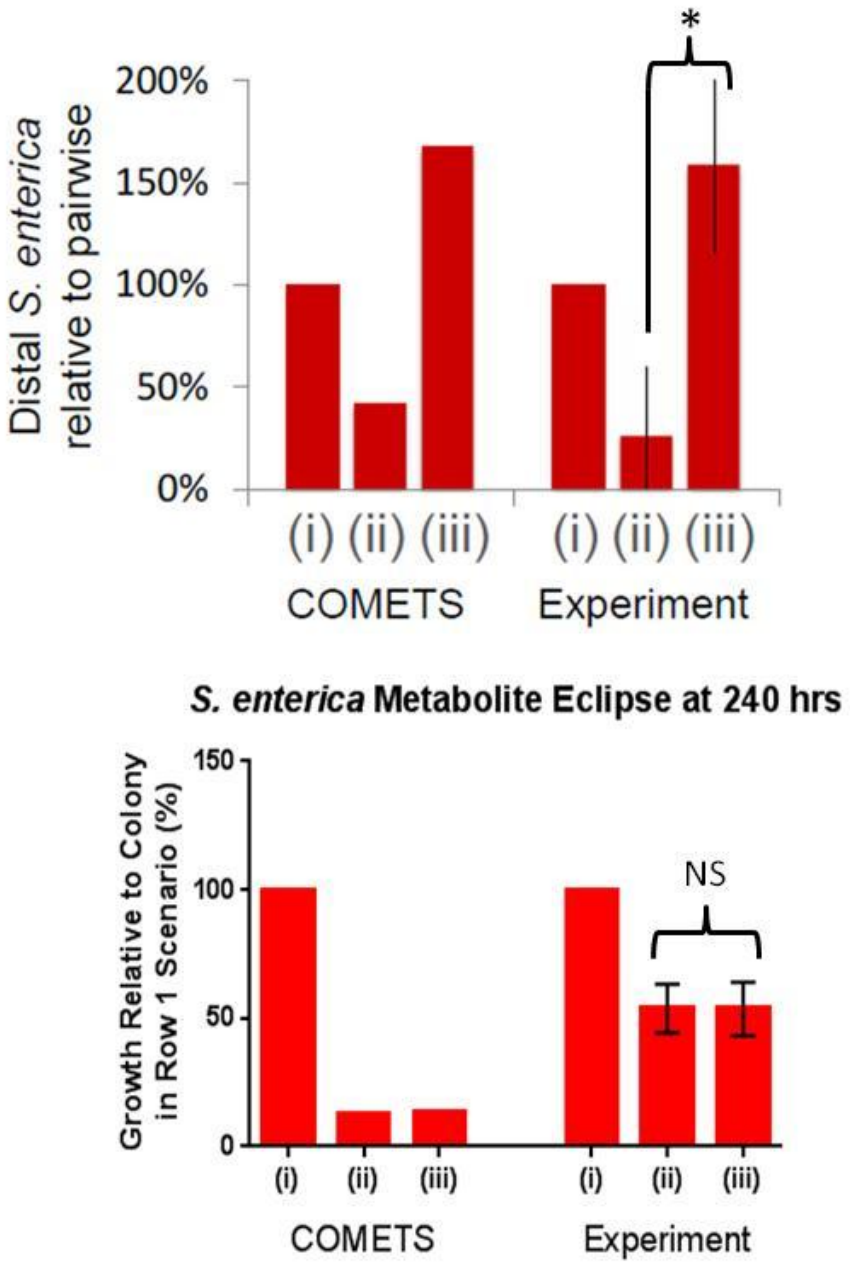

Figure 11. Comparison of the eclipse dilemma scenarios on the macro-scale (above), reproduced with permission from [16], and the micro-scale (below). Both macro and micro COMETS simulations were generated when D = $5x10^{-6}$ cm^2/sec. On the macro-scale, scenarios 2 and 3 were found to be significantly different using a two tailed t-test (p value = 0.02). This is in contrast to the micro-scale experiments where the differences between scenarios 2 and 3 experimental results were not significantly different using an identical test (p value = 0.99). As the size scale closer approaches the single-cell level, the predictive ability of the COMETS model appears to diminish. Error bars represent standard deviation.

5.4. Discussion

After patterning microcolonies of cells, resulting colony growth was monitored and quantified to provide necessary data to compare to the COMETS model predictions of distance-dependence on the diffusion driven metabolite-sharing events between the syntrophic strains. Preliminary cross-feeding experiments revealed strong distance dependence between the printed micro-colonies of the consortium when the partners were patterned at increasing spatial separations (from 1 mm to 3. 5 mm). These results suggested that cross-feeding becomes less effective as the diffusion path is increased, which was readily reflected in the COMETS model's predictions of syntrophic interaction across increasing spatial separations on the micro-scale when using parameters that were similar the experimental conditions.

Comparison of the distance dependence trials to COMETS simulations revealed that the growth exhibited by the pairs of *E. coli* and *S. enterica* cross-feeding partners aligned best for most separation distances when the predictions were generated with metabolite diffusion coefficients of $5x10^{-6}$ cm^2/sec and $1x10^{-6}$ cm^2/sec, respectively. A possible explanation for the experimental diffusion dependence data matching better for different diffusion coefficients is the ability of agarose to bind anions within its gel matrix [32]. The diffusible carbon source which the *E. coli* is providing to the *S. enterica* is likely acetate [29]. This could account for *S. enterica*'s growth trend in the experimental scenario matching the simulation data generated using the lower diffusion coefficient, as diffusion of the acetate is possibly being somewhat inhibited due to binding to the substrate. Additionally, acetate will likely convert to acetic acid quickly upon its release to the extracellular environment. Acetic acid possess a vapor pressure similar to, albeit slightly lower than, water which makes it likely that diffusion of *S. enterica*'s carbon-source is being inhibited due to its slow loss from the substrate due to evaporation.

These nutrient losses due to evaporation may also be contributing to *S. enterica*'s growth matching better to the *in silico* data generated with the lower diffusion coefficient of $1x10^{-6}$ cm^2/sec. Despite these complications, comparison of the COMETS simulation predictions to the experimental data reveals good agreement across the resulting growth trends. The COMETS model was able to accurately predict the trend and the ratio, of colony growth based solely on the distance between cross-feeding populations, with colony growth decreasing as separation distance between partners is increased. This demonstrates the initial steps of recapitulating a micro-scale, non-homogenous, spatially-dependent bacterial population behavior in a laboratory environment with a predictive growth model.

COMETS was used to generate predictions on several "eclipse dilemma" scenarios. These predictions were challenged in the laboratory by micropatterning competitor strains in the path of nutrient exchange between the consortium partners in order to evaluate the effects of competition on the resulting fluorescence intensity of the consortium colonies. The simulations produced by COMETS on both the macro- and micro-scales predicted that competitors that utilized both metabolites would decrease cross-feeding, causing the growth of both partners to decrease relative to scenario 1. Both macroscale plating [16] and micro-scale bioprinting experiments revealed that this hypothesis is supported as consortium partners in this scenario (scenario 2) exhibited the least growth among the scenarios tested. COMETS also correctly predicted that *E. coli* in scenario 3 would benefit from the inclusion of additional *S. enterica* WH212 colonies producing methionine, while the focal *S. enterica* WH212 colony would suffer a decrease in relative biomass, relative to the scenario 1 control, if the same methionine-producing strain was placed in the path of nutrient exchange. The presence of the conspecific competitors in scenario 3 was predicted to inhibit the *S. enterica* growth to approximately the

same degree as when in the presence of the full competitor, *S. enterica* WT, in scenario 2 which was readily reflected by the micro-scale *in vitro* experiments. This sharply contrasts the macro-scale results when scenario 3 was modeled in COMETS and reproduced in the laboratory using macro-scale plating, where both results agreed that *S. enterica* colony would increase in biomass due to the enhanced growth of *E. coli* [16]. The focal *S. enterica* colony's decreased growth in scenario 3 relative to the macro-scale experiments is unlikely to be simply an effect of substituting a single intervening colony for a "wall" of seven intervening colonies. If this effect were due solely to the presence of a 7-fold larger wall colony, an appreciable increase in growth between the biomass of *S. enterica* in scenario 3 relative to scenario 2 would likely still be observed due to the increased amount of acetate production coming from the approximately 16-fold larger *E. coli* colony in scenario 3. This outcome highlights how the examination of similar interactions on different scales is necessary as they may not produce similar results. In addition, this highlights the ability of COMETS to predict such non-intuitive outcomes. In regards to scenario 4 COMETS predicted that if the additional methionine-producing colonies were placed outside the path of nutrient exchange the focal *E. coli* colony would once again experience an increased biomass relative to *E. coli* in the scenario 1 control. However COMETS predicted that this increase in biomass of the *E. coli* focal colony would only result in a growth increase of 6% over the *E. coli* focal colony in scenario 1. This represents the least accurate prediction made by COMETS over the course of the investigation as the *E. coli* colony in scenario 4 was found to have an average growth of 429% relative to the average growth recorded for *E. coli* in scenario 1 when examined *in vitro*. Interestingly, COMETS predicted that the focal *S. enterica* colony in the scenario 4 would grow more slowly than it would in the control scenario, despite the increased biomass of the *E. coli* colony, due to a "diffusion sink" created by the line of

conspecific competitor colonies. The rapid utilization of acetate by the line of *S. enterica* colonies was predicted to create a depletion zone which would slow diffusion of acetate in the region between the *E. coli* colony and the focal *S. enterica* colony as some metabolites would back-flow from this zone of higher concentration back toward the depletion zone. Additionally, COMETS indicated that after 144 hours the *E. coli* colony would have reached the point where it had utilized all available lactose within the media local to the colony, forcing *E. coli* to begin utilizing acetate as a substitute carbon source, adding yet another acetate competitor to the scenario. These predications were supported with bioprinting experiments, with *E. coli* exhibiting the highest and second highest average fluorescence intensity in scenarios 4 and 3, respectively. COMETS prediction of the focal *S. enterica* colony's relative biomass in scenario 3 is also supported by the *in vitro* experiments as they exhibited nearly the same value for fluorescence intensity at hour 240 as they did for scenario 2. Overall, the relative growth of the colonies within each scenario observed during the "eclipse dilemma" printing experiments agreed strongly with general trends predicted by COMETS; however magnitude of relative growth observed *in vitro* was not readily reflected within the simulations. This demonstrates the utility of using micro-patterning techniques to examine microbial interactions with spatiotemporal dependencies, such as diffusible nutrient competition, as the cellular behavior at such small scales may not coincide with observations made on larger scales.

It should be noted that the eclipse dilemma *in vitro* data aligned better with COMETS predictions generated using a lower diffusion coefficient in comparison to the distance dependence results. Better prediction of the growth relative to scenario 1 was attained with simulations generated using diffusion coefficients of $1x10^{-6}$ cm^2/sec and $5x10^{-7}$ cm^2/sec for *E. coli* and *S. enterica*, respectively. As with the distance dependence scenario *S. enterica* matched

better with a diffusion coefficient 5-fold lower than that of *E. coli*, once again suggesting the diffusion of acetate is being inhibited relative to methionine. However, better matching with overall lower diffusion coefficients as compared to the diffusion dependence scenarios could be at least partially explained by the experimental setup differences between the two sets of trials. Unlike the distance-dependence experiment, each eclipse scenario sample was patterned in isolation, upon separate surfaces. This may account for the *in vitro* data aligning better with the simulation data generated with lower diffusion coefficients. It is possible that despite the large separations (5 mm) between cross-feeding pairs used in the distance dependence experiments, some metabolite diffusion between the groups did occur. If this was the case, then more metabolites would be available for each colony than COMETS would assume during a given simulation, resulting in the *in vitro* data aligning better with higher diffusion coefficients for the distance dependence trials. This could be corrected by revisiting the distance dependence experiments and patterning each cross-feeding pair on isolated surfaces to prevent any possibility of cross-interaction between pairs.

Cellular deposition using a liquid-based printing system always results in colonies which are non-uniform in terms of cell number, both across the colony surface and between printed colonies. All printed colonies exhibited a ring-shaped morphology which is caused by the differential evaporation of the cell-laden droplets, with liquid at the edges evaporating faster than at the center. This phenomenon results in greater cell numbers being deposited at the edges of the colony. Evaporation causes the bacteria at the edges to deposit on top of one another, leading to higher intensity fluorescence in these regions. The random selection of a small volume (approx. 200 nL) of solution containing cells from a larger volume (4 µL) performed by the print pin during patterning is similar to randomly sampling a subpopulation from a larger population

with a Gaussian distribution. Some patterned colonies will have cell densities very close to the average cell density within the original solution, while others will have cell density values which vary about the average. Due to this variability in patterned cell number per colony, it is highly likely that the initial biomass printed for each scenario was also variable. Throughout all the simulations described here COMETS was programmed with the assumption that each printed colony had the same initial biomass value, which was estimated to be $1x10^{-6}$ g. As this biomass value was only an estimate it is a likely candidate for adjustment to better match the initial biomass of the printed colonies *in vitro*, which may lead to better agreement between the *in silico* and *in vitro* results. It is possible that the growth ratios and trends predicted by COMETS would come even closer to the *in vitro* results if the more challenging to control experimental parameters, such as exact starting biomass per printed colony, could be used as input parameters for each simulation.

The conversion of fluorescence intensity to biomass can be accomplished with the data gathered from the experiment which related colony intensity to cell number. By using the common approximation that the average bacterial cell has a mass of $1x10^{-12}$ g, each fluorescence intensity measurement gathered over the 96 to 192 hours of observation during the experimental trials can be converted into a value for biomass. Once biomass estimates for each experimental colony are acquired the initial biomasses of all colonies directly after printing can be calculated. Initially, accurate measurements of fluorescence intensity were impeded when imaging was previously attempted on freshly printed colonies due to the relatively low cell densities present after patterning. However, by generating best-fit curves for each *in vitro* data set the y-intercepts of each curve can be readily calculated, leading to reasonable estimates for the biomass of each

colony directly post-printing. This would result in the acquisition of more precise initial biomasses for each colony within each experimental scenario for input into COMETS..

Another possible factor for the inconsistencies between the growth ratios predicted by COMETS and those observed during experimentation the model's assumption of a two-dimensional surface. This assumption simplifies the calculations of metabolite diffusion between the colonies. However, the inherent three-dimensional nature of the *in vitro* patterned surfaces causes some metabolites to be lost to the z-direction (into the substrate). While modifying the diffusion coefficients is an imperfect approach to correcting for this difference between experiment and model, it does slow the overall exchange of metabolites in the model, resulting in slightly better agreement between simulation and experiment. A more appropriate correction, which is currently under development, will require modification and refinement of the COMETS model itself in order to accurately recapitulate diffusion processes in three-dimensions. Despite the current general estimates used to tune COMETS' starting parameters, the accuracy of COMETS simulations indicates that complex, spatially-defined metabolic interactions between multiple species can be predicted over short time intervals within a well controlled environment on the micro-scale.

5.5. Conclusions on Bioprinting for Computational Model Validation

The bioprinting approach permits the fabrication of patterned, multi-species micro-cultures with parameters, such as colony population density, environmental dimensions and spatial distribution of cells and nutrients, which can be readily input as modeling parameters for the COMETS system. This can also work in reverse, with COMETS modeling parameters used

to design a laboratory experiment to test the predictions of a de novo simulation. We have developed a method of cellular patterning which enables the observation of complex intercellular interactions on the micro-scale with defined spatial characteristics. Using this approach we have investigated the dynamics of mutualistic microbial cross-feeding and evaluated the effects of competition on nutrient exchange on the micro-scale. Additionally we have shown that the results of these interactions are appreciably different than those found on the macro-scale. This suggests that any microbial interaction which relies upon spatiotemporal dynamics should be evaluated on multiple scales as the resulting effects can differ drastically when scale is altered. We have also demonstrated the utility of the COMETS platform and its ability to predict the general trend of many of these outcomes based on their spatial organization and scale. This bioprinting approach could be used to challenge any model, such as COMETS, which strives to predict bacterial interactions with spatiotemporal dependencies. When used in combination with COMETS, this approach demonstrates the power of using a computational model in conjunction with the means of readily recapitulating the model's parameters on the micro-scale in order to confirm or refute the *in silico* predictions *in vitro*.

References Cited

[1] K. Brenner, L. You, and F. H. Arnold, "Engineering microbial consortia: a new frontier in synthetic biology," *Trends Biotechnol.*, vol. 26, no. 9, pp. 483–489, 2008.

[2] S. Stolyar, S. Van Dien, K. L. Hillesland, N. Pinel, T. J. Lie, J. a Leigh, and D. a Stahl, "Metabolic modeling of a mutualistic microbial community.," *Mol. Syst. Biol.*, vol. 3, no. 92, pp. 1–14, 2007.

[3] H. J. Kim, J. Q. Boedicker, J. W. Choi, and R. F. Ismagilov, "Defined spatial structure stabilizes a synthetic multispecies bacterial community.," *Proc. Natl. Acad. Sci. U. S. A.*, vol. 105, no. 47, pp. 18188–18193, 2008.

[4] M. Mee and H. Wang, “Engineering Ecosystems and Synthetic Ecologies,” *Mol. Biosyst.*, vol. 8, no. 10, pp. 2470–2483, 2012.

[5] B. Niu, H. Wang, Q. Duan, and L. Li, “Biomimicry of quorum sensing using bacterial lifecycle model.,” *BMC Bioinformatics*, vol. 14 Suppl 8, no. Suppl 8, p. S8, Jan. 2013.

[6] P. a. Iglesias and P. N. Devreotes, “Navigating through models of chemotaxis,” *Curr. Opin. Cell Biol.*, vol. 20, no. 1, pp. 35–40, 2008.

[7] D. (Colorado C. Brown, “Bulletin of Mathematical Biology: Linking molecular and population processes in mathematical models of quorum sensing,” *Bull. Math. Biol.*, vol. 75, no. 10, pp. 1813–1839, 2013.

[8] K. Brenner, D. K. Karig, R. Weiss, and F. H. Arnold, “Engineered bidirectional communication mediates a consensus in a microbial biofilm consortium.,” *Proc. Natl. Acad. Sci. U. S. A.*, vol. 104, no. 44, pp. 17300–4, Oct. 2007.

[9] W. S. Choi, M. Kim, S. Park, S. K. Lee, and T. Kim, “Patterning and transferring hydrogel-encapsulated bacterial cells for quantitative analysis of synthetically engineered genetic circuits.,” *Biomaterials*, vol. 33, no. 2, pp. 624–33, Jan. 2012.

[10] D. S. Weaver, I. M. Keseler, A. Mackie, I. T. Paulsen, and P. D. Karp, “Open Access A genome-scale metabolic flux model of Escherichia coli K – 12 derived from the EcoCyc database,” *BMC Syst. Biol.*, vol. 8, no. 79, pp. 1–24, 2014.

[11] S. Louca and M. Doebeli, “Calibration and analysis of genome-based models for microbial ecology,” *Elife*, vol. 4, no. OCTOBER2015, pp. 1–17, 2015.

[12] a. Varma and B. O. Palsson, “Stoichiometric flux balance models quantitatively predict growth and metabolic by-product secretion in wild-type Escherichia coli W3110,” *Appl. Environ. Microbiol.*, vol. 60, no. 10, pp. 3724–3731, 1994.

[13] B. Kerr, M. a Riley, M. W. Feldman, and B. J. M. Bohannan, “Local dispersal promotes biodiversity in a real-life game of rock-paper-scissors.,” *Nature*, vol. 418, no. 6894, pp. 171–174, 2002.

[14] A. Konopka, “What is microbial community ecology?,” *ISME J.*, vol. 3, no. 11, pp. 1223–1230, 2009.

[15] E. Tzamali, P. Poirazi, I. G. Tollis, and M. Reczko, “A computational exploration of bacterial metabolic diversity identifying metabolic interactions and growth-efficient strain communities.,” *BMC Syst. Biol.*, vol. 5, no. 1, p. 167, Jan. 2011.

[16] W. R. Harcombe, W. J. Riehl, I. Dukovski, B. R. Granger, A. H. Lang, G. Bonilla, A. Kar, N. Leiby, P. Mehta, C. J. Marx, and D. Segrè, “Metabolic resource allocation in individual

microbes determines ecosystem interactions and spatial dynamics," *Cell Rep.*, vol. 7, no. 4, pp. 1104–1115, 2014.

[17] H. Song and L. You, "Methods in molecular biology: Modeling spatiotemporal dynamics of bacterial populations," *Methods Mol. Biol.*, vol. 880, pp. 243–254, 2012.

[18] M. Schaechter, "From growth physiology to systems biology," *Int. Microbiol.*, vol. 9, pp. 157–161, 2006.

[19] M. C. Te Giffel and M. H. Zwietering, "Validation of predictive models describing the growth of Listeria monocytogenes," *Int. J. Food Microbiol.*, vol. 46, no. 2, pp. 135–149, 1999.

[20] D. B. Kolesky, R. L. Truby, a. S. Gladman, T. a. Busbee, K. a. Homan, and J. a. Lewis, "3D bioprinting of vascularized, heterogeneous cell-laden tissue constructs," *Adv. Mater.*, vol. 26, no. 19, pp. 3124–3130, 2014.

[21] S. V Murphy and A. Atala, "3D bioprinting of tissues and organs.," *Nat. Biotechnol.*, vol. 32, no. 8, pp. 773–785, 2014.

[22] W. F. Hynes, N. J. Doty, T. I. Zarembinski, M. P. Schwartz, M. W. Toepke, W. L. Murphy, S. K. Atzet, R. Clark, J. Andres Melendez, and N. C. Cady, "Micropatterning of 3D microenvironments for living biosensor applications," *Biosensors*, vol. 4, no. 1, pp. 28–44, 2014.

[23] B. Lorber, W.-K. Hsiao, I. M. Hutchings, and K. R. Martin, "Adult rat retinal ganglion cells and glia can be printed by piezoelectric inkjet printing.," *Biofabrication*, vol. 6, no. 1, p. 015001, 2014.

[24] X. Cui, T. Boland, D. D. D'Lima, and M. K. Lotz, "Thermal inkjet printing in tissue engineering and regenerative medicine.," *Recent Pat. Drug Deliv. Formul.*, vol. 6, no. 2, pp. 149–55, 2012.

[25] A. Skardal, M. Devarasetty, H.-W. Kang, I. Mead, C. Bishop, T. Shupe, S. J. Lee, J. Jackson, J. Yoo, S. Soker, and A. Atala, "A hydrogel bioink toolkit for mimicking native tissue biochemical and mechanical properties in bioprinted tissue constructs," *Acta Biomater.*, vol. 25, pp. 24–34, 2015.

[26] A. Dolatshahi-Pirouz, M. Nikkhah, A. K. Gaharwar, B. Hashmi, E. Guermani, H. Aliabadi, G. Camci-Unal, T. Ferrante, M. Foss, D. E. Ingber, and A. Khademhosseini, "A combinatorial cell-laden gel microarray for inducing osteogenic differentiation of human mesenchymal stem cells.," *Sci. Rep.*, vol. 4, p. 3896, 2014.

[27] M. Ali, E. Pages, A. Ducom, A. Fontaine, and F. Guillemot, "Controlling laser-induced jet formation for bioprinting mesenchymal stem cells with high viability and high resolution," *Biofabrication*, vol. 6, no. 4, p. 045001, 2014.

[28] M. L. Clarke, J. Y. Lee, D. V. Samarov, D. W. Allen, M. Litorja, R. Nossal, and J. Hwang, "Designing microarray phantoms for hyperspectral imaging validation," *Biomed. Opt. Express*, vol. 3, no. 6, p. 1291, 2012.

[29] W. Harcombe, "Novel Cooperation Experimentally Evolved Between Species," *Evolution (N. Y).*, vol. 64, no. 7, pp. 2166–2172, 2010.

[30] C. J. Gantzer and H. G. Stefan, "A model of microbial activity in lake sediments in response to periodic water-column mixing," *Water Res.*, vol. 37, no. 12, pp. 2833–2846, 2003.

[31] W. T. Tan and J. K. Goh, "Electrochemical Oxidation of Methionine Mediated by a Fullerene-C 60 Modified Gold Electrode," *Electroanalysis*, vol. 20, no. 22, pp. 2447–2453, 2008.

[32] L. Piculell and S. Nilsson, "Anion-specific salt effects in aqueous agarose systems. II: Nuclear spin relaxation of ions in agarose gels and solutions," *J. Phys. Chem.*, vol. 93, no. 1 7, pp. 5602–5611, 1989.

Chapter 6: Summary and Conclusions

In summary of the findings discussed in the previous chapters, I have shown that two-dimensional bioprinting is a powerful tool that can be applied to many novel cell signaling and sensing applications. Additionally I have shown that two-dimensional, biocompatible cell printing can be achieved using microarray and molecular printers by performing specific modifications, including incorporation of a suitable matrix material and maintaining high humidity within the tool during patterning [1]. I have demonstrated that mammalian cells patterned and encapsulated within biocompatible, three-dimensional microenvironments can be used to detect the presence of toxins when they are engineered to express the appropriate detection probe. This approach could be readily used to develop a variety of different of cell-based assays or biosensors designed to evaluate the effects of therapeutic compounds or to detect the presence of specific toxins. In this case, I have used this approach to develop the first reported printed, cell-based biosensor capable of sensing the cell's redox environment by responding to the presence of reactive oxygen species and reducing agents [2].

After verifying the function of this proof-of-concept ROS biosensor, the next steps for improving the utility and function of the sensor would be to incorporate cells which are engineered to express the redox sensitive roGFP at different intracellular sites. This would improve the sensor's ability to evaluate the intracellular availability and activity of the exogenous redox agents by monitoring their action at cellular organelles such as the mitochondria, nucleus, endoplasmic reticulum, etc. Inversely, such a sensor could be used to examine the activity of potential antioxidant compounds and their ability to mitigate the

intracellular exposure of both exogenous and endogenous ROS at multiple cell sites simultaneously. The sensor itself could also be incorporated into a microfluidic chamber permitting for acute or chronic exposure of ROS or antioxidants to the immobilized cells in a controlled manner. Utilizing this general process flow for biosensor fabrication, additional cell-based sensors could be developed which respond to the presence of a variety of different molecules. Such sensors would incorporate cells engineered to express intracellular probes at predetermined cellular locations which are capable of responding to specific analytes. Possible examples of expressible fluorescent probes used for these sensors include Ca^{2+} sensitive proteins such as G-CaMP [3] and pH sensitive proteins such as GFPmull [4].

Two-dimensional bioprinting was also used to challenge complex predictions of an experimental bacterial growth model, an entirely novel application for bioprinting that, to our knowledge, has not been attempted before. The predictions generated by the COMETS model depended heavily upon the spatiotemporal organization of the syntrophic bacterial micro-colonies, a situation which could be recapitulated in the laboratory using our two-dimensional printing approach. This work represents a first for both the fields of bioprinting and computational biology and could be used as a framework for the experimental validation and refinement of any current or future bacterial growth model which generates its predictions based on spatiotemporal dynamics [5].

Future directions for using microprinted bacterial co-cultures to validate the COMETS model will begin with the quantification of the specific conditions present during the laboratory experiments in order to accurately adjust the initial modeling parameters. By tuning COMETS initial parameters to better match the experimental conditions it may be possible to generate more accurate predictions of colony biomass accumulation. Currently, COMETS is programmed

with parameters which assume equal starting biomass of the colonies, equal metabolite diffusion coefficients, and an ideal two dimensional surface. Estimation of the true starting biomasses of each micro-colony within each experimental scenario is possible by converting the fluorescence intensity over time growth trends recorded during each experiment into cell number over time trends. By estimating the y-intercept of each growth trend, and using a common measure of biomass per cell, the biomass of each micro-colony can be estimated and directly input into COMETS for prediction adjustment. Based on evidence that acetate is potentially evaporating, thereby slowing its diffusion relative to methionine, the next steps will be to set the diffusion coefficients for the exchanged metabolites independently within a single simulation. The final steps will be to implement the version of COMETS which extends its diffusion simulation capabilities to three dimensions to more accurately replicate the metabolite exchange within the experiments.

Finally, I have demonstrated that microcontact printing, the earliest method of bioprinting, is still finding use in the field of fundamental biology. Our collaborative effort highlighted the continuing utility of this two-dimensional bioprinting approach for investigating receptor-mediated signaling. Utilizing engineered surfaces composed of micropatterned IgG and poly-L-lysine, the role and mechanism of PKC-ε in macrophage phagocytosis was elucidated. The work performed by Dr. Lennartz using my IgG-modified substrates revealed for the first time that PKC-ε enters the phagosome on vesicles, which traffic from the Golgi on microtubules and that each domain of PKC-ε plays a specific, critical role in this process [6].

Throughout the course of these investigations it has become clear that while bioprinting in three dimensions is being actively leveraged for advanced tissue engineered applications, two-dimensional bioprinting remains a highly promising technology which has not yet been fully

exploited. Whether it is utilizing microcontact printing to investigate the role of a specific protein kinase, using microarray-based bioprinting to challenge a computational bacterial growth model, or for the development of novel biosensors, two-dimensional bioprinting can be readily achieved with common laboratory instruments and without the need for sophisticated equipment or expertise. Development of an effective three dimensional bioprinting process requires expertise from three major disciplines, specifically biology, mechanical engineering, and materials science [7]. Alternatively, two-dimensional, microarray-based printing techniques do not require broad mechanical engineering knowledge on topics such as additive manufacturing, machine design and control, or CAD/CAM systems.

A specific example of this is the conversion of a thermal inkjet printer into a three-dimensional, or even two-dimensional, bioprinting tool. This conversion requires harvesting and reassembling the physical components of a commercially available printer, rewriting of the software drivers, and fine tuning of the printing parameters to avoid overheating of the printing solutions [8]. In contrast, standard pin-based microarray printers (like the SpotBot 3 used in some of my experiments) are already designed to pattern solutions in a large range of viscosities, with pins large enough to accommodate whole-cells (at least bacterial cells), using capillary force with no substantial modifications to its hardware and only minor software modification to permit printing of arbitrary geometries. Due to the prevalence of laboratory microarray printers and the minimal modifications required to pattern viable cells, many researchers can gain access to bona fide live-cell printers with relative ease.

As demonstrated by the applications examined above, two-dimensional bioprinting is especially useful for the investigation of fundamental and applied cellular signaling, sensing, and other diffusion-based phenomena. The general strength of bioprinting is the precise control over

the positioning of cells, signals, nutrients or toxins relative to one another, as well as their respective concentrations, all of which are of critical importance to the study of diffusion-based phenomena. When investigating these types of phenomena computationally researchers can benefit from beginning with a two-dimensional approaches they become more mathematically rigorous when the complexity of a third dimension is introduced. For example, diffusion-based phenomena such as metabolite sharing [9] and quorum sensing [10] can become substantially more challenging to simulate when additional dimensions are considered due to the increasing complexity of the requisite equations used to describe the system. Each of the applications explored in the previous chapters are excellent examples of situations where the evaluation of the third dimension is not only unnecessarily complicating, but also non-essential. While many researchers are focused upon more achieving and utilizing advanced three-dimensional bioprinting, two-dimensional bioprinting should, itself, be viewed as useful tool and not simply as a stepping-stone toward the third dimension.

6.1. Accomplishments

Publications

- "Establishing microbial communities via bioprinting for the experimental verification of a predictive bacterial growth model" In Preparation for Submission (2016)
- "Micropatterning of 3D Microenvironments for Living Biosensor Applications" *Biosensors* (2014)
- "Microscale Cell Printing in Photocrosslinkable Three Dimensional Matrix Materials", Abstract for MRS (2011) Fall Meeting & Exhibit
- "Direct Cell Printing With Microfabricated Quill-Pen Cantilevers", *Proceedings of the Materials Research Society* (2009)

Conference Presentations

- Materials Research Society (MRS) 2011 Fall Meeting & Exhibit (Dec 2nd 2011, Boston MA)

- Undergraduate Research Symposium (SUNY Albany) 2009 Spring (Apr 19th 2009, Albany NY)

Poster Presentations

- College of Nanoscale Science & Engineering Summer Internship Poster Session (SUNY CNSE) 2008 Summer (Aug 1st 2008, Albany NY)

References Cited

[1] W. F. Hynes, A. Gracias, N. M. Fahrenkopf, N. A. Raof, W. K. Raja, K. Lee, Y. Xie, M. Bergkvist, and N. C. Cady, "Direct Cell Printing With Microfabricated Quill-Pen Cantilevers," in *MRS Proceedings*, 2010, pp. 1235–RR06.

[2] W. F. Hynes, N. J. Doty, T. I. Zarembinski, M. P. Schwartz, M. W. Toepke, W. L. Murphy, S. K. Atzet, R. Clark, J. Andres Melendez, and N. C. Cady, "Micropatterning of 3D microenvironments for living biosensor applications," *Biosensors*, vol. 4, no. 1, pp. 28–44, 2014.

[3] J. Nakai, M. Ohkura, and K. Imoto, "A high signal-to-noise Ca(2+) probe composed of a single green fluorescent protein.," *Nat. Biotechnol.*, vol. 19, no. 2, pp. 137–41, 2001.

[4] J. Han and K. Burgess, "Fluorescent Indicators for Intracellular pH," *Chem. Rev.*, vol. 110, no. 5, pp. 2709–2728, 2010.

[5] W. F. Hynes, W. R. Harcombe, D. Segrè, C. J. Marx, and N. C. Cady, "Establishing microbial communities via bioprinting for the experimental validation of a predictive bacterial growth model," *Prep.*, vol. NA, 2016.

[6] A. C. Wong, K. Ho, T. Ueyama, X. Zhang, A. D'Amico, T. Wood-Cammock, W. F. Hynes, M. M. Barroso, C. M. Hanes, N. C. Cady, M. Trebak, N. Saito, and M. R. Lennartz, "Golgi-associated PKC-epsilon is delivered to phagocytic cups on vesicles: Role of PI4P," *Submiss. to J. Cell Biol.*, vol. NA, 2016.

[7] C. K. Chua and W. Y. Yeong, *Bioprinting: Principles and Applications*, 1st ed. Singapore: World Scientific, 2014.

[8] L. Pardo, W. Cris Wilson, and T. Boland, “Characterization of patterned self-assembled monolayers and protein arrays generated by the ink-jet method,” *Langmuir*, vol. 19, no. 5, pp. 1462–1466, 2003.

[9] H. J. Kim, J. Q. Boedicker, J. W. Choi, and R. F. Ismagilov, “Defined spatial structure stabilizes a synthetic multispecies bacterial community.,” *Proc. Natl. Acad. Sci. U. S. A.*, vol. 105, no. 47, pp. 18188–18193, 2008.

[10] K. Brenner, D. K. Karig, R. Weiss, and F. H. Arnold, “Engineered bidirectional communication mediates a consensus in a microbial biofilm consortium.,” *Proc. Natl. Acad. Sci. U. S. A.*, vol. 104, no. 44, pp. 17300–4, Oct. 2007.